Methods for rockfall risk assessment and estimation of runout zones: A case study in Gothenburg, SW Sweden

Laura Catalina Agudelo Motta

Dissertations in Geology at Lund University,
Master's thesis, no 593
(45 hp/ECTS credits)

Department of Geology
Lund University
2020

Methods for rockfall risk assessment and estimation of runout zones: A case study in Gothenburg, SW Sweden

Master's thesis

Laura Catalina Agudelo Motta

Department of Geology
Lund University
2020

Contents

Cover Picture: Rockfall occurred in 2017 in Fjällbo, Gothenburg. Photo taken by Mats Rundgren.

Methods for rockfall risk assessment and estimation of runout zones: A case study in Gothenburg, SW Sweden

LAURA CATALINA AGUDELO MOTTA

Agudelo Motta, Laura Catalina., 2020: Methods for rockfall risk assessment and estimation of runout zones: A case study in Gothenburg, SW Sweden. *Dissertations in Geology at Lund University*, No. 593, 58 pp. 45 hp (45 ECTS credits).

Abstract: Rockfalls occur around Sweden every year and the country lacks a national risk evaluation and an adequate regulatory framework for construction related to this natural hazard. The aim of this study is to address this problem by mapping areas under possible threat of rockfalls, considering two fundamental aspects: i) identification of the source areas and ii) estimation of the runout zones. The study was performed in the northeastern part of the Gothenburg municipality, particularly focusing on Fjällbo park, a popular climbing area where large talus slopes under the cliffs show evidence of both historic and recent rockfalls. The most recent event occurred in 2017. Potential rockfall source areas were outlined using a statistical method called Slope Angle Distribution (SAD), which combines information about the geology and topography of an area with the slope angle values extracted from a Digital Elevation Model (DEM). Runout zones were simulated using two programs: CONEFALL and RockfyFor3D, process-based software that use a DEM as a fundamental part of the analyses. CONEFALL uses the energy line method to estimate runout zones, whereas RockyFor3D considers different characteristics of the blocks, slopes, as well as protective effects from the forest density and tree sizes.

According to the SAD method, all angles above 40° - 42° are considered potential rockfall sources in the study area. CONEFALL generates rather conservative models and the outcomes are dependent on the topography and the height of the cliffs. Moreover, the lateral extent of the runout zones is overestimated by the software but can be adjusted by constraining its aperture angle. On the other hand, RockyFor3D generates more realistic outcomes and shows that the block shape affects the lateral extent of runout zones and block mass controls the energy dissipation of the blocks. Likewise, it shows that the bouncing behavior of the blocks on the surface is mostly controlled by the slope gradient and the coefficient of restitution, which is dependent on the type of soil or rock, and by the obstacles encountered on the way (their distribution and their sizes). Lastly, these simulations indicate that forests act as protective agents, as they may stop the falling blocks; however, the protection efficacy depends mainly on the density of the forest. The 2017 rockfall occurred in Fjällbo was included in the simulations performed using CONEFALL and RockyFor3D as a verification point of the applicability and accuracy of the two software models.

The SAD methodology for potential rockfall source detection, as well as the runout zone estimations obtained with CONEFALL and RockyFor3D models may serve as a foundation for further and more detailed risk assessment. These methods, however, are sensitive to topography, morphology and geology of the area, and, therefore, it is paramount to perform verifications of the study area with fieldwork and/or high-resolution remote sensing imagery. Depending on the topographical and geological information available, these methods can be used at both local and regional scales.

Keywords: Rockfall hazard, rockfall simulation, Gothenburg, Fjällbo, runout zones.

Supervisor(s): Johan Berglund (Swedish Geotechnical Institute) and Mats Rundgren (Lund University).

Subject: Bedrock Geology

Laura Catalina Agudelo Motta, Department of Geology, Lund University, Sölvegatan 12, SE-223 62 Lund, Sweden. E-mail: la6645ag-s@student.lu.se

Metoder för bedömning av bergras och uppskattning av utfallszoner: En fallstudie i Göteborg, SV Sverige

LAURA CATALINA AGUDELO MOTTA

Agudelo-Motta, Laura Catalina., 2020: Metoder för bedömning av bergras och uppskattning av utfallszoner: En fallstudie i Göteborg, SV Sverige. *Examensarbeten i geologi vid Lunds universitet*, Nr. 593, 58 sid. 45 hp.

Sammanfattning: Begras och blockutfall förekommer runt om i Sverige varje år och det saknas en nationell riskbedömning och tydligt regelverk relaterad till denna naturfara. Ett första steg för att ta itu med detta problem är att kartlägga områden där ras kan ske och eventuella faror kan uppstå, genom att beakta två grundläggande aspekter: i) identifiering av källområden och ii) uppskattning av utfallsområden. Denna studie har utförts för att testa metodik för detta i den nordöstra delen av Göteborgs kommun, särskilt med fokus på Fjällbo park, ett populärt klätterområde med omfattande talusbranter under klipporna. Detta är tydliga tecken på både historiska och recenta bergras, där det senaste inträffade 2017. Potentiella ras-/utfallskällor identifierades på en generell nivå med hjälp av en statistisk metod som kallas Slope Angle Distribution (SAD), vilken kombinerar information om geologin och topografin i ett område, där sluttningsvinklarna är erhållna från en digital höjdmodell (DEM). Utfallszoner simulerades med hjälp av två program: CONEFALL och RockfyFor3D, processbaserade mjukvaror som använder en DEM som en grundläggande del av analyserna. Utfallskällor för simulering i RockyFor3D lokaliserades manuellt. CONEFALL använder den så kallade energilinjemetoden för att uppskatta utfallszoner, medan RockyFor3D tar hänsyn till olika egenskaper hos blocken, sluttningarna, såväl som den skyddande effekten från skog och träd.

SAD-metoden indikerade att alla vinklar över 40° - 42° kan betraktas som potentiella utfallskällor i studieområdet. CONEFALL genererar relativt konservativa modeller och resultaten beror på topografin och höjden på klipporna. Dessutom överskattas den laterala utsträckningen av utfallszonerna av programvaran, men detta kan justeras genom att begränsa dess konvinkel. RockyFor3D genererar mer realistiska resultat och visar att blockformen har påverkar på den laterala utbredningen av utfallszoner och att blockmassan styr blockens energimängd. På samma sätt visar den att blockens studsbeteende mestadels styrs av sluttningens lutning och restitueringskoefficient, som beror på jord- eller bergartstyp, och av de hinder som blocken stöter på längs utfallsvägen (deras fördelning och deras storlekar). Slutligen indikerar dessa simuleringar att skog och träd har en skyddande effekt, då de kan helt stoppa, eller minska rörelseenergin för blocken. Dock beror skyddseffekten til stor del på skogens densitet. Det inträffade i Fjällbo 2017 är inkluderat för att försöka verifiera resultaten från genomförda simuleringar och därmed dess användbarhet och tillförlitlighet.

SAD-metodiken kan användas för preliminär identifiering av potentiella källor för bergutfall och ras. För uppskattning av utfallszoner i översiktliga bedömningar fungerar CONEFALL, meadn RockyFor3D kan utgöra grund för ytterligare och mer detaljerad riskbedömning. Samtliga dessa metoder är emellertid känsliga gällande områdets topografi, morfologi och geologi, och det är därför viktigt att utföra verifieringar av studieområden med hjälp av fältarbete och / eller högupplösta bilder för fjärranalys. Beroende på tillgänglig topografisk och geologisk information kan dessa metoder användas både på lokal och regional skala.

Nyckelord: Rasrisk, bergras, naturrisk, simulering, Göteborg, Fjällbo, utfallszoner.

Handledare: Johan Berglund (Statens geotekniska institut) och Mats Rundgren (Lunds universitet)

Ämnesinriktning: Berggrundsgeologi

Laura Catalina Agudelo Motta, Geologiska institutionen, Lunds Universitet, Sölvegatan 12, 223 62 Lund, Sverige.
E-post: la6645ag-s@student.lu.se

1 Introduction

Rockfalls are a type of mass movement that occur when a boulder becomes unstable and falls, bounces or rolls from a cliff or a steep slope; particularly in faulted or jointed outcrops, or slopes that are very exposed to erosion or subjected to human modifications (CGS 2020). Unlike similar types of mass movements (e.g. landslides), an important characteristic of rockfalls is that blocks or particles move freely and independently in relation to each other (Fig. 1; SGI 2018; SGI 2020).

In comparison to other geohazards, rockfalls usually impact small areas; nevertheless, depending on the location, the size of the falling blocks, and their velocity downslope, they might represent a serious threat for the surroundings (Volkwein et al. 2011; CGS 2020). For this reason, it is essential for public authorities to identify and delimit the spatial distribution of the areas where these natural hazards are prone to happen, and construct realistic risk zone maps to be used for mitigation of their negative effects without hindering urban expansion and economic activities (Monnet et al. 2010; Barnett 2016).

Rockfalls occur in Sweden every year. Although they typically do not lead to any fatalities or serious consequences, the country lacks a national risk evaluation and detailed documentation, as well as an adequate regulatory framework related to this natural hazard (SGI 2018; SGI 2019). Consequently, the extent of the problem is not well known today, which makes it difficult to highlight and give priority, in terms of protection, to zones under potential risk due to rockfalls (SGI 2018).

Numerous factors must be taken into consideration when establishing priorities to mitigate the damaging effects of natural hazards. Understanding rockfall mechanics is hence important to define a foundation for risk assessment related to this type of mass movements. Mapping of rockfall hazard should include two fundamental aspects: identification of source areas and estimation of runout zones (Toppe 1987).

The potential rockfall source areas can be outlined based on empirical approaches, i.e. fieldwork, interpretation from remote sensing imagery and evidence from previous rockfalls; or statistical approaches (e.g. the Slope Angle Distribution – SAD procedure, proposed by Loye et al. 2009). Likewise, runout zones can be delineated by using theoretical methods, like the energy line method (Onofri & Candian 1979; Toppe 1987; Evans & Hungr 1993; Jaboyedoff & Labiouse 2011); or by means of probabilistic process-based models that include diverse parameters, which are based on studies of the ground conditions in an area of interest (Dorren 2016).

Simulation of rockfalls in surface models offers a valuable and practical tool to calculate the reach or runout zone of falling blocks based on empirical and probabilistic methods. CONEFALL and RockyFor3D are modelling software developed by the Risk Analysis Group at the University of Lausanne and The International Association for Natural Hazard and Risk Management (ecorisQ), respectively. With these programs, it is possible to estimate runout zones from simple and rather conservative to more realistic approaches, and determine their vertical and horizontal extent for a specific source site (point or area), as well as evaluate forest protection, surface roughness effects, impact and bouncing properties.

1.1 Objective

In different areas around Sweden, there are steep rock slopes that can pose a potential danger to nearby infrastructure due to instabilities which can unpredictively lead to the collapse or fall of blocks (SGI 2019). The Swedish Geotechnical Institute (Statens Geotekniska Institut, SGI) and the Gothenburg Municipality (Göteborgs Stad) are currently working together on a municipal-level analysis of rockfall hazard using GIS tools, remote sensing imagery, and fieldwork observations and verifications to establish an optimal and systematic methodology that serves as a basis for rockfall risk assessment (SGI 2019).

Fjällbo park is located in SW Sweden, on the outskirts of Gothenburg urban sector. It is a popular climbing area where large talus slopes evidence both historic and recent rockfalls. Fjällbo is a very accessible and strategic site, and one of SGI's study areas, as well as the target of other studies. The most recent work was carried out by Hellman (2018), who performed an analysis of the rockfall susceptibility by acquiring and processing data from Unmanned Aerial Vehicles (UVAs) and studying the structural properties of the cliff.

This thesis follows up the studies by SGI and Hellman (2018) and presents an evaluation of the application of modelling software, in combination with field observations, for the Fjällbo area. The main objective of this work is to serve as a pilot study in

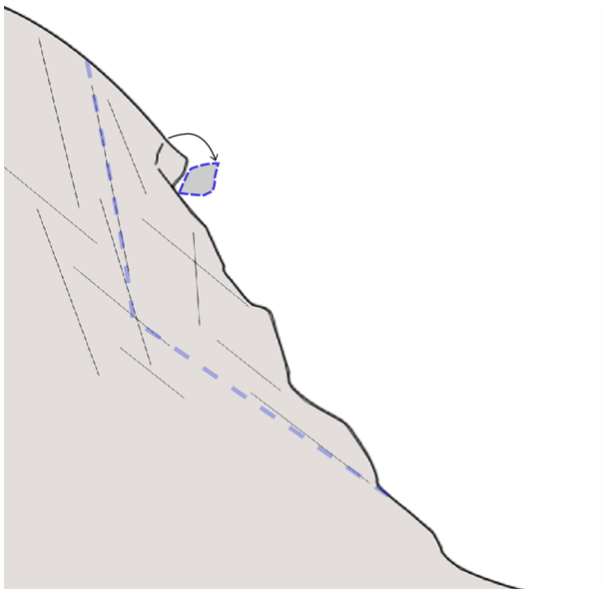

Fig. 1. Illustration of a rockfall showing a block detaching from the cliff or rock wall. This movement occurs individually for each of the blocks or particles involved. To highlight the relevance of this definition, the dashed line shows a situation where a large portion of a rock slope detaches and slides downhill. This movement is called rockslide. Illustration made by Johan Berglund (SGI).

Sweden since the methods to be used to detect potential rockfall sources and delimit runout zones were designed considering alpine conditions and tested in alpine settings. To see their applications in a Swedish environment, only natural slopes are taken into account. This study not only considers slope angle values but other aspects of the slope, like type of soil/ rock, block shape, block dimensions, topographic relief, tree protection, coefficient of restitution and surface roughness in order to examine and visualize the influence and importance of separate rockfall parameters in the extent of outfall distances. It is important to highlight, however, that calculation of the probability of rockfall occurrence is not part of this thesis.

Although this study focuses on Fjällbo, it also includes analyzes for its surroundings to test the applicability of these methods on a larger scale and determine whether they are useful and may contribute to the development of a comprehensive regional and national rockfall risk assessment.

2 Conceptual framework

2.1 Rockfalls

Mass movement phenomena cover a wide variety of processes that result in the fall and propagation of different materials found in slopes, including rocks, soil, artificial fillings, and the combination of these (Varnes 1978; Highland 2004).

Rockfalls are relatively small, but abrupt movements of individual and superficial boulders located at a cliff (CGS 2020); the mechanism is rather simple: rock blocks become detached from steep slopes or cliffs by the effects of weathering, erosion, presence of interstitial water, and the natural action of gravity (Dorren 2003; Highland 2004; Fanos & Pradhan 2018). Rockfalls are common where the cliffs are fractured, faulted, or jointed; or where steep outcrops are undercut either by natural processes or human activities (Highland 2004; CGS 2020).

Once the material has lost support and starts to move, and depending on the mean slope gradient, it continues downslope through one or several of the following modes of motion: freefall, rolling, bouncing or sliding (Fig. 2; Varnes 1978; Dorren 2003). In areas where these events continuously happen, it is common to find accumulations of rock that create talus or scree slopes (Evans & Hungr 1993).

As shown in Figure 2, freefall of rocks occurs at very steep slope angles, i.e. if the mean slope gradient is larger than 70°; although this may vary depending on the geological conditions of the area (Ritchie 1963; Dorren 2003). During the freefall, there is a temporary loss of ground contact and an increase in acceleration through the descent (Richards 1988; Peng 2000). As the slope gradient decreases in the downslope segment, the rock eventually hits the surface, and the transition from freefalling to bouncing takes place (Dorren 2003); the block bouncing behavior is determined by the physical characteristics of the slope (Ritchie 1963; Peng 2000). If the slope gradient is less than 45°, the bouncing block gains rotational momentum and the motion mode progressively converts into rolling (Dorren 2003).

During the initial and final phases of a rockfall, sliding over the slope surface generally occurs. In these stages either the sliding rock gains energy and starts falling, bouncing or rolling due to an increase in the slope gradient, or loses its energy by cause of friction when the block is finally reaching a stopping point (Dorren 2003).

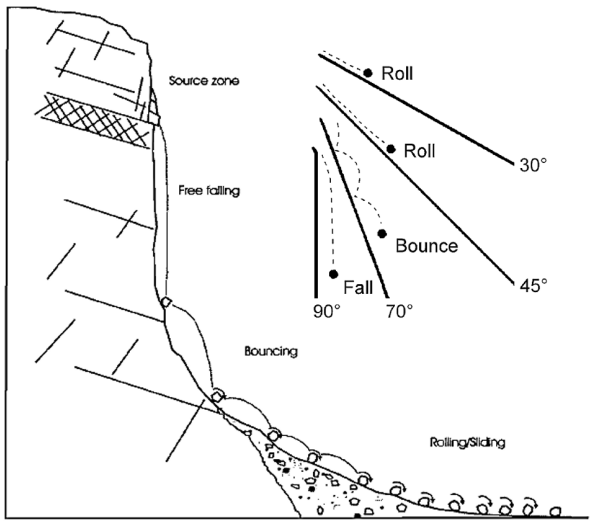

Fig.2. Schematic diagram showing the typical rockfall modes of motion. From Peng (2000).

2.2 Slope stability

The environmental factors known to influence the occurrence of rockfalls have been called "determinant" or "preparatory" factors and they account for the overall slope stability condition (Dai et al. 2002; Jiménez-Perálvarez et al. 2009; Barnett 2016).These variables determine the probability of a mass movement to happen in a particular area since they create the conditions for the blocks to be susceptible to detachment from the rock face without actually initiating it (Dai et al. 2002; Barnett 2016).

The above-mentioned variables include, but are not restricted to, geology (lithology and structural features), slope angle and aspect, topography, soil properties, vegetation cover and weathering (Dai et al. 2002; SGI 2018). A selection of the most significant determinant factors is therefore the first step when performing rockfall hazard evaluation (Jiménez-Perálvarez et al. 2009).

The composition of the rocks and their mechanical properties determine how brittle and ductile structures develop in a particular region. The nature of geological contacts, foliation in the rocks, and presence of fractures, as well as their intensity and characteristics, have a very high influence on slope stability, as these discontinuities control the strength of the geological units (SGI 2018; SGI 2019).

Elevation and geomorphological evolution of an area determine the slope gradient (Fanos & Pradhan 2018). Gravity-driven geohazards are closely associated with the steepness of the topography and the relief morphology (Montgomery & Brandon 2002); and hence one of the main, and probably the most relevant

and necessary factors for rockfall initiation is a steep slope angle (Jiménez-Perálvarez et al. 2009; Loye et al. 2009). Downslope direction (aspect) is also determined by the topography and relief characteristics. It specifies the direction of maximum change rate and consequently, defines the fall path (Fanos & Pradhan 2018).

The effects of weathering and erosion vary widely depending on the local characteristics of the slope; nevertheless, the time factor is very relevant, since the longer these processes act, the greater is the probability that the strength of individual structures approaches a critical limit (SGI 2018). The likelihood of a mass movement to occur also depends on the triggering mechanisms (e.g. freeze-thaw activity, anthropogenic activity), however, these mechanisms may change over short periods, and thus are very challenging to estimate (Dai et al. 2002; Jiménez-Perálvarez et al. 2009).

It is also important to pinpoint the difference between constructed and natural slopes: natural slopes are the ones that have not been subject to changes as a result of human activity, while constructed slopes are the ones that have been manufactured or excavated (SGI 2019). The latter are not part of the scope of this study. In Sweden, a high frequency of rockfalls is associated with the last deglaciation period (~10.000 years ago) and has decreased since. As a consequence, an overall stable condition is now seen in the natural slopes (SGI 2018, SGI 2019). Nevertheless, there is a substantial number of rockfalls occurring in Sweden every year, although serious accidents are exceptional. However, due to the generally high strength of the rocks, which provides a good foundation for construction, in some parts of Sweden, it is common to build residential or recreational infrastructure near steep slopes without a thorough evaluation of the conditions and probabilities of the blocks to move downslope (SGI 2018, SGI 2019).

2.3 Source areas and runout zones

A rockfall trajectory starts from the release zone or source area where a block (or group of blocks) loses support and starts to move downslope while gaining acceleration (Fig. 3; Richards 1988; Peng 2000) and ends where the block slows down and finally stops at the runout or deposit zone (Fig 3; Fanos & Pradhan 2018). The block descends through the transition zone and the combination and shift among modes of motion (See section 2.1) from the release area to runout zone draws the path of a rockfall trajectory (Ritchie 1963; Fanos & Pradhan 2018) and thereby delineates the propagation area, i.e. the area potentially under the threat of rockfall (Jaboyedoff & Labiouse 2011). Figure 3 shows a typical rockfall trajectory.

Ideally, the detached rock starts its movement by freefalling, then bounces, rolls, and finally stops (Peng 2000); sliding can occur at different points (Dorren 2003). However, the characteristics of rock trajectories may differ depending on the dimensions and the shape of the boulder, slope angle, physical characteristics of the slope surface, height of the cliff, rock and soil type, velocity and time (Ritchie 1963).

Identifying the potential sources or releasing points of rockfalls is one of the most essential yet challenging steps when modelling rockfall trajectories (Loye et al. 2009; Fanos & Pradhan 2018). The selection and spatial representation of specific blocks or areas allows us to define the primary conditions of the rockfall paths, which will determine the hypothetical but most likely propagation track and thereby influence the results of the runout modelling (Fanos & Pradhan 2018).

From a simple perspective, unstable rock slopes can be defined with respect to the steepness of the topography by specifying a slope angle threshold, which can be identified from distinguishing evidence, i.e. cliffs lying above talus slopes, field evidence or records from historical events (Toppe 1987; Dorren & Seijmonsbergen 2003; Jaboyedoff & Labiouse 2003; Michoud et al. 2012). According to field observations and tests, slopes with starting angles between 30° and 35° can be considered as potential starting zones; this lower limit is proposed as it guarantees enough inclination for the blocks to start moving downslope (Toppe 1987; Jaboyedoff & Labiouse 2011). Nevertheless, the influence and significance of the additional parameters related to rock slope stability as well as the boulder internal factors that affect material stability over the surface cannot be neglected (Michoud et al. 2012).

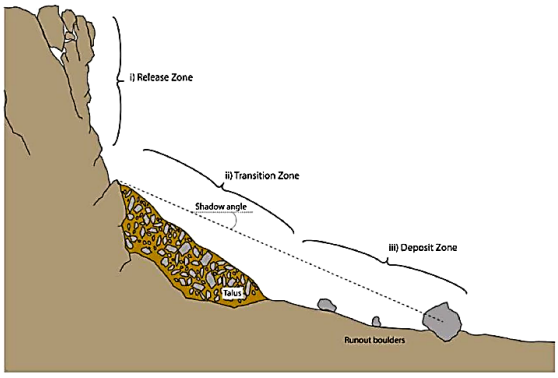

Fig. 3. Schematic rockfall trajectory: source, transition and deposit zone. From Fanos & Pradhan (2018).

2.3.1 Detection of potential source areas – a statistical approach

Geomorphometric analysis using Digital Elevation Models (DEMs) in combination with the geological data of an area can be used to detect potential rockfall source area with the Slope Angle Distribution procedure (SAD; Loye et al. 2009; Michoud et al. 2012). This method was proposed by Roullier (1998) and improved by Loye et al. (2009). It operates under the principle that different relief and rock types generate a restricted range of slope angle values that are distinctive for a specific morphotectonic setting (Strahler 1950; Loye et al. 2009), and hence the topography can be used as a proxy to detect potential source locations (Michoud et al. 2012).

To carry out such analysis, it is required to classify the study area into homogeneous morphometric areas (HMA). These are areas with

similar geological and tectonic history and morphology (Loye et al. 2009). Given that the type of relief of a terrain displays distinctive slope angles that can be directly related to geomorphic processes, different morphological units (MU) might be encountered within each HMA (Loye et al. 2009; Michoud et al. 2012). This methodology has been developed for regional studies and tested in alpine environments, and the MU proposed by Loye et al. (2009) are presented below; however, these may differ from region to region:

- Plains (low slope angles) associated with fluvio-glacial deposits.
- Footslopes or hillslopes (moderate slope angles) related to alluvial fans, debris flow and landslide deposits.
- Steep slopes formed by talus slopes and valley flanks. These are associated with till deposits, screes and rocky outcrops covered with vegetation and/or soil.
- Cliffs (very steep slope angles).

Slope angle values of the HMA are extracted from the DEM using GIS tools, and the Slope Angle Frequency Distribution (SAFD) is calculated and then decomposed into several Gaussian distributions f, each one corresponding to a morphological unit (GDMU) by means of Equation 1 (Michoud et al. 2012):

$$f(s) = w * \frac{1}{\sigma\sqrt{2\pi}} * exp\left[-\frac{1}{2} * \left(\frac{s - m_c}{\sigma}\right)^2\right]$$

where s is the slope angle value, w is a weighting factor related to the proportions among MU inside the study area, m_c and σ are the mean and standard deviation of the slope angle value, respectively. As a final step, the GDMUs are summed up, and compared to the SAFD curve, if the sum of GDMUs fits well with the SAFD, the topography of the study area is well represented and the method is valid for extraction of potential rockfall sources (Fig. 4, 5; Loye et al. 2009).

Rockfall source areas are most likely found in the steepest MU (Michoud et al. 2012); consequently, the slope angle value above which the cliffs lie must be extracted from the SAFD. This limit is defined as the slope angle value where the normal distribution of the cliffs MU becomes dominant over that of the steep slopes MU, i.e. the intersection between the GDMUs (A in Fig. 4, 5; Loye et al. 2009; Michoud et al. 2012). As a result, the areas with slope angle values above this threshold are considered as potential rockfall sources (Fig. 6; Michoud et al. 2012). However, the cliffs MU can have very low slope angle values (even 0°) where rockfalls are very unlikely to initiate, hence, only slope angle values above the mode of the steep slopes MU (B in Fig. 4, 5) are considered for the SAFD computation of the cliffs MU (Michoud et al. 2012).

Loye et al. (2009) proposed a modification of the methodology for areas with large flat terrains. The SAFD is decomposed into three instead of four GDMUs, as follows:

- Plains corresponding to the large flat terrain or areas of low steepness.
- Hillslopes corresponding to the sides of the small hills.
- Steep slopes and cliffs are grouped into areas of rugged topography.

With this modification, A is defined by the intersect between the hillslopes MU and the steep slopes and cliffs MU, and B is the mode of the hillslopes MU (Fig. 5).

2.3.2 Empirical methods to estimate runout zones

The *Fahrböschung* principle was proposed by Heim (1932) and has later been applied to hazard analysis by other authors (Onofri & Candian 1979; Toppe 1987; Jaboyedoff & Labiouse 2011) in order to predict runout zones of potential rockfall events. The *Fahrböschung* is the angle between the horizontal plane and the "energy line" that connects the top of a rockfall source scar and the longest runout boulder for a given rockfall (Fig. 7; Dorren 2003; Volkwein et al. 2011).

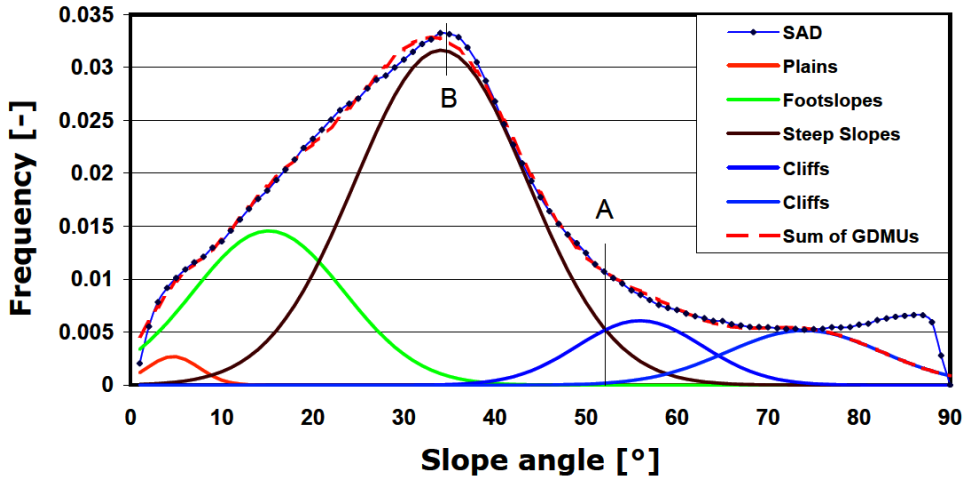

Fig. 4. Example of the Slope angle distribution (SAD) analysis in an Alpine terrain. A indicates the limit where cliff slopes become dominant over the steep slopes MU and defines the potential rockfall source areas. In this particular example, the cliffs MU is divided into two units, due to the very steep topography of the area. B indicates the mode of the steep slopes. From Loye et al. (2009).

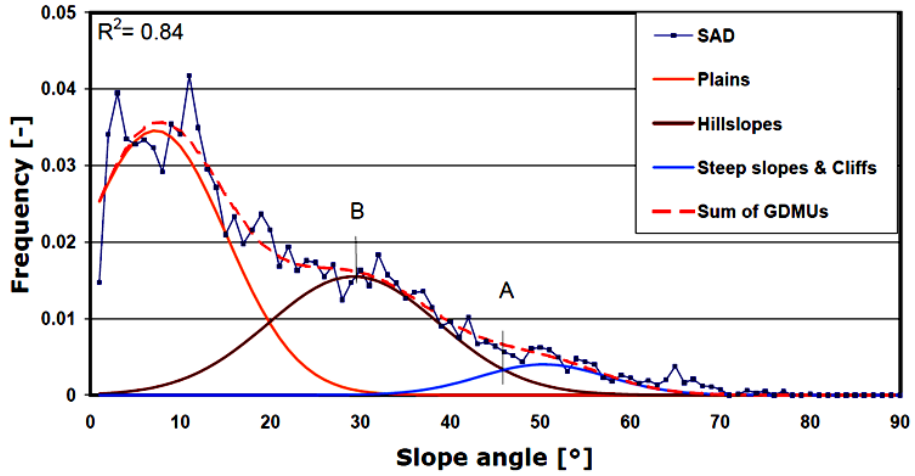

Fig. 5. Slope angle distribution (SAD) modification for areas with large flat terrains. A indicates the limit where the steep slopes and cliffs MU becomes dominant over the hillslopes MU and defines the lowest threshold for potential rockfall source areas. B indicates the mode of the steep slopes. R^2 corresponds to the coefficient of determination of the sum of GDMUs. If this value is close to 1, the curve represents a good fit of the SAFD. From Loye et al. (2009).

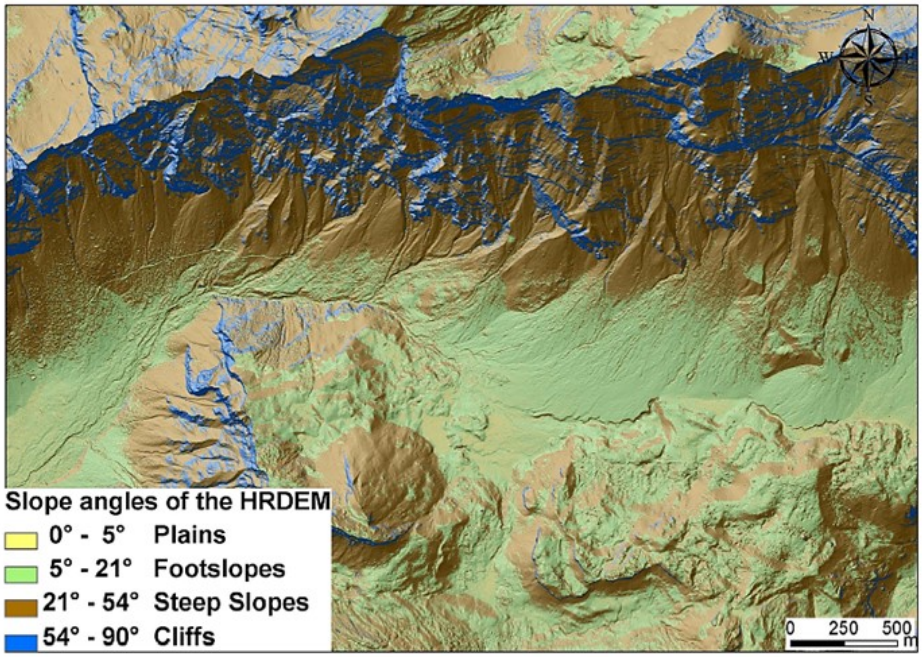

Fig. 6. Graphical distribution of the slope angles corresponding to each MU after performing the SAD analysis in the Alpine terrain. From Loye et al. (2009).

Evans and Hungr (1993) developed a similar approach called the shadow angle. The principle is fundamentally the same as in the *Fahrböschung* angle, but in this case, the energy line goes from the highest point of the talus or scree slope to the deposit zone for a given rockfall (Fig. 7; Dorren 2003).

The empirical values for both the *Fahrböschung* and the shadow angle ($ø_p$) can vary with respect to assumptions and field conditions (Jaboyedoff and Labiouse 2011). The estimated angles for the energy line method range between 22° and 37° (Fig. 8; Dorren 2003; Jaboyedoff & Labiouse 2011). Onofri & Candian (1979) reported that 50% of blocks are stopped for $ø_p > 33.5°$, 72% for $ø_p > 32°$, and 100% for $ø_p > 28.5°$. Domaas (1985) observed that 50% of the rockfall fragments stop for $ø_p = 45°$ and 95% for $ø_p > 32°$ (Toppe 1987), and Gerber (1994) recognized three limits deriving in 100% of blocks

being halted: 33°, 35° and 37°, depending on the geological settings (Jaboyedoff 2011). Lied (1977) stated that all the blocks are stopped at an angle $ø_p$ between 28°-30°, and Evans and Hungr (1993) proposed an empirical shadow angle of 27.5° based on several field studies. Modelling rockfall scenarios with this low angle limit provides the most conservative approach, i.e. the worst-case scenario for hazard analysis (Pfeiffer & Higgins 1990; Nilsen 2008).

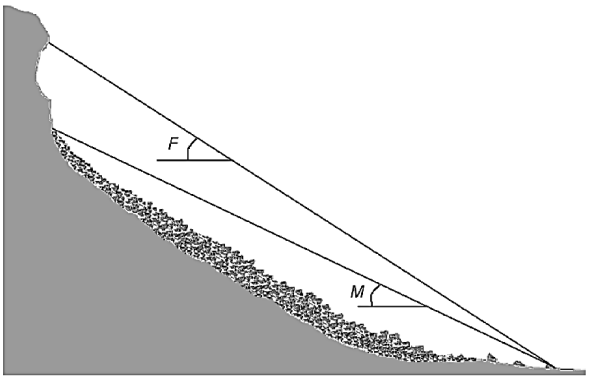

Fig. 7. Representation of the Fahrböschung (F) and the minimum shadow angle (M) energy line methods. From Dorren (2003).

2.4 Rockfall parameters

The falling behavior of a block is controlled by the rock properties, as well as the surface characteristics of the slope. The latter are, in turn, defined mainly by two parameters: the coefficient of restitution and surface roughness (Peng 2000; Fanos & Pradhan 2018).

The coefficient of restitution is a dimensionless value that expresses the amount of energy dissipated after collision with a surface (Nilsen 2008; Wang et al. 2018). In the context of rockfall studies, it is used to explain the bouncing phenomena (Thorbjörnson Lind 2016). This parameter has a normal (Rn) and a tangential (Rt) component, which measure the energy loss perpendicular to the slope and the resistance to move parallel to the slope, respectively (Peng 2000; Fanos & Pradhan 2018). The coefficient of restitution can show values between 0 and 1, where CR = 1 corresponds to a perfect elastic collision, i.e. the impact and rebound velocities are the same, and CR = 0 is a perfect inelastic collision where the block, depending on the slope gradient, either starts to roll or stops completely (Azzoni et al. 1995; Thorbjörnson Lind 2016). For rockfall analyses, the coefficient of restitution is assumed to be only a function of the slope material (Heidenreich 2004; Nilsen 2008).

On the other hand, the surface roughness describes the slope surface irregularities or obstacles, i.e. the slope angle variation from the average slope angle that accounts for most of the fall direction changes recorded and energy loss during a rebound on the surface among rockfalls, as these obstacles might alter the angle at which a block hits the slope (Peng 2000; Dorren 2016; Fanos & Pradhan 2018).

2.5 Block shape and mass

Hu et al. (2018) performed several laboratory tests in order to analyze the effect that block shape and mass have on runout distance and lateral dispersion of rockfall trajectories. The experiments show longer runout distances and shorter lateral dispersion for spherical blocks in comparison with cubical and wedgy blocks (Fig. 9A). The authors concluded that cubical and wedgy blocks have larger frictional

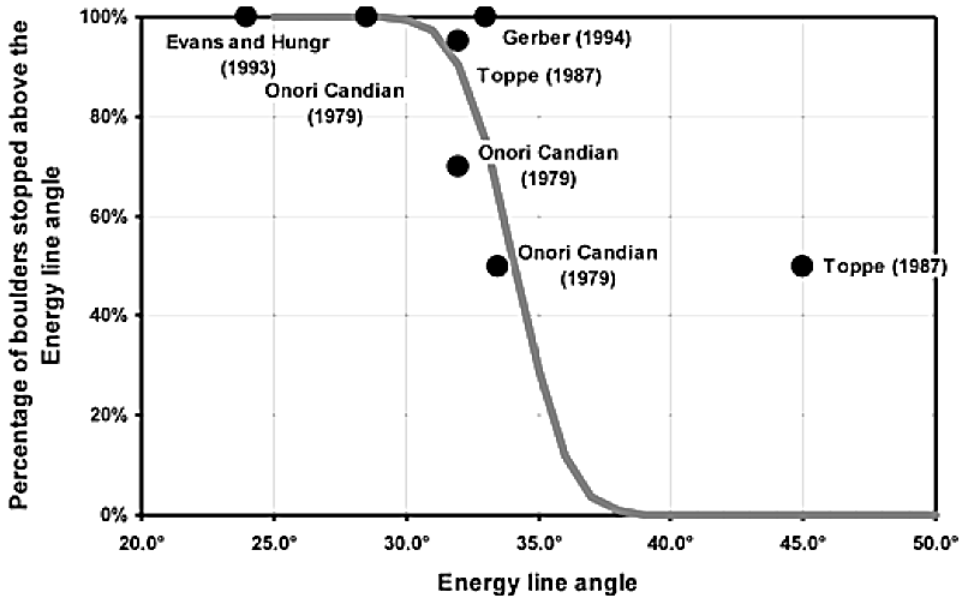

Fig. 8. Relationships between energy line angles and proportion of blocks stopped. From Jaboyedoff & Labiouse (2011).

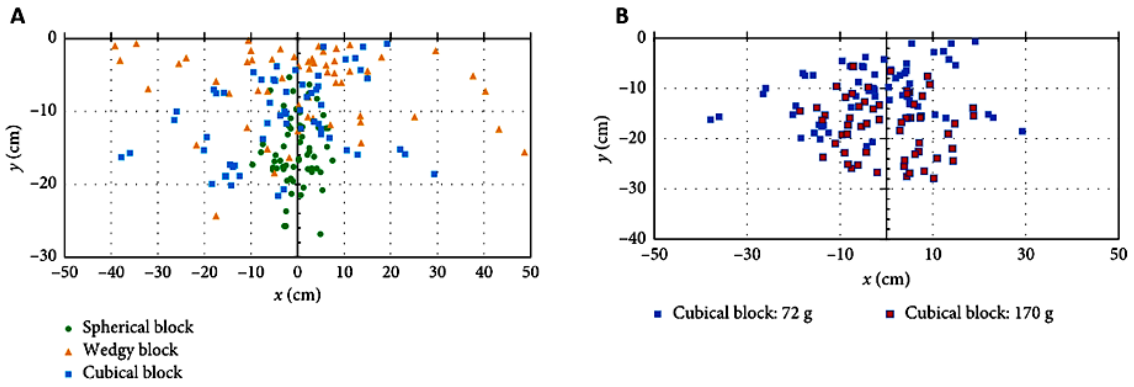

Fig. 9. A) Runout distances and lateral dispersion for three different block shapes (x axis) vs. Vertical distance (y axis). B) Runout distances and lateral dispersion for two blocks with different mass vs. Vertical distance (y axis). Results according to laboratory tests performed by Hu et al. (2018). Figure modified after Hu et al. (2018).

resistance, which results in a shorter runout distance. When it comes to rebound, these types of blocks have more ways to impact the surface, (e.g. with a side, an edge, or a corner) which generates more variation in lateral dispersion, in contrast with spherical blocks that impact with the same configuration in every rebound.

Similarly, the mass effect was tested, and the heavier blocks showed greater runout distances, while the lateral extent range tends to decrease as mass increases (Fig. 9B; Hu et al. 2018); however, the depth of penetration is not mentioned in this analysis. This variable is highly relevant to rockfall trajectories, as during penetration the block's impact energy is absorbed, which means that the block decelerates as penetration progresses and the maximum depth of penetration is reached when the impact energy is fully dissipated (Fig.10; Wang & Cavers 2008). Depth of penetration is dependent on mass, impact velocity and physical characteristics of the block Pichler et al. 2005).

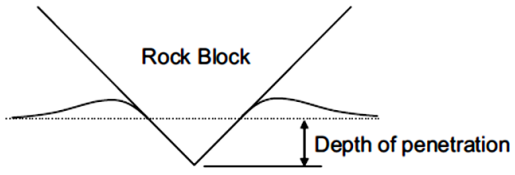

Fig. 10. Depth of penetration after block impact on ground. From Wang & Cavers (2008).

2.6 Tree protection

Protection structures are vital to mitigate rockfall threats. Their purpose is to halt or deflect falling blocks from their original path, and to resist their impact energy (Fanos & Pradhan 2018). These include technical and natural protective measures as nets, dams, galleries, and forests (Dorren et al. 2011).

Forests comprise a natural barrier or shield against mass movements representing a risk for adjacent urban areas or infrastructure like railroads or highways (Dorren et al. 2006). Forested slopes not only provide protection against rockfalls, but also against soil erosion and consequently contribute to the general slope stability (Dorren & Seijmonsbergen 2003; Fanos & Pradhan 2018).

These protective effects are often neglected and as a consequence, the rockfall hazard may be overestimated resulting in expensive and unnecessary protective actions taken by the authorities (Dorren et al. 2006). In fact, the first paragraph of the Mountain Forest Protocol of the Alpine Convention states: "Mountain forests provide the most effective, the least expensive and the most aesthetic protection against natural hazards." (Dorren et al. 2006). Protective effects, however, depend on different aspects of the slope and the forest itself (e.g. stem diameter, density, and tree species), and recent modifications to rockfall models allow incorporation of these characteristics to calculate the protection efficacy provided by forests (Dorren et al. 2006; Dorren 2016).

2.7 Modelling software

There are different software available for rockfall simulation (e.g. Flow-R, NMM, RAMMS::Rockfall, RocFall, Rockfall Analyst, CADMA), which are based on empirical, process-based or GIS-based methods (Vo 2015). For this study, two modelling programs were used: CONEFALL and RockyFor3D. CONEFALL was chosen because it is an easily accessible, user-friendly, and free software that requires just a few files as input data and generates 2D rockfall models. On the other hand, RockyFor3D was selected because it is a program that involves several parameters (to be presented below), and therefore, it is possible to test the influence of each of them on the runout zones estimations.

The two programs are briefly described in this section:

2.7.1 CONEFALL

Jaboyedoff & Labiouse (2003) developed a rockfall modelling software with the objective of getting a fast and preliminarily estimation of rockfall propagation areas and runout distance of any block of rock. Their model is based on the energy line principle explained in section 2.3.2.

The program predicts the runout zones from two grid files taken as input data: one that contains the elevation information of the study area (DEM) and another grid file with the boolean values -1 and 1 for areas that do not represent any risk and for potential source points, respectively. The method proposed by Jaboyedoff & Labiouse (2003) and further described by Jaboyedoff & Labiouse (2011) consists of allocating the cells of the DEM that are lowest in altitude within a cone that has its appex on the corresponding source cell in the grid file (Fig. 11) to measure the respective propagation area. The program allows the user to choose the evaluation method: the cone center in the middle of the cell (representing the top of the cliff for the *Fahrböschung* method) or on the borders of the cell (representing the bottom of the cliff for the shadow angle).

CONEFALL calculates the rockfall propagation area by checking whether a DEM cell is located below the energy line or not, and this is checked with the following mathematical expression (Equation 2):

$$0 < \Delta x^2 + \Delta y^2 - \left(tg\left(\frac{\pi}{2} - \emptyset_p\right)\right)^2 * (Z_0 - Z)^2$$

where Δx and Δy are the horizontal distances between the source point and each of the tested points, Z_0 is the elevation of the source point and Z the elevation of the evaluated point (Jaboyedoff & Labiouse 2003).

In CONEFALL, the main parameter controlling the propagation is the cone angle which has a fixed value provided by the user (Jaboyedoff 2003). CONEFALL accepts values between 0° and 90°; however, the recommended values range between 27° and 37° since this method is based on the empirical values calculated for the energy line method (Section 2.3.2; Fig. 11; Jaboyedoff 2003). In addition, the lateral dispersion of the blocks is defined by the intersection of the cone with the topography, which might lead to an overestimation of the lateral extent of the cone, so the program offers the option to restrict the aperture of the angle according to the local conditions of the study area (Jaboyedoff 2003; Jaboyedoff & Labiouse 2003).

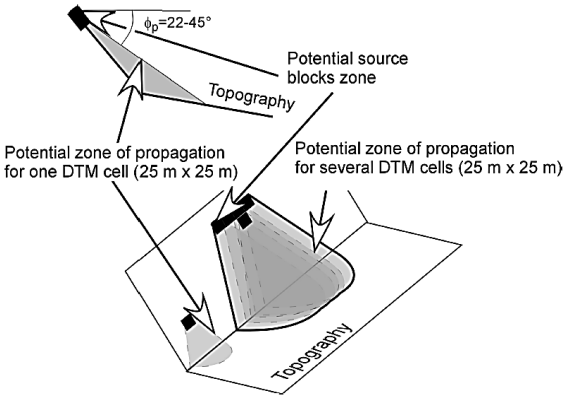

Fig. 11. Illustration of the cone method. The black cells are the source areas. From Jaboyedoff & Labiouse (2011).

2.7.2 RockyFor3D

Rockyfor3D is a software that calculates trajectories of falling rocks in 3D at a local and regional level (Monnet et al. 2010). It is defined as a "probabilistic process-based rockfall trajectory model since it combines deterministic algorithms with stochastic or random approaches" (Dorren 2003; Dorren 2016).

The model simulates the rockfall trajectory by assuming parabolic free falls for each of the blocks involved, the subsequent rebounds on the slope surface, and the change of direction and protection provided by forests (Monnet et al. 2010).

Since trajectories are predominantly governed by topography, it must be realistically represented by the input data (Dorren et al. 2006). Dorren (2016) presents the requirements and operation of Rockyfor3D, and these are briefly summarized below:

The input data consists of a minimum of ten ASCII raster files, including elevation, slope surface, forest and block characteristics.

Soil type	General description of the substrate	Mean Rn value	Rn value range
0	River, or swamp, or material in which a rock could penetrate completely	0	0
1	Fine soil material (depth > ~100 cm)	0.23	0.21-0.25
2	Fine soil material (depth < ~100 cm), or sand/gravel mix in the valley	0.28	0.25-0.31
3	Scree (Ø < ~10 cm), or medium compact soil with small rock fragments, or forest road	0.33	0.30-036
4	Talus slope (Ø > ~10 cm), or compact soil with large rock fragments	0.38	0.34-0.42
5	Bedrock with thin weathered material or soil cover	0.43	0.39-0.47
6	Bedrock	0.53	0.48-0.58
7	Asphalt road	0.35	0.32-0.39

Table 1. Soil types classification used by Rockyfor3D and their associated Rn values. From Dorren (2016).

Deviation angle (°)	0-5	5-10	10-15	15-20	20-25	25-30	30-35	35-40	40-45	45-50	50-55
V < 10 m/s	49	15	9	6	5	4	3	3	3	2	2
10 < V < 15 m/s	53	14	8	6	4	4	3	3	2	2	2
V > 15 m/s	46	16	10	7	5	4	4	3	3	2	0

Table 2. Percentage of probabilities (%) for different deviation angles after rebound. V = velocity of the block before the rebound. From Dorren (2016).

Impact type	Probabilities (%)		
	0°-22.5° deviation	22.5°-67.5° deviation	67.5°-76° deviation
Frontal	44	50	6
Lateral	11	84	5
Scratch	72	24	4

Table 3. Percentage of probabilities for deviation angle after tree impact. From Dorren (2016).

- Digital Elevation Model: A file that contains information about the topography of the area. From this file, the program extracts the slope values and aspect map.
- Rock density: A raster map with the rock density in each cell. The values should span 2000 – 3300 (kg/m^3) for the source cells and must be zero (0) for the rest.
- Block dimensions (d1, d2, d3): A set of three raster files that contains the size in meters of the falling blocks d1= height, d2= width and d3= length.
- Block shape: A raster file that includes the form of the falling block for each source cell. The cells in this raster must have one of the following values:
  - ◊ 0 No block
  - ◊ 1 Rectangular block
  - ◊ 2 Ellipsoidal block
  - ◊ 3 Spherical block
  - ◊ 4 Disc-shaped block

  The block shape is used to determine the block's volume and mass, and the moment of inertia (I). These calculations are dependent on the block shape but also on the block dimensions (d1, d2 and d3).

- Surface roughness: Three raster maps defining the mean obstacle height (MOH), i.e., rocks that are lying on the slope and form obstacles for the falling block. Each of these raster files corresponds to 70%, 20% and 10% (Rg70, Rg20, Rg10) of the mean diameters of block sizes covering the slope according to these percentages (Fig. 12).

  Roughness values range from 0 to 100 m, and they are used to calculate the tangential coefficient of restitution (Rt), and thus estimate energy loss during bouncing.

  During the simulation, the size of the obstacle encountered by the falling block is randomly chosen from the three files based on their probabilities, i.e. material within the 70% file is most likely to affect the simulated falling block than material in the 10% file.

- ◊ Soil type: A raster map that describes the type of substrate. The soil type is directly linked to the normal coefficient of restitution (Rn; see Table 1).

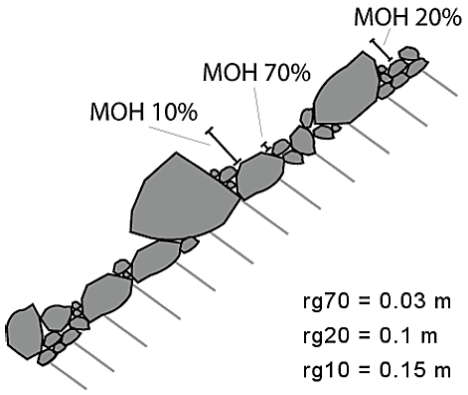

Fig. 12. Illustration of the mean obstacle height (MOH) corresponding to 70%, 20% and 10% of the surface in a particular slope. If the slope surface is smooth, the roughness value is 0. From Dorren (2016).

The method assumes an initial parabolic free fall with fixed velocity values i.e. initial horizontal velocity Vhor = 0.5 m/s and vertical velocity Vvert = -0.5 m/s. After the first impact, these velocities are converted to normal (V_n) and tangential velocity (V_t), and the depth of penetration (Dp) is calculated as a function of Rn, Rt, the dimensions and mass of the block and the impact velocity of the falling block for each rebound (bouncing) until the maximum Dp is reached. Rolling is assumed for slopes with a gradient between 0° and 30° and is represented by a sequence of short-distance rebounds. Sliding is not modelled by this software.

Direction change when bouncing on the slope surface is determined by the topography, the falling direction of the block (aspect) and the velocity of the block (Dorren et al. 2006; Dorren 2016). During each rebound, the block deviates from its original direction towards the falling direction of the raster cell in which the block bounces. How much the block is deviated is defined by a random number and its probability of occurrence depends on the velocity of the block according to statistical analysis performed by Dorren et al. (2006) (Fig. 13; Table 2). In the same way, changes in fall direction can occur after impact with trees. The probabilities of deviation are calculated on the basis of impact types (Fig. 14) combined with a uniformly distributed random number (Table 3).

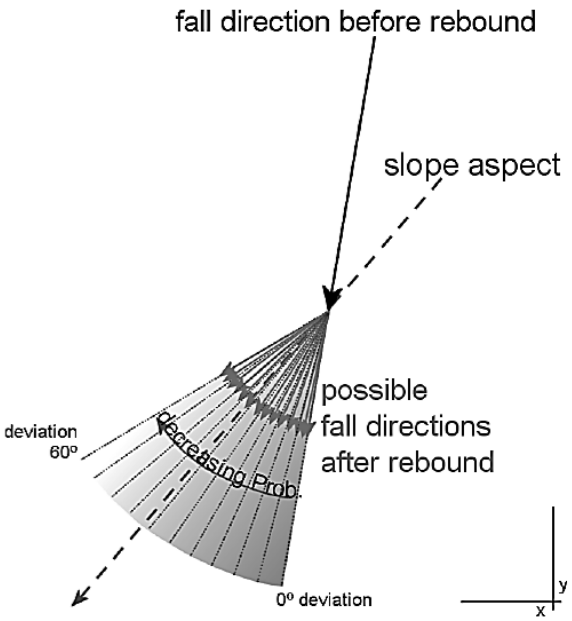

Fig. 13. Illustration of an example of possible changes in fall direction after a rebound. From Dorren (2016).

3 Study area and regional geology

Fjällbo park is located in SW Sweden, in the outskirts of Gothenburg urban region (Fig. 15). It is a

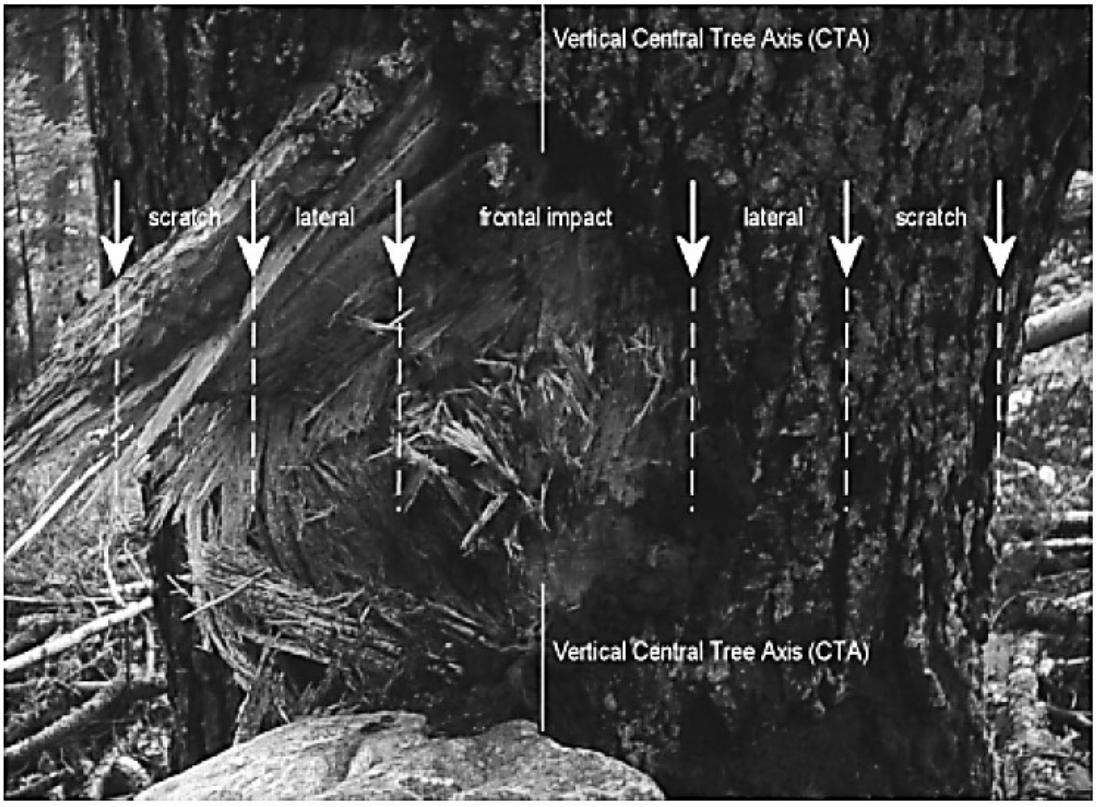

Fig. 14. Impact tree types. They are defined by the horizontal distance between the impact and the position of the central tree axis (CTA). From Dorren (2016).

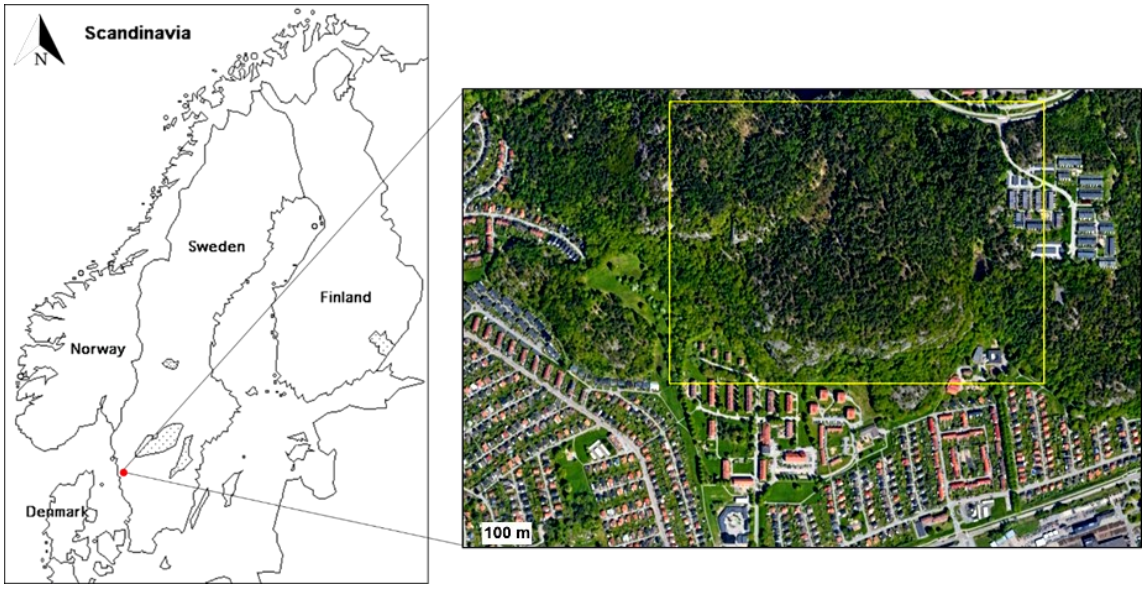

Fig. 15. Location of the study area. Fjällbo climbing park is framed in the yellow rectangle. Satellite image taken from Google Earth.

popular climbing area where cliffs can reach more than 90 meters in height. The rock walls display numerous discontinuities (joints and fractures), which represent weak points and, therefore, potential rockfall sources. A large rockfall was documented in 2017 after a pillar of approximately 150 Ton detached from the rock wall (See section 4.2). This rockfall destroyed a renowned climbing route and impacted near a hiking trail transited by locals and visitors every day (Hellman 2018); moreover, a growing residential area is situated approximately 40 to 50 m from the base of the cliffs. Fjällbo is a very accessible site that has evidence of historic and recent rockfalls, and thus provides the possibility for validation of the accuracy and applicability of rockfall simulations.

3.1 Bedrock geology

The Idefjorden terrane is located in the region west of the Trans-Scandinavian Igneous Belt (TIB; Fig. 16). It is part of the Sveconorwegian orogen and extends from south of Gothenburg to the southeastern part of Norway (Fig 17; Stephens et al. 2020). Towards the east, the Idefjorden terrane is delimited by the Mylonite Zone (MZ), one of the major shear zones in western Sweden (Andersson et al. 2002), which separates it from the Eastern segment of the Sveconorwegian orogen (Starmer 1996). The Idefjorden terrane is, in turn, divided into Median and Western segments, which are separated by the Dalsland Boundary Thrust (DB) in the north and the Göta Älv Shear Zone (GÄ) towards the south (Fig. 16, 17; Park et al. 1991; Starmer 1996).

Intrusive and sedimentary sequences that compose the Idefjorden terrane were formed and assembled mainly during the Gothian Orogeny (1.66-1.52 Ga; Åhäll & Connelly 2008; Bingen et al. 2008) and were severely affected by the Sveconorwegian Orogeny (1.05-1.03 Ga; Starmer 1996; Söderlund et al. 2008). At least two episodes of Sveconorwegian ductile deformation are suggested in the area (≥1.03 Ga and at 0.92 Ga, Scherstén et al. 2004), and no evidence of Gothian metamorphism has been found (Bergström et al. 2020).

Fjällbo and its surroundings are located in the Median Segment of the Idefjorden terrane. The main geological units in the area are the Åmål group, Göteborg intrusive suite, and the Hisingen suite (Fig. 18; Bergström et al. 2020).

The Göteborg suite comprises mostly intrusive
units emplaced at 1.63 – 1.59 Ga (Bergström et al. 2020). Geochemical data show compositions ranging from granite to quartz diorite and gabbro, passing through granioditiorte and tonalite fields (Bergström et al. 2020). Metamorphism in this suite corresponds to amphibolite facies with local migmatization (Åhäll & Connelly 2008). A specific component of the Göteborg suite is an augen-bearing orthogneiss with bands of variable width, interpreted as an originally coarsely porphyritic plutonic rock (Bergström et al. 2020).

Coevally, the supracrustal rocks of the Åmål group were deposited. This group includes volcanic rocks erupted at 1.63–1.61 Ga intercalated with sedimentary sequences. The rocks within this group are well preserved as metamorphism occurred under greenschist to lower amphibolite facies (Bergström et al. 2020).

The Hisingen Suite consists principally of granitoid intrusions that occurred around 1.58-1.52 Ga, although mafic to felsic bodies are also found (Åhäll & Connelly 2008). Evidence of mixing and mingling between mafic and felsic magmas is commonly encountered (Bergström et al. 2020). Deformation within this group is heterogeneous, ranging from migmatized to almost undeformed units (Åhäll & Connelly 2008). Later episodes of magmatism are associated with the Sveconorwegian orogeny in the Idefjorden terrane, mostly consisting of pegmatite and granite intrusions with ages of 1.04–1.03 and 0.98 Ga (Bergström et al. 2020).

The augen-bearing orthogneisses in the area are folded on a regional scale (Fig. 19; Samuelsson 1978; Bergström et al. 2020). The folds strike NNW-SSE and gently plunge SSE (Samuelsson 1978). They are normally isoclinal and bend towards the west into the GÄ (Bergström et al. 2020). This large-scale structure has been influenced by the strong foliation and mylonitization along the GÄ and MZ and crosscut by pegmatitic intrusions (Samuelsson 1978). Later reactivation along the GÄ in the brittle regime has been suggested (Bergström et al. 2020).

On a large scale, the relief in south Sweden is the result of tectonic and denudational events since the Late Proterozoic, as well as a product of differential deep weathering of bedrock structures (Johansson et al. 2001; Olvmo & Johansson 2002). The effect of ice-sheet sculpturing can be seen in local-scale landforms; especially in hilly areas that have been subjected to enhanced glacial erosion (Johansson et al. 2001; Olvmo & Johansson 2002). Reshaping of large landforms due to glacial erosion occurs only to a limited extent and the original landforms are not totally erased (Johansson et al. 2001).

SGI and the Gothenburg municipality are conducting a cooperative analysis of rockfall hazard for the region based on field observations, structural data measurements, evidence from previous rockfalls and data processing using GIS tools. An important conclusion of this work is that the morphology of the slopes is mainly controlled by the structural features, i.e. fractures and foliation (schistosity) in the outcrops. In order to visualize the general hazard extent in the area, but, at the same time, disregard slopes that do not pose a threat of rockfall, 40° has been proposed as the lowest slope angle value for potential rockfall sources (SGI 2019).

Specifically for Fjällbo climbing area, structural data from Hellman (2018) indicates three joint sets with dip directions and dips of 230°/14°, 231°/74° and 139°/86° according to measurements in the field, and, similarly, 244°/11°, 233°/81° and 148°/88° after digital extraction from remote sensing data processing. Hellman (2018) concluded that the wedge shaped, blocky and jagged character of the cliff is controlled by the steeply dipping sets and undercut by the more gently dipping joint set.

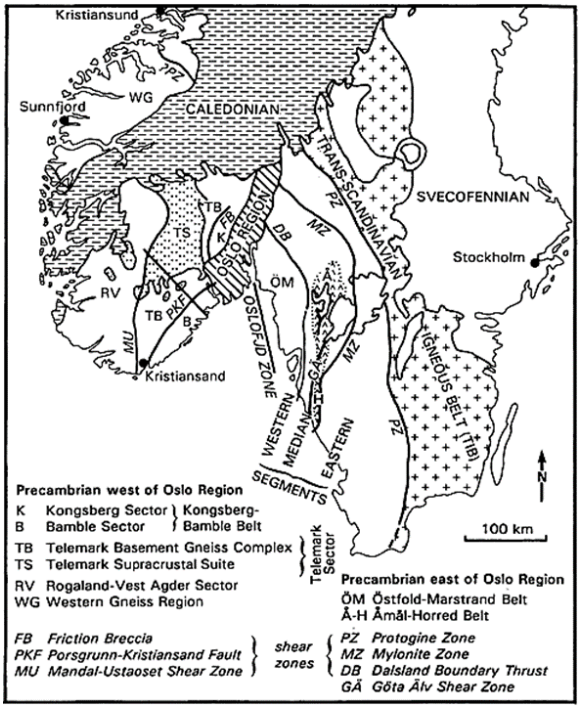

Fig. 16. Structural division of southern Scandinavia. From (Starmer 1996).

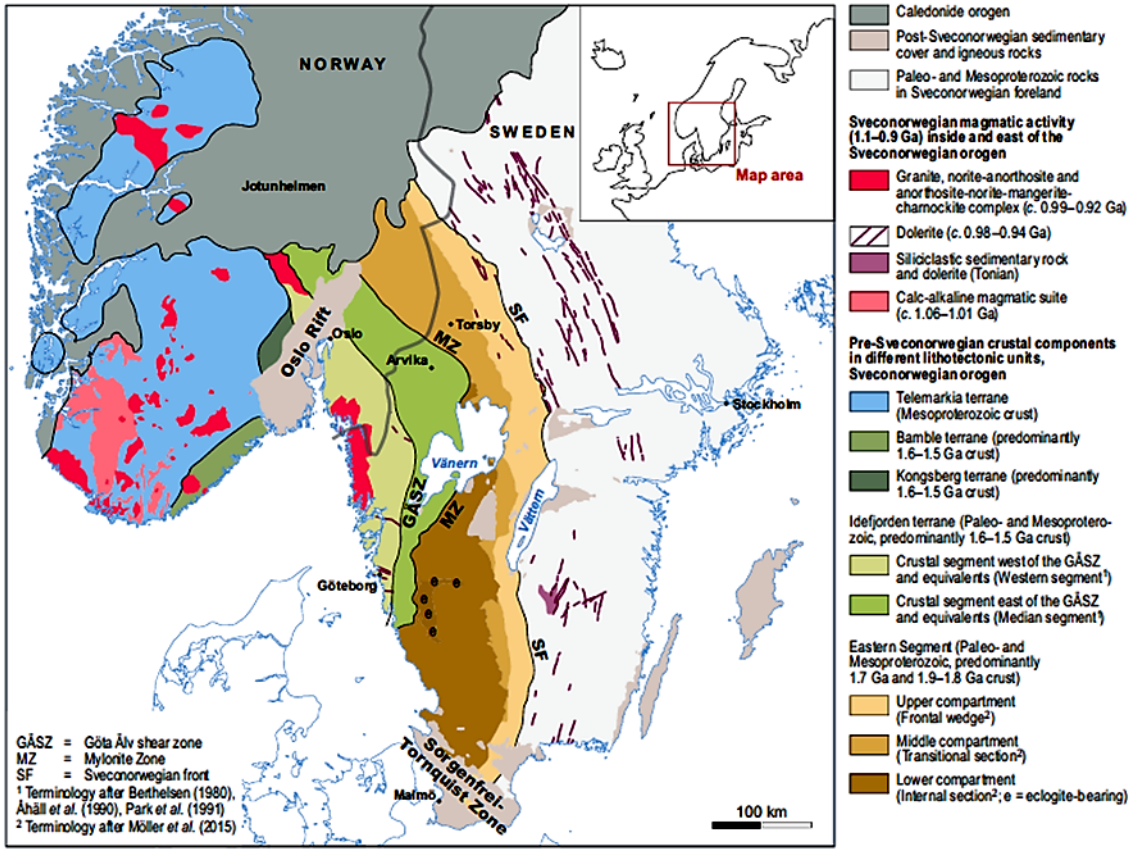

Fig. 17. Major Sveconorwegian lithotectonic units. From Stephens et al. (2020).

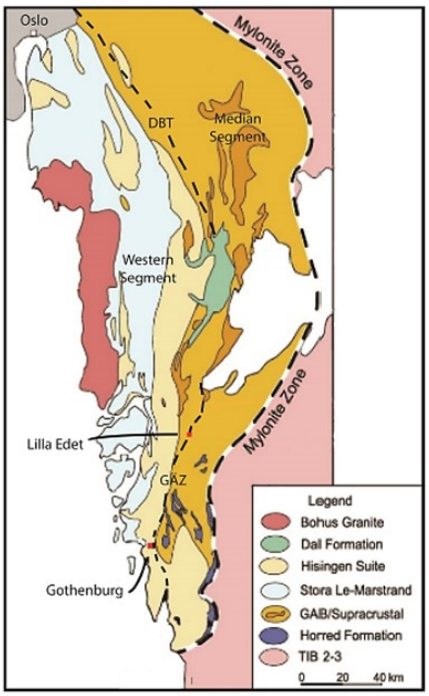

Fig. 18. Principal geological units in the Idefjorden Terrane. GAB/Supracrustal corresponds to Göteborg Åmål Belt (Suite)/Supracrustal rocks. From Sartell (2019), modified after Åhäll & Connelly (2008).

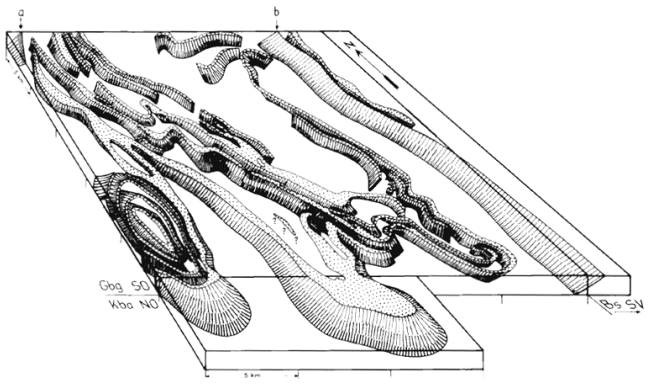

Fig. 19. Augen gneisses folded on a regional scale. a is the location of Göta Älv river and b the location of the Mylonite zone. Gbg SO, Kba NO and Bs SV correspond to the map sheets covered by this structure. From Samuelsson (1978).

3.1 Quaternary geology

The deglaciation of the Weichselian ice sheet in southern Sweden was characterized by a mainly terrestrial ice marginal retreat (Stroeven et al. 2016). This retreat is marked along the Swedish southwest coast by different marginal moraine ridges (Fig 20; Lundqvist & Wohlfarth 2000; Stroeven et al. 2016). Radiocarbon, varve and cosmogenic nuclide dating suggest ages approximately between 18 and 13 cal kyr BP for the formation of these moraines (Lundqvist & Wohlfarth 2000; Anjar et al. 2014; Stroeven et al. 2016).

In the study area, part of the Gothenburg moraine can be followed. It starts in the south, in the western part of Stora Delsjön, then it passes through the eastern part of Gothenburg, and continues northwards; near Lärjeholm it probably transects the valley of the Göta Älv river (Fig 21; Magnusson 1978).

During and after deglaciation, land uplift occurred as a result of isostatic rebound and exposed areas below the highest level reached by the sea during late-glacial times (highest coastline; Påsse 1987; Stevens & Hellgren 1990). However, the global melting of ice sheets during the last deglaciation caused an eustatic sea level rise, which occasionally occurred at a faster rate than the uplift, resulting in temporary transgressions of the sea (Stevens & Hellgren 1990).

The following description of the glacial and postglacial deposits encountered in the area, is based on Magnusson (1978):

Till is scarce in the area, and where it is found, it occurs as a thin layer. This thin cover is mostly found in plateau areas located at high altitudes (between 100 and 150 m), above the highest coastline. Drumlin-like ridges are the most remarkable landforms related to these deposits. Sandy till is the most commonly found type although gravelly till, and, in minor proportions, till dominated by fine sand and silt is also encountered. A low primary deposition, rather than loss because of erosion is suggested to explain the low abundance of till in the area.

Glaciofluvial deposits are found in the valley of the Säveån river. Usually they are covered by clay and have been detected after drilling within the area. Variations in the dimensions of the glaciofluvial deposits are interpreted to indicate periodicity of ice retreat. Some beach deposits are associated with these deposits.

Fine-grained glacial and postglacial sediments are the most widespread deposits in the area. They consist mainly of clay and silt. Glacial clays were deposited in late glacial fiords. Later reworking and redeposition by wave action resulted in formation of postglacial clays. South of Kviberg, approximately 2.5 km from Fjällbo, the thickest deposit (100 m) is found. In some parts, the postglacial clays show traces of organic matter. A few peat deposits occur in the area, and they usually do not exceed 4 – 5 m in thickness.

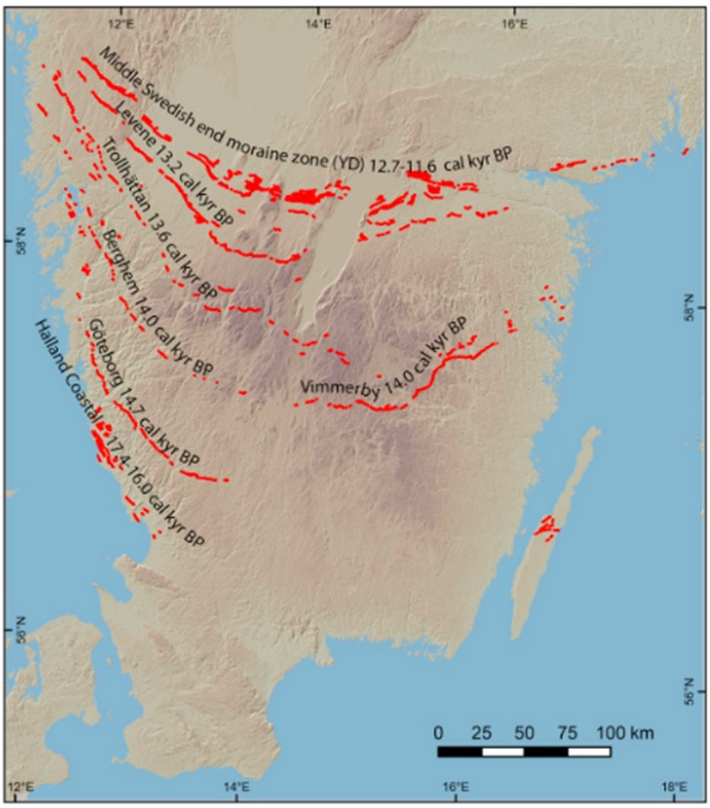

Fig. 20. Major moraines in southern Sweden. From Stroeven et al. (2016).

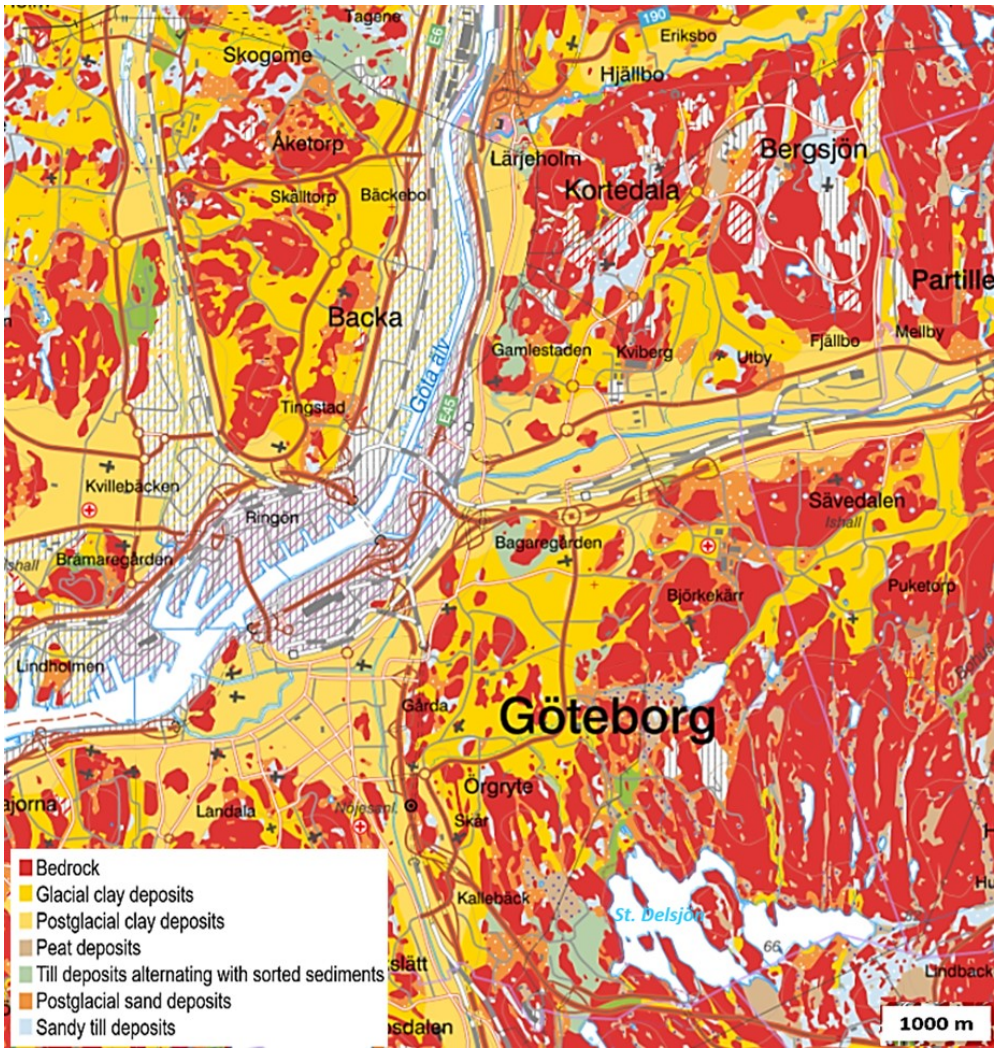

Fig. 21. Quaternary deposits of the Fjällbo area and its surroundings (SGU 2020).

4 Methodology

4.1 Digital data

Elevation data (XYZ) for the Gothenburg municipality was acquired using Light Detection and Ranging (LiDAR) by the company COWI AB in 2017. The following parameters for data acquisition were reported:

Point density > 11 pt / m², laser overlap: 21%, altitude: 1750 m above ground, opening angle 15.0°, frequency of the pulse: 487 kHz, multipulse mode: 3, scanning frequency: 40.0 Hz, and speed: 115 kN.

The measurements were performed with laser systems Leica ALS80-HP-8238 from aircraft BN2A-21 Islander OY-CKS, and laser systems Leica ALS80-HP 8236 from aircraft-D FCAE Cessna 208.

A DEM of the area was extracted from the LiDAR data. Orthophotos of the region were obtained from Google Earth imagery, and orthophotos for Fjällbo climbing area were available from Axel Hellman's master's thesis work (Hellman 2018). These were taken with a 3DR UVA owned by Gothenburg University, equipped with a 12-megapixel camera and GPS and GLONASS positioning.

Bedrock and quaternary deposits maps (Scale 1:25 000 – 1:100 000) were downloaded in shape format from the Geodata Extraction Tool from Lantmäteriet and the Swedish Geological Survey (SGU). The scale of the maps is not uniform as different mapping methods were used, including field mapping and remote sensing images interpretation. The estimated position error ranges from 25 – 150 m (SGU 2014).

The SAD analysis data were processed using Histofit 1.0, an Excel tool developed by Loye et al. (2009), the same authors that proposed the method. CONEFALL was downloaded for free from Risk Analysis Group at the Univer-

sity of Lausanne (https://wp.unil.ch/risk/software/conefall/). The license for Rockyfor3D was purchased by SGI and borrowed for this study.

Vector and raster data were processed with ArcMap 10.5.1 under the license of Lund University. Data gridding and conversion was done with Surfer 17. Maps generation was performed by using these two programs.

The coordinate reference system used for all data is SWEREF99 12TM.

4.2 Fieldwork

In November 2019 and March 2020, two field campaigns were carried out in Fjällbo park. The first one was for reconnaissance of the area and the second to perform observations, take notes and pictures of the rock wall (rock type, composition and structures), the quaternary deposits, and the evidence of previous rockfalls (talus slopes). Moreover, measurements of the height of the blocks in the talus slopes, as well as the diameter of the trees were performed, and tree species were identified. Finally, the locations of the three potential block sources for rockfall simulations (See section 5.4) were checked, as well as the location of the 2017 rockfall source and its approximate extent. These locations were previously chosen and measured using aerial photos, i.e. apparently loose blocks along the cliff were identified and measured in ArcMap and Google Earth.

Location of the trees in the area was marked in a GPS to keep track of their distribution. The accuracy of the tree positions is estimated at ±2m. The circumference of the trees was measured to later calculate the diameter at breast height (DBH) and run simulations including the forest. This procedure was performed using a metric tape and wrapping it around the tree stems.

The mean obstacle height (MOH) was measured on the slopes located under the chosen rockfall sources for simulation purposes. As explained in section 2.7.2, the MOH in the slope is divided in three parts: 70%, 20% and 10%; therefore 70, 20 and 10 blocks were measured for each case. Measurements were based on the block distribution in the terrain, i.e. the area was inspected and the distribution of the size of the blocks was estimated in percentage. For example, if 70% of the blocks had medium size, 70 blocks of this similar size were measured to calculate the average and obtain the MOH.

4.3 SAD analysis

In order to evaluate the usefulness of the SAD procedure at different scales, two additional areas (named Area 2 and Area 3; Fig. 22) around Fjällbo were included in the study, both of them related to the same genetic processes, and thereby belonging to the same HMA. The Göta Älv river was taken as the western limit for the three areas since it represents a natural tectonic limit. The east boundary is delimited by the end of the LiDAR data acquired. The north-south extent of Fjällbo and Area 2 are the same (1 km); Area 3 has an extent of 8 km along the north-south direction, and this area covers a large part of the regional-scale fold in the bedrock and parts of the Gothenburg moraine (See section 3). The DEM cell size used for this analysis was 5 m, i.e. 25 m^2 per pixel, considering that the geology mapping is not very detailed nor uniform (See section 4.1). Even though this pixel size does not represent the highest resolution for the original LiDAR data, it provides a good resolution of the slope data without affecting the range of slope angle values, considering that for lower resolutions, high slope gradients can be missed in the analysis.

According to the modification of the SAD analysis for flat terrains proposed by Loye et al. (2009) (Section 2.3.1), and the geological processes involved in the study area, three morphological units were used: plains, till slopes, steep slopes. The steep slopes MU also includes cliffs but here the name was simplified. Vector soil data was categorized according to the MU as follows:

- Plains related to glaciofluvial and postglacial deposits.
- Till slopes associated with moraines.
- Steep slopes associated with bedrock units.

All slope angle values equal to zero, as well as water bodies and artificial fillings (named “Others” in Fig. 27, 28, 29) were discarded from the SAD analysis.

For the three areas, slope angle values were extracted from the DEM raster using the slope function in ArcMap, which generates a raster with the slope angle values. From the attribute table, the values and their respective number of pixels (which are translated into area) were exported to Excel and processed using Histofit 1.0. This tool uses the following input data: the slope angle values from 1° to 90° in steps of one degree, as well as the weight, mean and standard deviation that corresponds to each of the MU. It calculates the frequency for each slope value, creates a histogram with bin size = 1, and subsequently calculates the sum of the GDMUs in order to find the best fitting curve to the SAFD. Finally, the intercepts between plains and till slopes MU, and between till slopes and steep slopes MU, as well as the mode of the till slopes MU are extracted from this curve (See section 2.3.1).

4.4 CONEFALL

XYZ elevation data was converted to a Surfer Grid (GRD) file in order to generate the DEM in the

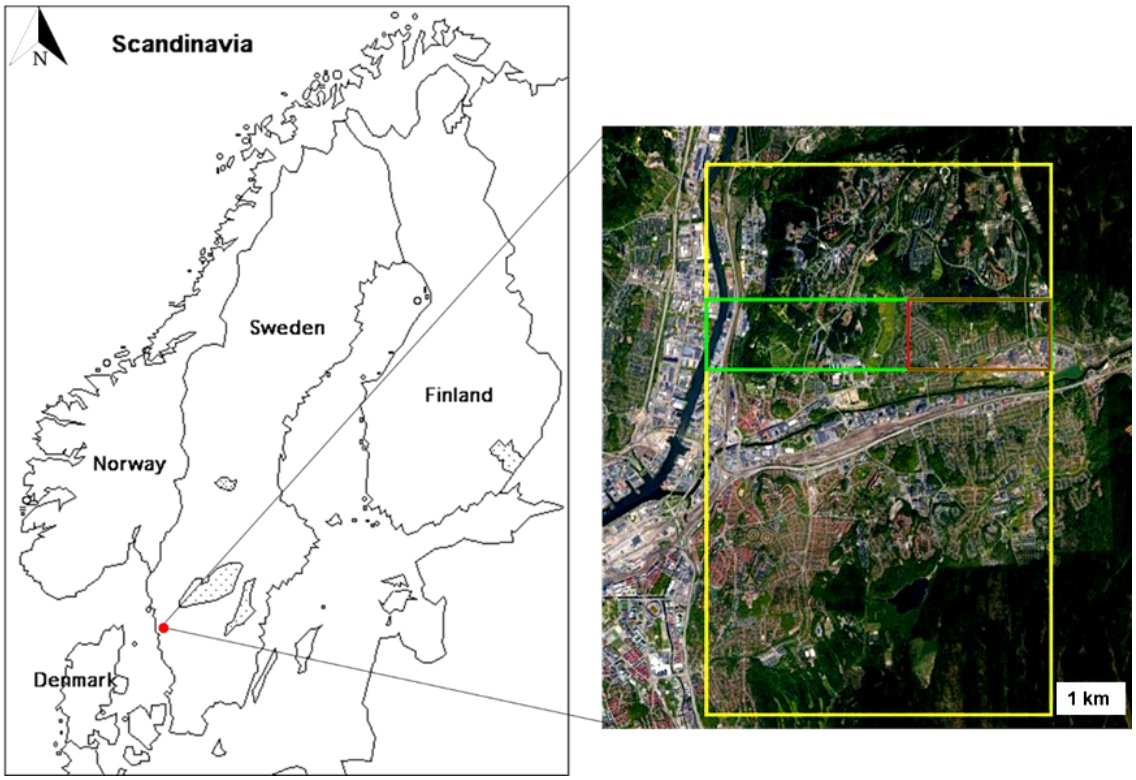

Fig. 22. Areas chosen for SAD analysis. Fjällbo area is framed in the red rectangle. Area 2 corresponds to the green rectangle and Area 3 to the yellow rectangle.

correct format for the program. The nearest neighbor was used as gridding method with spacing of 1 in x and y directions to guarantee maximum smoothing of curves; otherwise curves would look blocky as a result of the gridding. In the same way, the gridding of the source files was conducted.

The source areas were selected after obtaining the SAD analysis results, by converting the slope raster to an ASCII file to perform the gridding procedure. Additionally, for the Fjällbo climbing area, three specific source areas, named West, Center and East (according to their location with respect to the geographical north), as well as the 2017 rockfall source, were selected based on interpretation from aerial images and verification of their location in the field. These sources were chosen due to their position with respect to the growing residential area in Fjällbo and also because of the presence of talus slopes and topographic changes, in order to test the effect of these changing conditions when performing rockfall simulations (See section 5.4 for details on the characteristics of the sources and the slopes). In both cases, a value of 1 was assigned to the marked areas as potential sources and -1 to the rest of the grid, and using the same extent as the DEM.

The output type was selected as -1 and 1 where all the points with the value 1 correspond to the runout zone. The results were tested with and without an aperture angle limit. The results in grid format, were processed in Surfer to generate the contours and superimpose them to create the final maps. To have a clearer visualization of the runout distances in relation to the topography, they were also superimposed to the hillshade of the corresponding areas.

4.5 RockyFor3D

The same three potential rockfall sources described in Section 4.4 (West, Center and East) and the 2017 rockfall source in the Fjällbo area were selected for rockfall simulations in RockyFor3D. A polygon was created and digitized for each of the required attributes, i.e. block shape, block dimensions, soil type, surface roughness, block density. The files were then rasterized as this is the format accepted by the program (See section 2.7.2). In all cases, the density of the rock was assumed as ~ 2700 kg/m^3,

based on an average density for this type of granitoid-dominated gneissic terranes (Schön 2015).

Block dimensions were measured using orthophotos to simulate realistic conditions. The model calculates mass (M) of the blocks according to Equation 3, and their volume (V) according to their dimensions using Equations 4 and 5 (Dorren 2016).

$$Mass = Density * Volume$$

Rectangular block volume = $Height * Width * Length$

Spherical block volume = $\frac{4}{3} * \pi * (\frac{Height}{2})^3$

The MOH was calculated from the data measured in the field for each slope by calculating the average size of the blocks in the 70%, 20% and 10% groups (See Annex 1). Similarly, the DBH was calculated using Equation 6 and. A txt file containing the location of the trees and their DBH, as well as a raster file with the percentage of coniferous trees in the area were added to the input data.

$$Diameter = \frac{Circumference}{\pi}$$

The simulations were run testing the sensitivity of different parameters by varying them (See Section 5.4). 1000 simulations were run for every single case. To display the results and represent the morphology and topography of the terrain in high resolution, a Triangle Irregular Network (TIN) was created in ArcMap from the elevation data. Thee runout zones were superimposed and measured on the TIN. The resolution was 0.5 m, i.e. 0.25 m^2 per pixel for every case. This resolution was chosen as the point density of the elevation data is very high, and the field measurements were detailed.

5 Results

5.1 Field observations and measurements

The bedrock geology of the area consists mostly of coarse and fine-grained augen gneisses with feldspar porphyroblasts of varying size (~2-6 cm; Fig. 23 A, B) and associated quartz, plagioclase, and biotite in different proportions. Gneissic banding is clearer in fine-grained gneisses (Fig. 23A). Large amounts of biotite are found in the blocks on top of the 2017 fall (Fig. 23C), suggesting that this was a factor that contributed to develop weak planes in the rock wall that eventually collapsed. Parts of the outcrops and loose blocks show pegmatite intrusions (Fig. 23D), as well as amphibolites, mafic dikes and evidence of magma mingling (Fig. 25 D).

The joints, fractures and foliation in the cliff provide perfect conditions for climbers as several parts of the wall stick out, but, at the same time, these discontinuities represent planes of weakness and thus potential rockfall sources (Fig. 24). The soil at the lowest part of the rock wall consists of clay, the texture is very sticky and stiff, and it shows a yellowish tone. A total of 459 trees were measured (Annex 1).

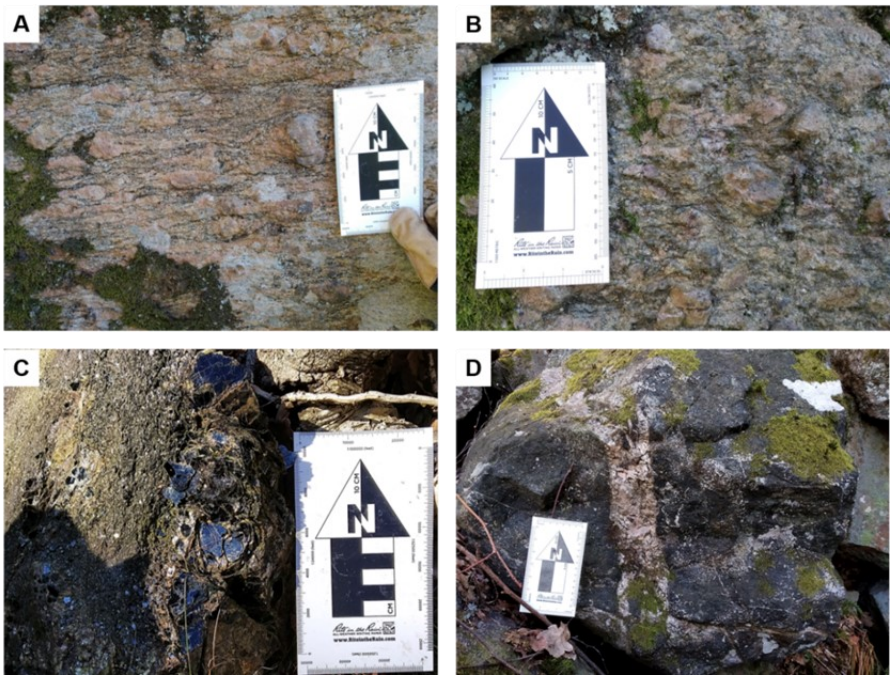

Fig. 23. A) Augen gneiss in a fine-grained matrix, showing a clear banding. B) Coarse augen gneiss. C) Blocks with abundant biotite content. Crystal size varies between mm to ~5 cm. D) Pegmatitic intrusion in mafic block.

Fig. 24. Some of the climbing walls of Fjällbo. The discontinuities in the rock represent planes of weakness and thus potential rockfall sources.

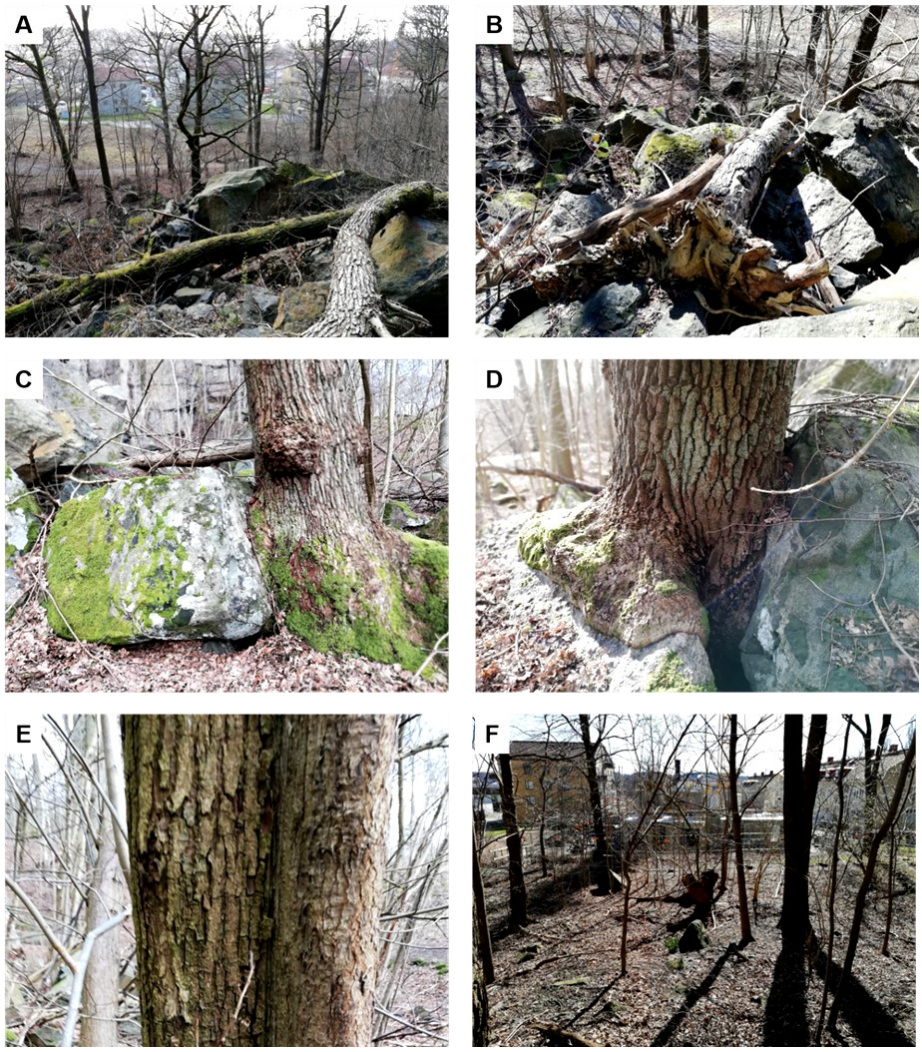

Fig. 25. A, B) Trees broken by the action of the 2017 rockfall. C, D) Trees growing between loose blocks. In Figure D, the block to the right exhibits evidence of magma mixing and mingling. E) Stem showing overgrowth, this suggests healing after being affected by a block. F) Longest extent of the loose blocks in the area.

Fig. 26. The 2017 rockfall. Front view to the left, lateral view to the right. To see details of the extent of the rockfall, see Section 5.4.

Most of the trees are deciduous (oak, hazel, aspen, birch), and just a few coniferous (pine). The abundance of coniferous trees increases towards the top of the cliff. Several trees in the area were observed to be knocked down by the action of the 2017 rockfall (Figure 25 A, B). Growth of trees between blocks as well as stem recovery also show evidence of the effects of rockfalls (Fig. 25 C, D, E).

The height of 300 blocks in total (100 blocks per slope) was measured for the three chosen slopes (West, Center, East; See section 4.4), each of them divided in three parts: 70%, 20% and 10% according to the distribution of the blocks (Annex 2).

A sign for the public describes the 2017 event and explains that a pillar collapsed from the rock wall, allegedly due to the action of water and ice during a prolonged time. The size of the largest boulder is estimated to be 150 Ton and a total of 500 Ton collapsed. The 2017 rockfall occurred along the "Ulf and Susan's path" (according to a climber encountered in the field), a very renowned climbing route (Fig. 26). The distribution of the blocks in the area also suggests evidence of older rockfalls. A simple correlation was done by inspecting the block that are more weathered and more covered by moss in comparison to the fresh blocks related to the 2017 rockfall. Moreover, some individual blocks went beyond the talus field below the cliff and passed the hiking trail, getting close to the constructed buildings (~ 40 m) and are located even closer to the under-construction structures (~ 20 – 30 m; Fig. 25 F).

5.2 SAD analysis

As stated in Section 4.3, three different areas of different size were selected to perform the SAD analysis procedure (Fig. 26). Figures 27, 28 and 29 show both the slope angle map and the categorized geological map according to the MU for each of the cases.

After the first extraction of the slope angle values in combination with the geological data according to the classification in MU, the SAFD was calculated for each case. The low slope angle values show the highest frequency in all cases and a decreasing trend towards the high values (Fig. 30, 31, 32). Both the slope values corresponding to the plains and steep slopes MU range between low and high angle values (1° and 84° in both cases); their mean and standard deviation values are very similar (Tables 4 and 5). The sum of GMDUs was not a good fit for to the SAFD curve, and hence no intersections between MU could be used for the SAD analysis (Fig. 30, 31, 32). The till slopes MU, however, show a different pattern, with values ranging between (2° and 40°). The mode of these MU was calculated in order to discard low slope angle values that do not pose a potential threat of rockfalls (Fig. 30, 31, 32).

Mean		Study area		
		Fjällbo	Area 2	Area 3
MU	Plains	32.5	38	25
	Till slopes	18.5	21	24.5
	Steep slopes	40.5	40.5	39

Table 4. Original mean values of slope angles for MU in the three study areas.

Standard deviation		Study area		
		Fjällbo	Area 2	Area 3
MU	Plains	18.04	21.32	14.29
	Till slopes	9.96	11.40	14.00
	Steep slopes	22.66	22.66	22.37

T*able 5. Original standard deviation values of slope angles for MU in the three study areas.*

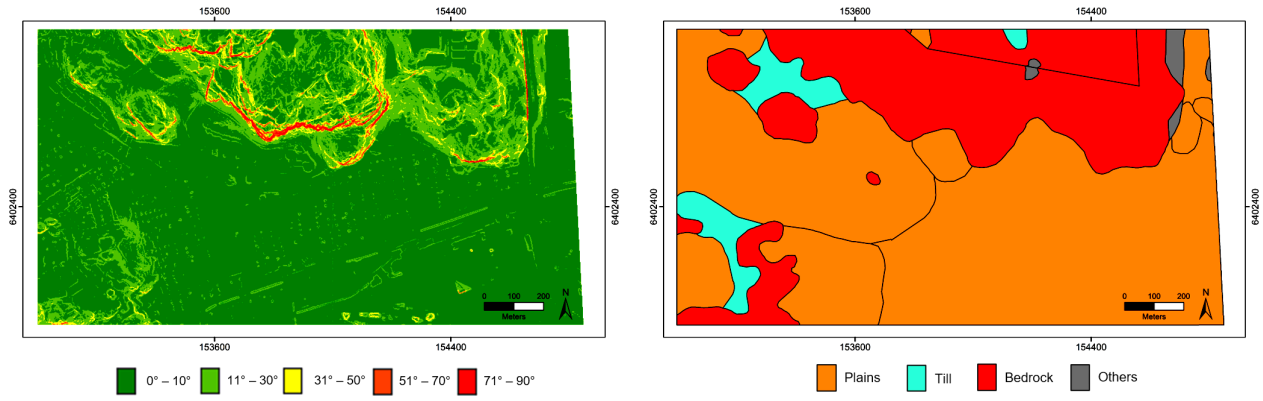

Fig 27. The Fjällbo area (approximately 2 km^2). Towards the east, the limit of the map is slightly irregular due to uneven data acquisition. To the left: Slope angle map. To the right: classified geological map according to the proposed MU (See section 4.3).

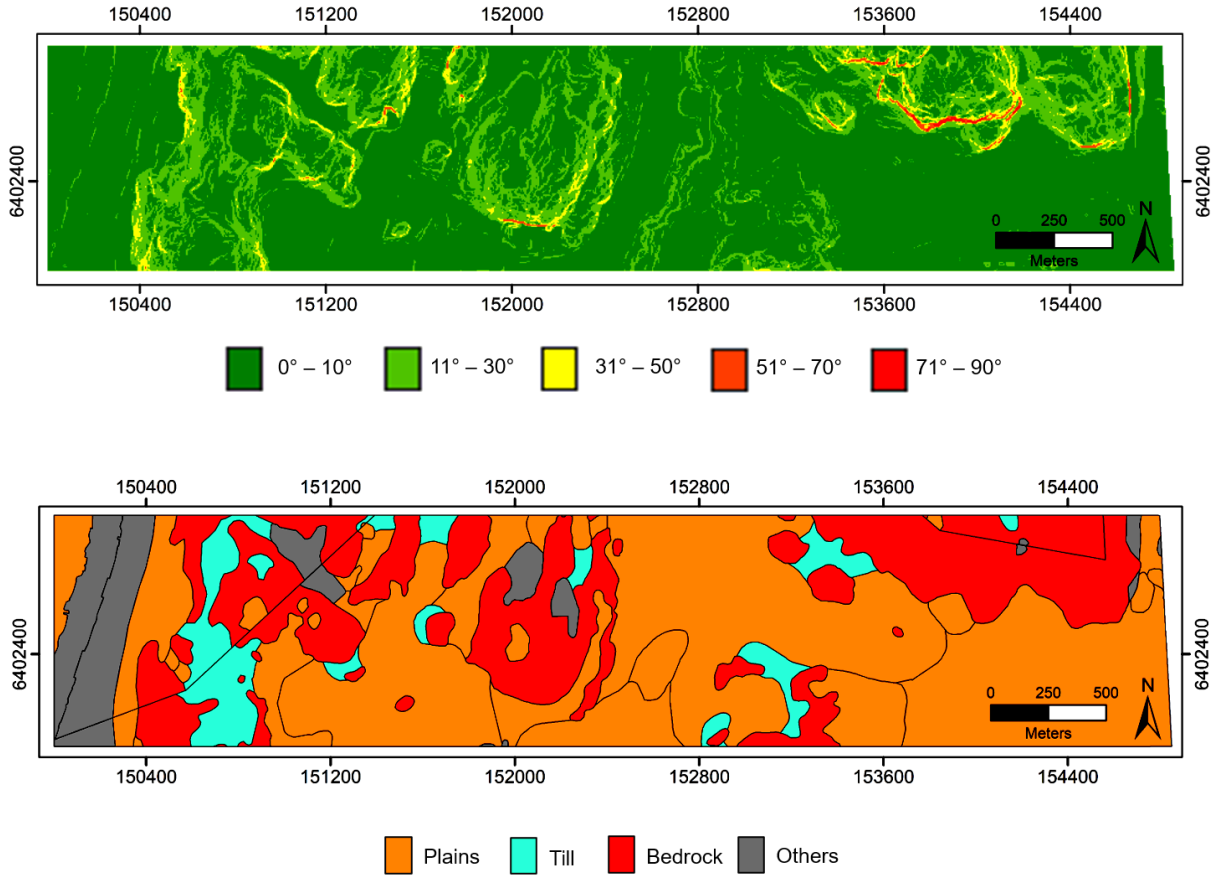

Fig. 28. Area 2 (approximately 5 km2). Towards the east, the limit of the map is slightly irregular due to uneven data acquisition. To the left: Slope angle map. To the right: classified geologic map according to the proposed MU (See section 4.3).

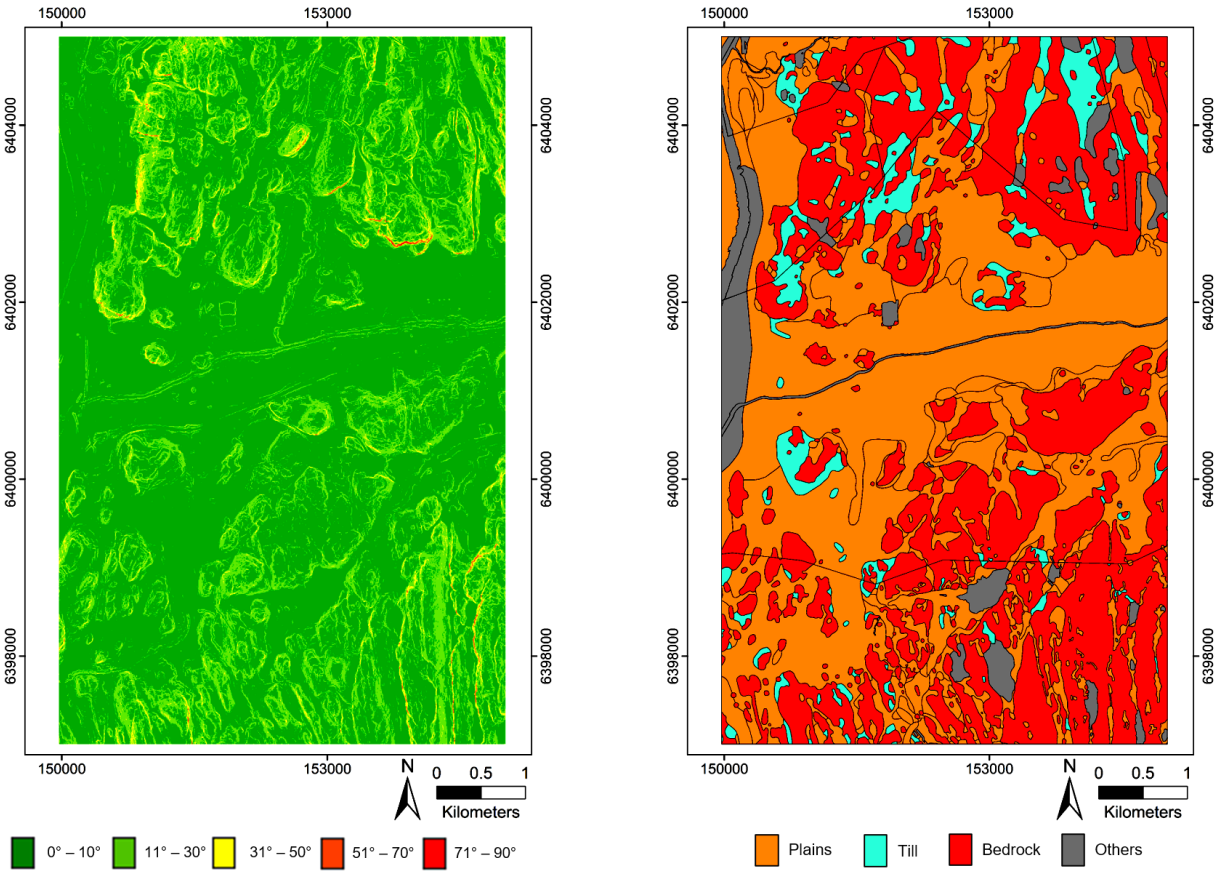

Fig. 29. *Area 3 (approximately 40 km^2). To the left: Slope angle map. To the right: classified geological map according to the proposed MU (See section 4.3).*

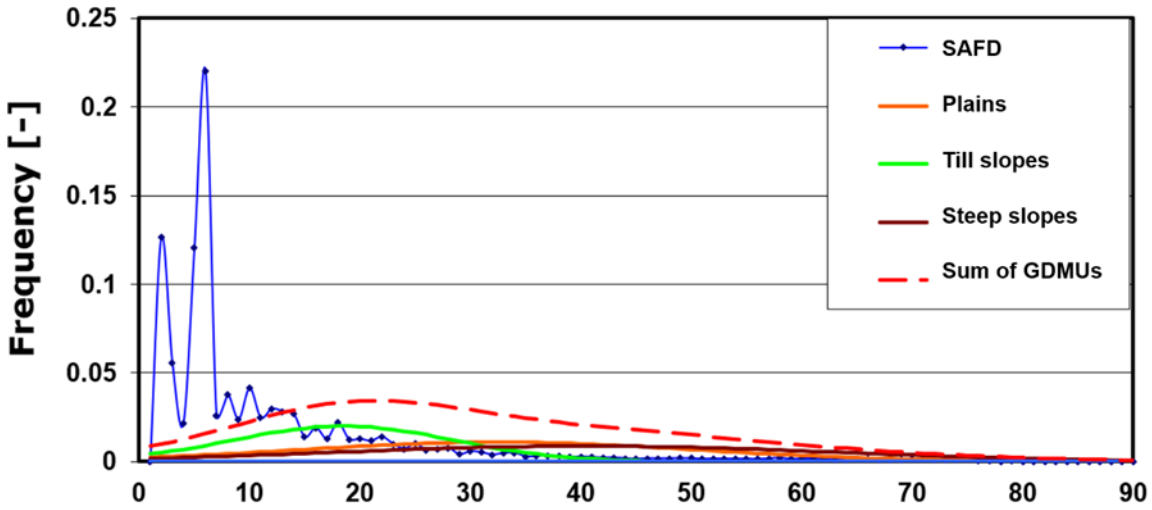

Fig. 30. Original SAD analysis for the Fjällbo area. Mode of till slopes = 18°.

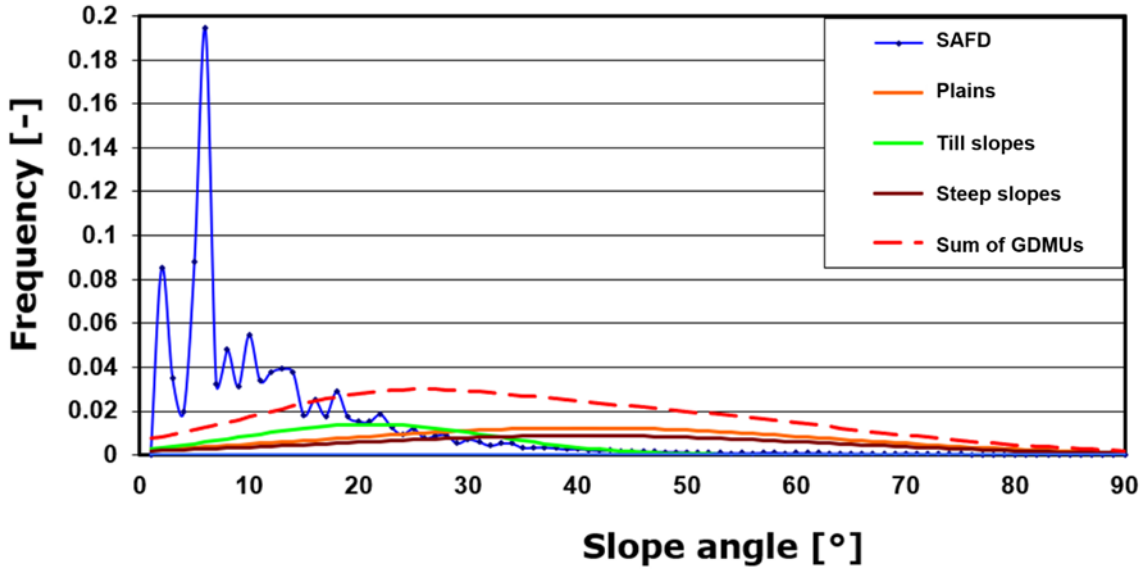

Fig. 31. Original SAD analysis for Area 2. Mode of till slopes = 23°.

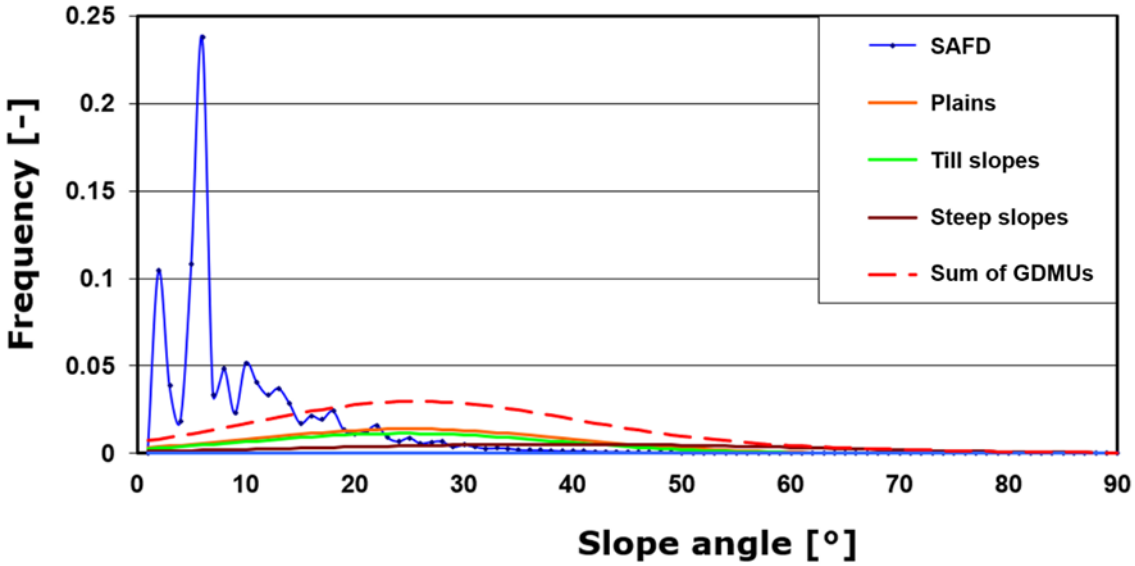

Fig. 32. Original SAD analysis for Area 3. Mode of till slopes = 22°.

When comparing the slope angle map to the soil data, specifically for the plains MU, some high values stand out, mostly in the contacts with bedrock units (Fig. 33, 34, 35). As for the steep slopes MU, all values below the calculated mode of the till slopes were discarded, as they do not represent potential rockfall sources, as explained in Section 4.3. The calculation of the mean and standard deviation values without these outliers is shown in Tables 6 and 7. The values for the till slopes MU remain the same as in the original data. The outliers in the plains MU for the Fjällbo area are mostly related to the central part of the cliff (Fig. 33). For Area 2, the outliers are clear in both the Fjällbo climbing area, and other cliffs towards the west. Within Area 3, less outliers were found, most of them are in the northwestern part of the area, and they are not only associated with bedrock units, but also with till deposits. In all cases the white areas correspond to the outliers within the steep slopes MU, i.e., the slope angle values below the value of the mode of the till slopes MU for each area.

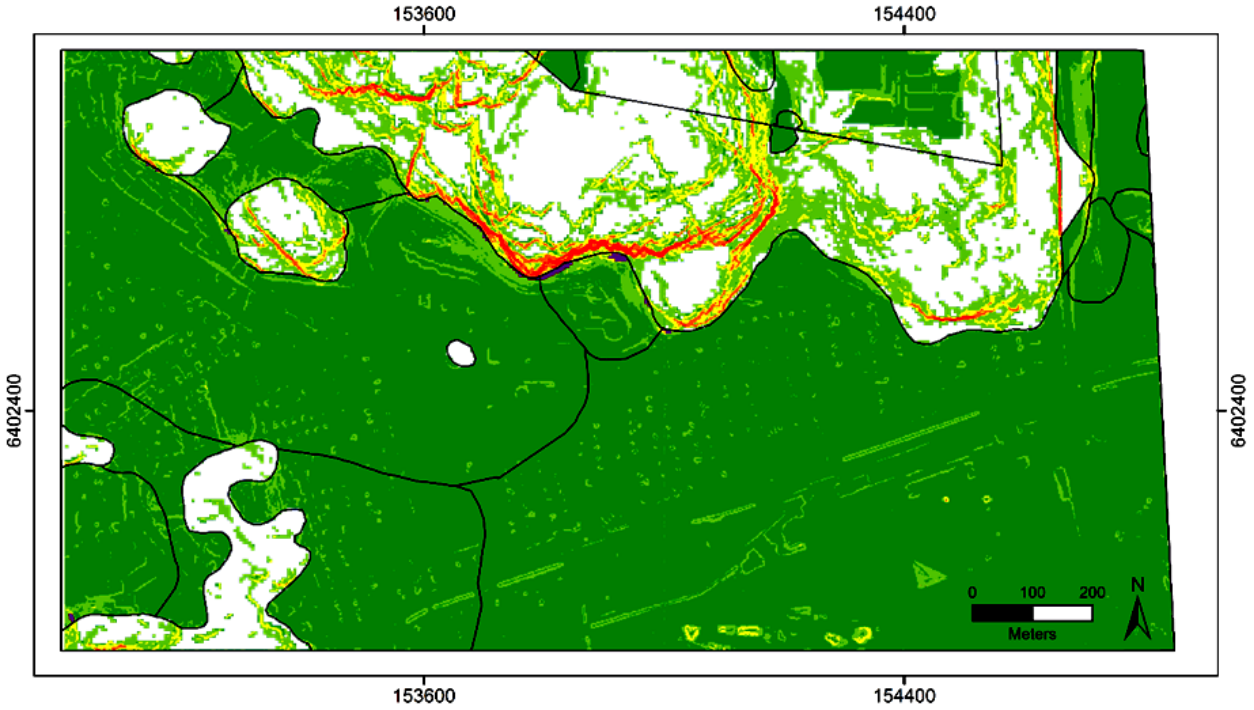

Fig. 33. Slope angle map for the Fjällbo area. The slope angle value outliers for the plains MU are highlighted in purple. Likewise, the slope angle value outliers for the steep slopes MU are highlighted in white.

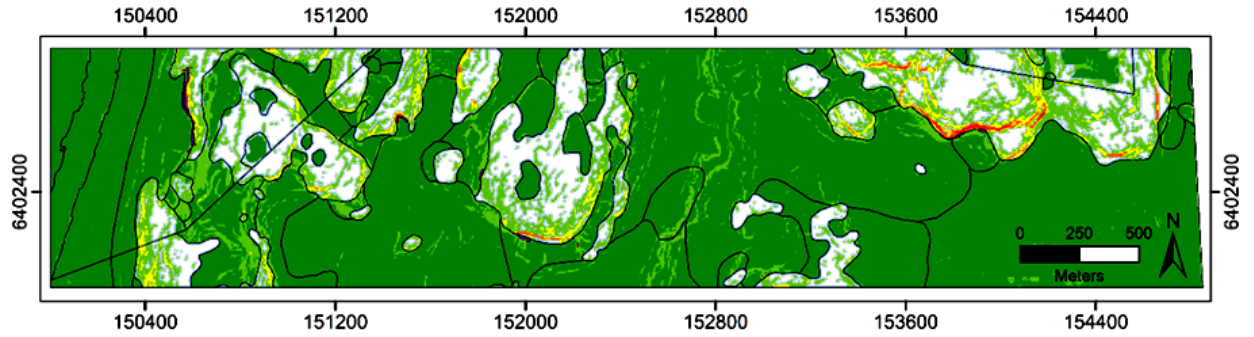

Fig. 34. Slope angle map for Area 2. The slope angle value outliers for the plains MU are highlighted in purple. Likewise, the slope angle value outliers for the steep slopes MU are highlighted in white.

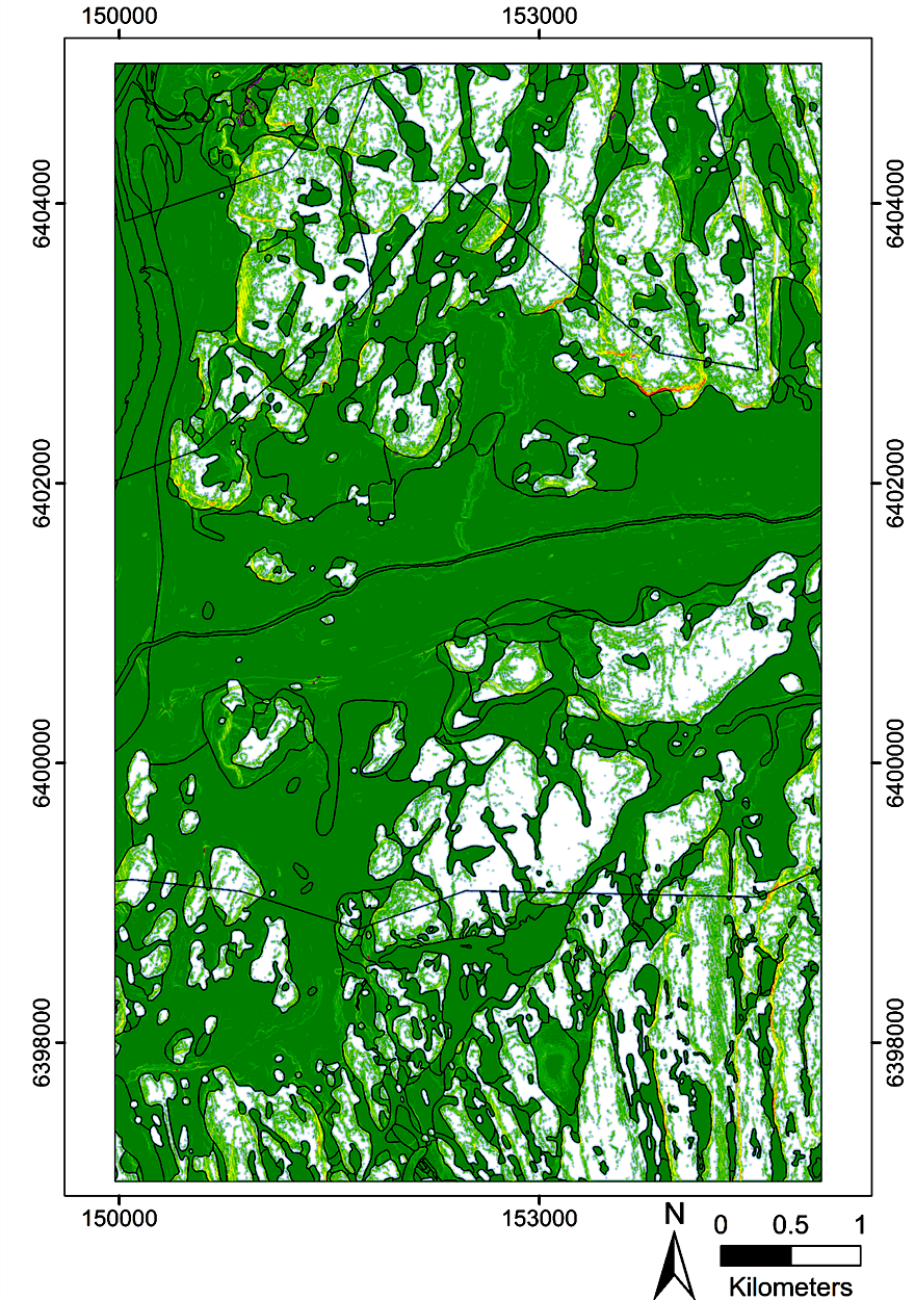

Fig. 35. Slope angle map for Area 3. The slope angle value outliers for the plains MU are highlighted in purple. Likewise, the slope angle value outliers for the steep slopes MU are highlighted in white.

Mean		Study area		
		Fjällbo	Area 2	Area 3
MU	Plains	10	10	10.5
	Till slopes	18.5	21	21.5
	Steep slopes	54	51	47.5

Table 6. Mean values of slope angles for MU in the three study areas after elimination of outliers.

Standard deviation		Study area		
		Fjällbo	Area 2	Area 3
MU	Plains	5.05	5.05	5.92
	Till slopes	9.96	11.40	12.27
	Steep slopes	14.87	16.60	17.46

Table 7. Standard deviation values of slope angles for MU in the three study areas after elimination of outliers.

The results, after elimination of outliers, for the Fjällbo area are shown in Figures 36 and 37. The slope angle intersection between the plains MU and the till slopes MU is at 17°. The mode of the till slopes MU is at 18°; below this value, the slope angles in the steep slopes MU were discarded as potential rockfall sources. The intersection between the till slopes MU and the steep slopes MU is at 40°, indicating the lowest angle at which slopes should be considered as potential rockfall sources, according to the SAD method. Figure 37 shows the new classification of the slope angle map according to the values extracted from the SAD analysis and their relationship with the topography, as they were superimposed on the hillshade map. The potential rockfall sources are located along the cliffs at the Fjällbo climbing area. The sum of GDMUs has a $R^2 = 0.89$.

For Area 2, the results after elimination of outliers are shown in Figures 38 and 39. The slope angle intersection between the plains MU and the till slopes MU is at 19°. The mode of the till slopes MU is at 23°. The intersection between the till slopes MU and the steep slopes MU (A) is at 42°. The potential rockfall sources are associated with the bedrock topography in the area, again in the Fjällbo area as well as in other cliffs in the west, near Utby and Kviberg. $R^2 = 0.9$ for the sum of GDMUs in this area. Figure 39 shows the new slope map according to the values extracted from the SAD analysis and their relationship with the topography.

Lastly, the results after elimination of outliers for Area 3 are shown in Figures 40 and 41. The slope angle intersection between the plains MU and the till slopes MU is at 22°, as well as the mode of the till

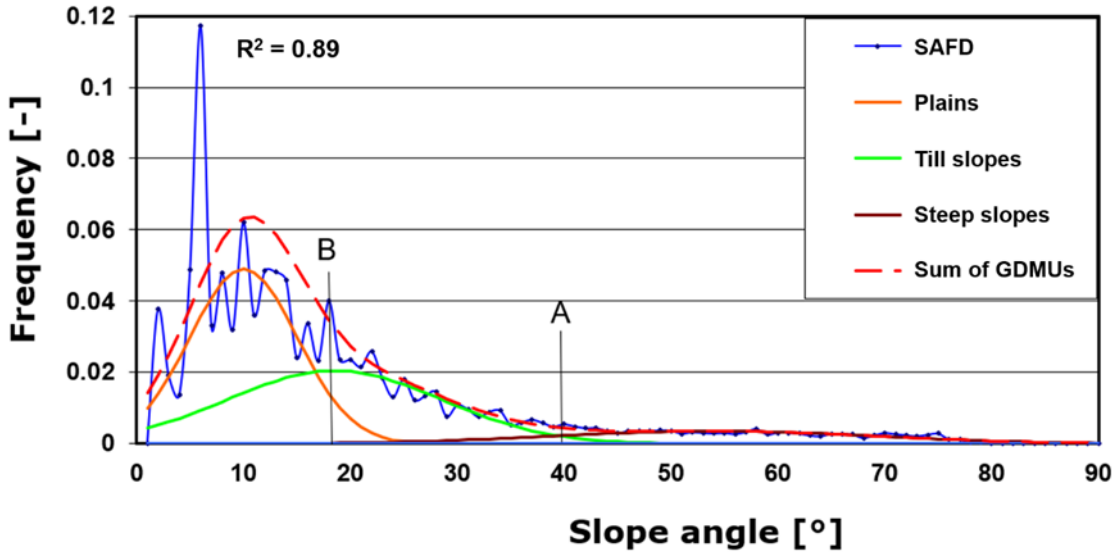

Fig. 36. SAD analysis for the Fjällbo area after elimination of outliers. A = 40°, B= 18° and $R^2 = 0.89$.

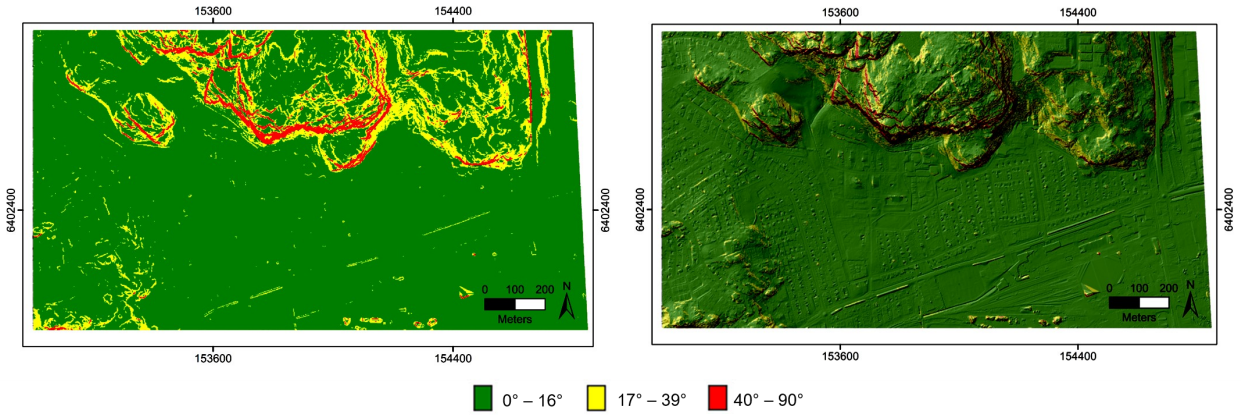

Fig. 37. To the left: Reclassification of the slope angle values according to the SAD analysis results for the Fjällbo area. To the right: Relationship of the slope distribution and the topography. Colors appear darker because the slope map has 50% of transparency to make the topography (hillshade) visible.

slopes MU. The intersection (A) between the till slopes MU and the steep slopes MU is at 42°. The sum of GDMUs for this area has the highest coefficient of determination out of the three tests (R^2 = 0.93).The potential rockfall sources are associated with the bedrock topography in this area, as in the previous analyzes (the Fjällbo area and Area 2), and the abundance of potential rockfall sources is higher in the northern part. In the south, the slope angle values for bedrock units are not larger than 30°, with some marked exceptions in the southwestern part of the study area (Fig. 29, 41). Figure 41 shows the new slope map according to the values extracted from the SAD analysis and their relationship with the topography.

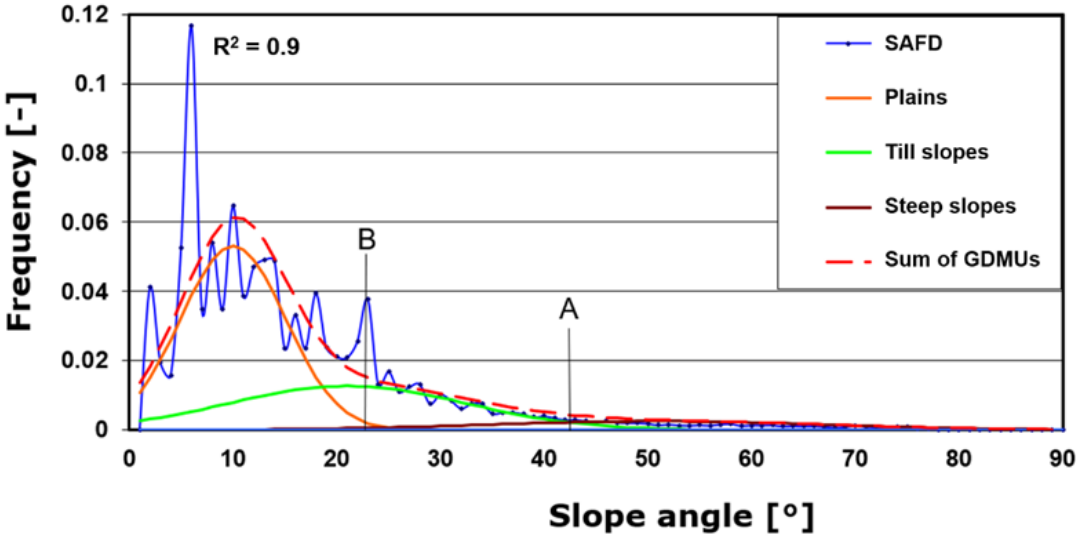

Fig. 38. SAD analysis for Area 2 after elimination of outliers. A = 42°, B= 23° and R^2 = 0.9.

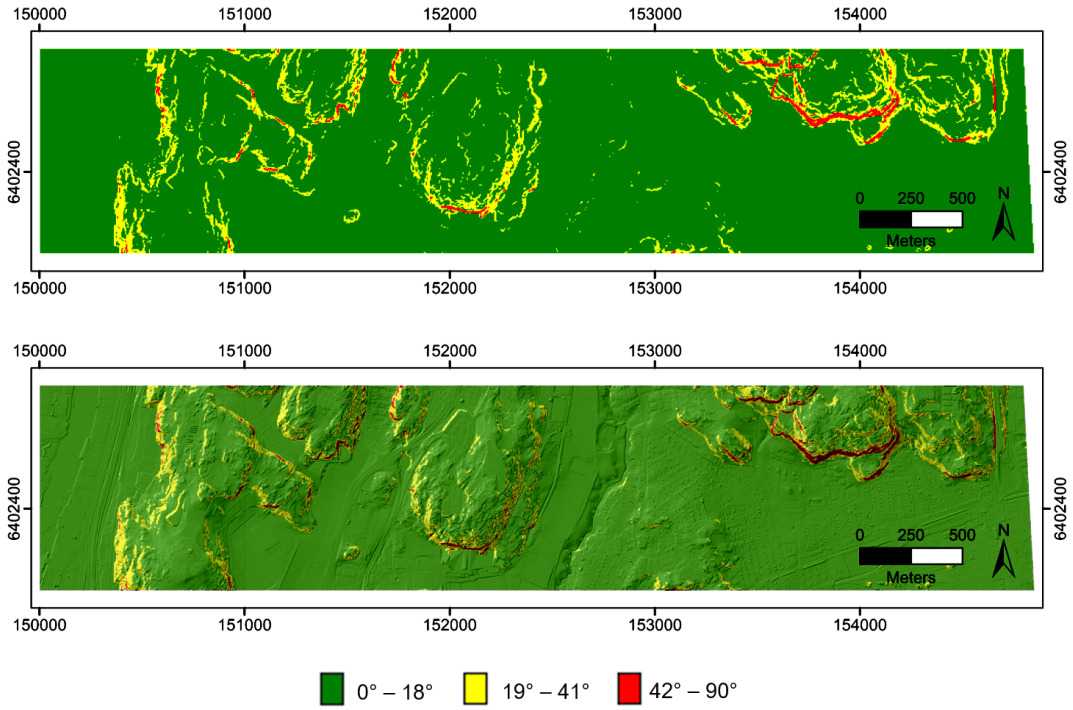

Fig. 39. Top: Reclassification of the slope angle values according to the SAD analysis results for Area 2. Bottom: Relationship of the slope distribution and the topography. Colors look darker because the slope map has 50% of transparency to make the topography (hillshade) visible.

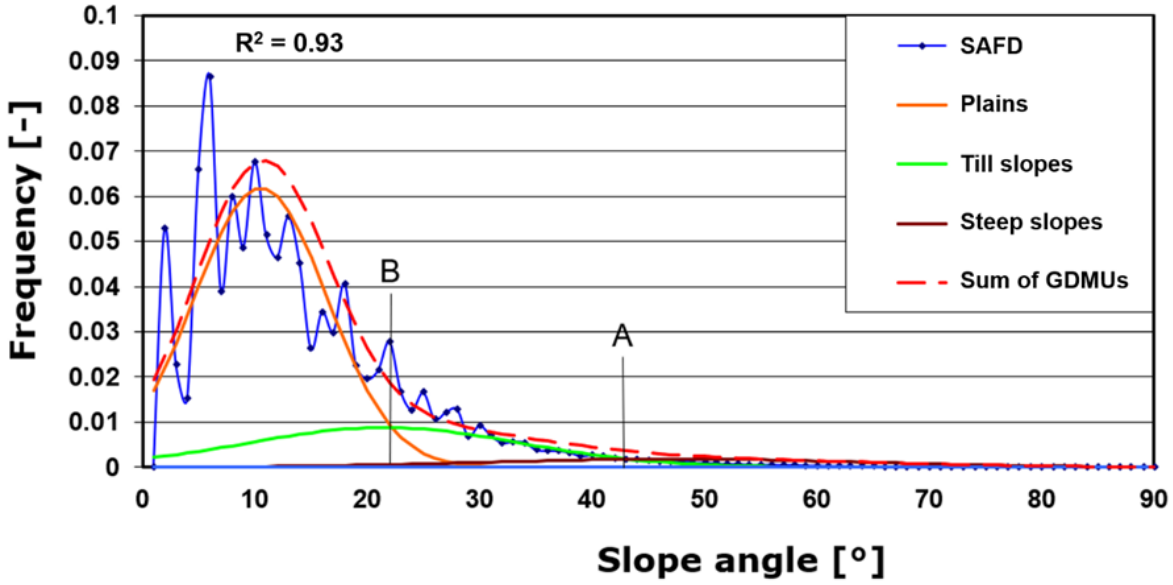

Fig. 40. SAD analysis for Area3 after elimination of outliers. A = 42°, B= 22° and R^2 = 0.93.

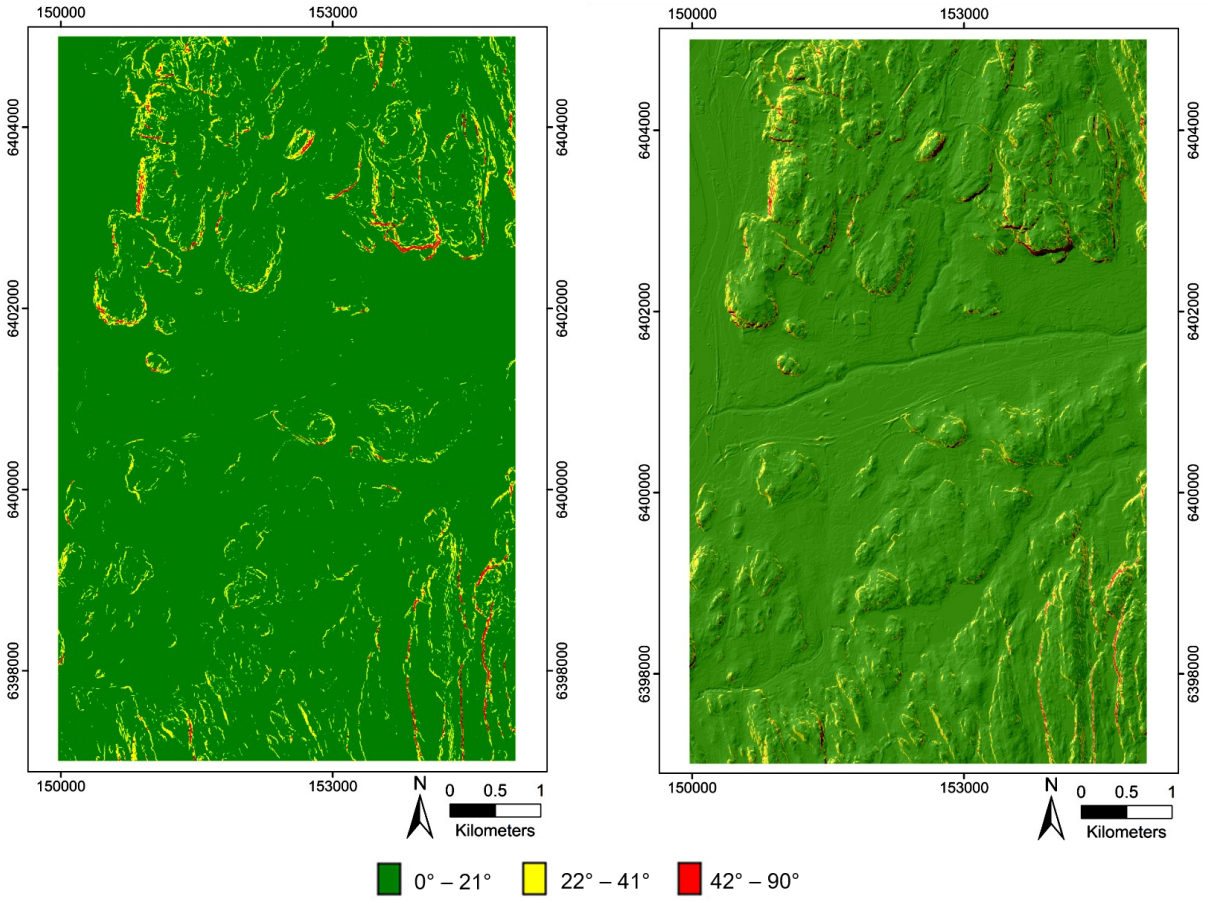

Fig. 41. To the left: Reclassification of the slope angle values according to the SAD analysis results for Area 3. To the right: Relationship of the slope distribution and the topography. Colors appear darker because the slope map has 50% of transparency to make the topography (hillshade) visible.

5.3 CONEFALL

5.3.1 Rockfall simulation using sources extracted with the SAD method

CONEFALL suggests the user to set an initial cone slope angle value between 27° and 37°, as it is based on the energy line method (See section 2.7.1). According to the empirical values, between 70% and 100% of the blocks are stopped at an energy line angle (cone slope angle in CONEFALL) of approximately 33° (Fig. 8). This value was hence chosen for all the rockfall simulations performed with this software.

For the Fjällbo area, the longest runout is located below the most prominent and high cliffs, where the climbing area is located. The runout distance ranges between 59 and 82 m. For the small nearby cliffs, the runout zones span 20 to 37 m (Fig. 42, 43). The longest runout in Area 2 is still located in the cliffs of the Fjällbo climbing area and has the same values as described above. The shortest runout distances are located towards the west, and range between 25 and 29 m (Fig. 44, 45).

In Area 3, the northern part has the longest runout distance, ranging between 75 and 84 m. In the southwestern part of the study area the runout zones are shorter, ranging between 38 and 46 m (Fig. 46, 47).

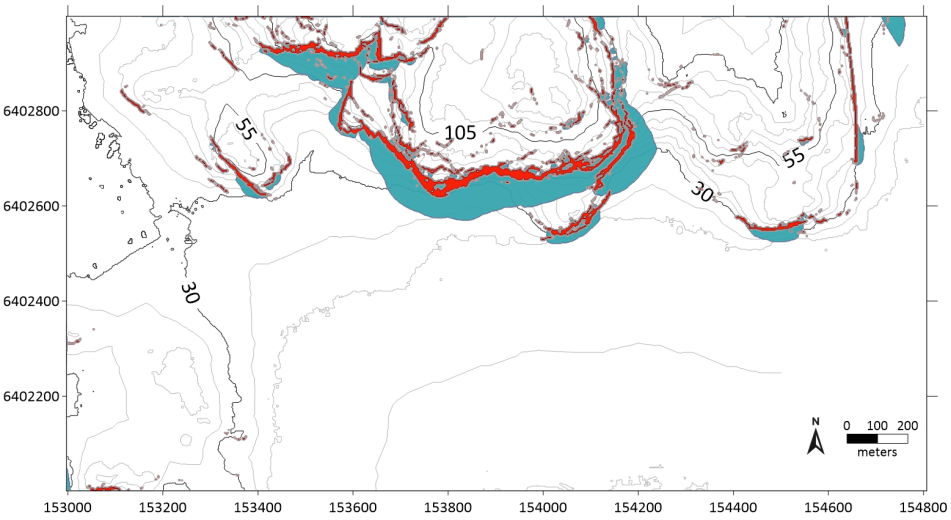

Fig. 42. Simulated runout zones using a cone slope angle of 33° in the Fjällbo area. Rockfall sources are highlighted in red and runout distances in blue. Contours, sources, and runout zones were extracted from the GRD files generated by CONEFALL and mapped in Surfer 17.

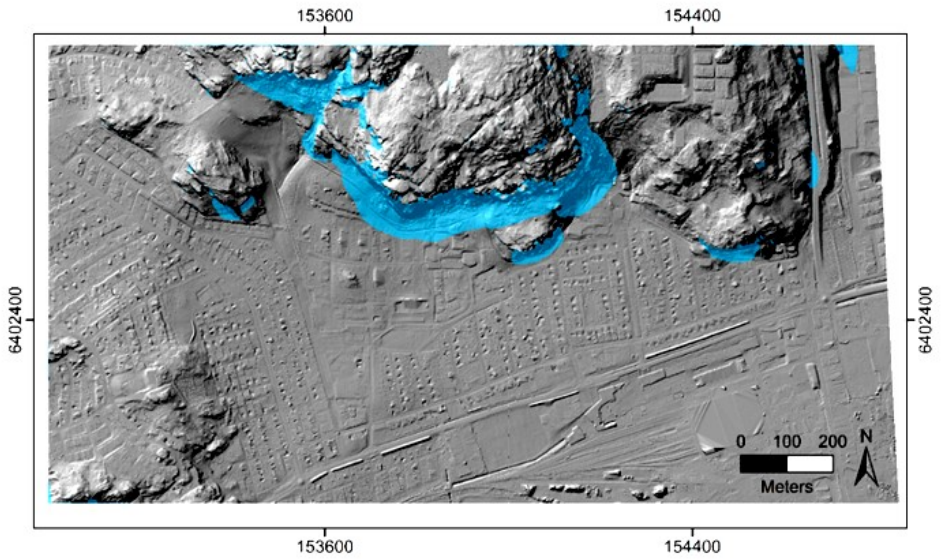

Fig. 43. Simulated runout zones (blue) superimposed on the hillshade map of the Fjällbo area

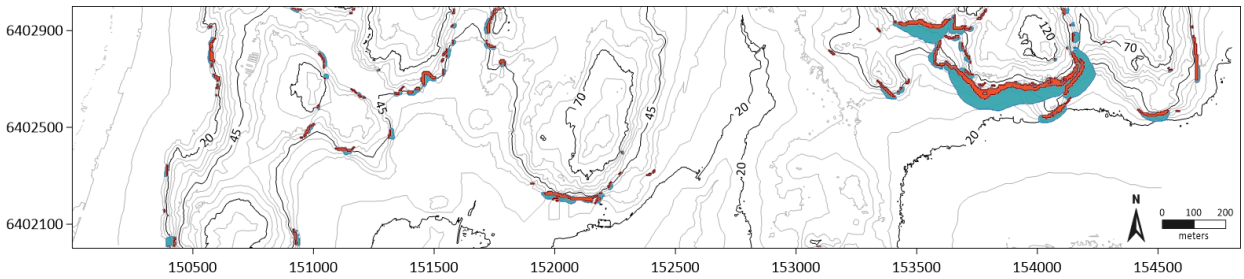

Fig. 44. Simulated runout zones using a cone slope angle of 33° in Area 2. Rockfall sources are highlighted in red and runout distances in blue. Contours, sources, and runout zones were extracted from the GRD files generated by CONEFALL and mapped in Surfer 17.

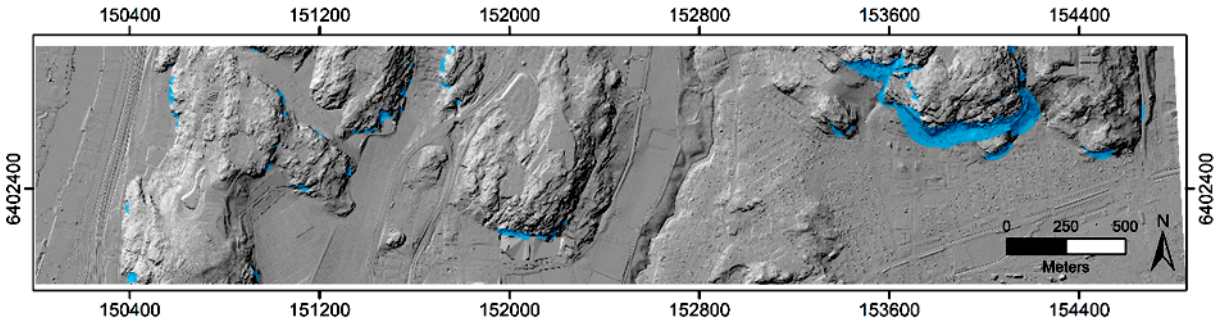

Fig. 45. Simulated runout zones (blue) superimposed on the hillshade map of Area 2.

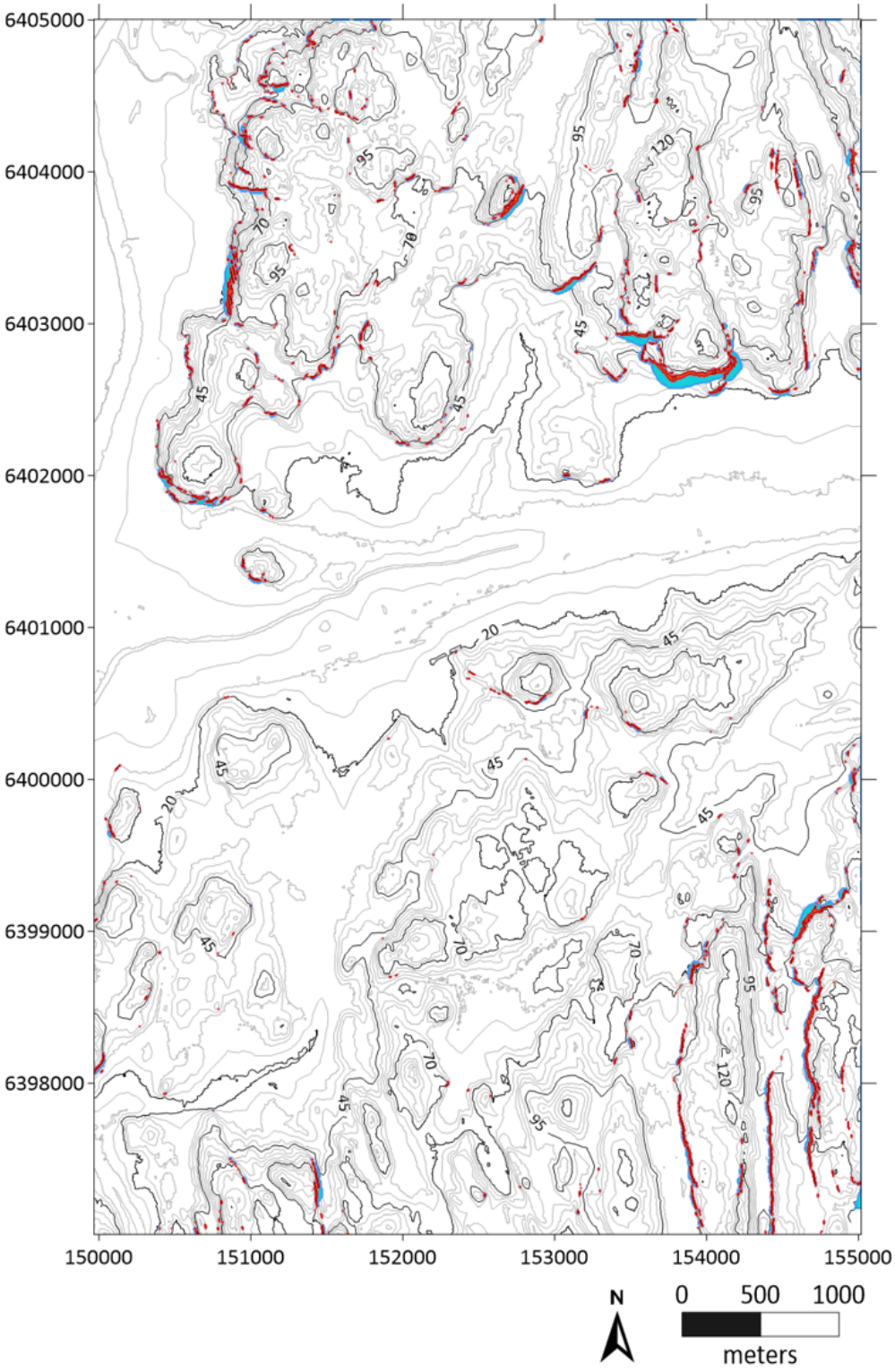

Fig. 46. Simulated runout zones using a cone slope angle of 33° in Area 3. Rockfall sources are highlighted in red and runout distances in blue. Contours, sources, and runout zones were extracted from the GRD files generated by CONEFALL and mapped in Surfer 17.

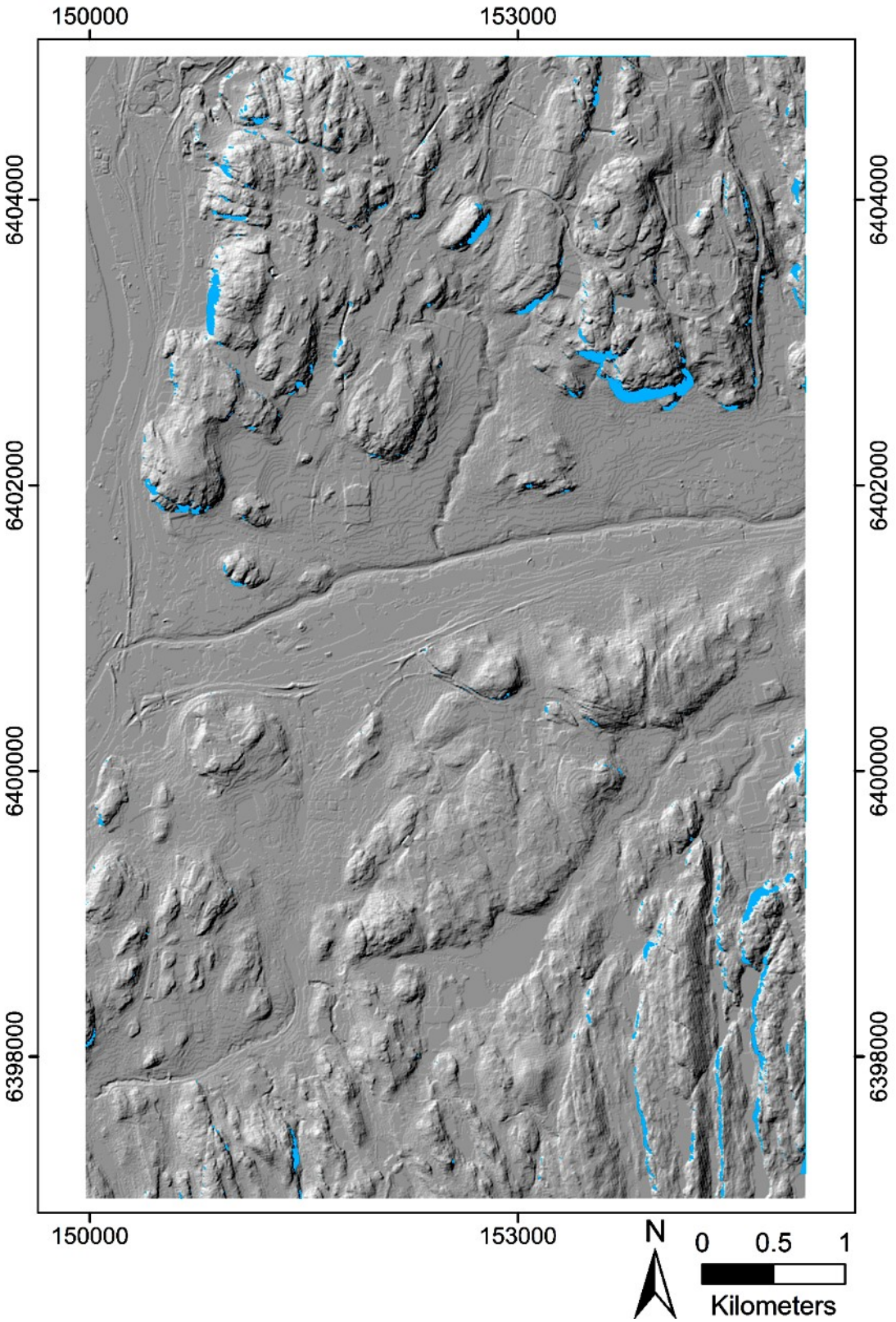

Fig. 47. Simulated runout zones (blue) superimposed on the hillshade map of Area 3.

5.3.2 Rockfall simulation using individual sources in Fjällbo park

A more local approach was taken by choosing individual sources (individual blocks) within the Fjällbo area (West, Center and East. See section 4.4). The same cone slope angle, i.e. 33° as in the previous simulations was used. These potential rockfall sources show a runout distance of 93 m, 76 m and 67 m for West, Center and East, respectively. Their longest lateral extent is 141 m, 115 m and 108 m for West, Center and East, respectively (Fig. 48, 49).

The lateral extent on top of the cliffs does not represent a realistic scenario when considering the topography and morphology of the cliff, i.e. the runouts extend at high lateral angles along the steep cliff. The default value for the lateral extent in CONEFALL is 360°, which results in runout zones that can be seen in Figure 48 and 49. With the help of field observations, orthophotos and the hillshade extraction in ArcMap, an aperture angle of 35° in direction south-north was selected to represent a more realistic lateral extent in each of the cases.

After constraining the aperture angle, the lateral extent is 94 m, 74 m and 68 m for West, Center and East, respectively at the longest runout. Vertical runout distances remain the same (Fig. 50, 51). In the figures, some of the contours have blocky corners. This is a result of the data gridding although these are the smoothest results obtained using a spacing of 1 for the grids (See section 4.4).

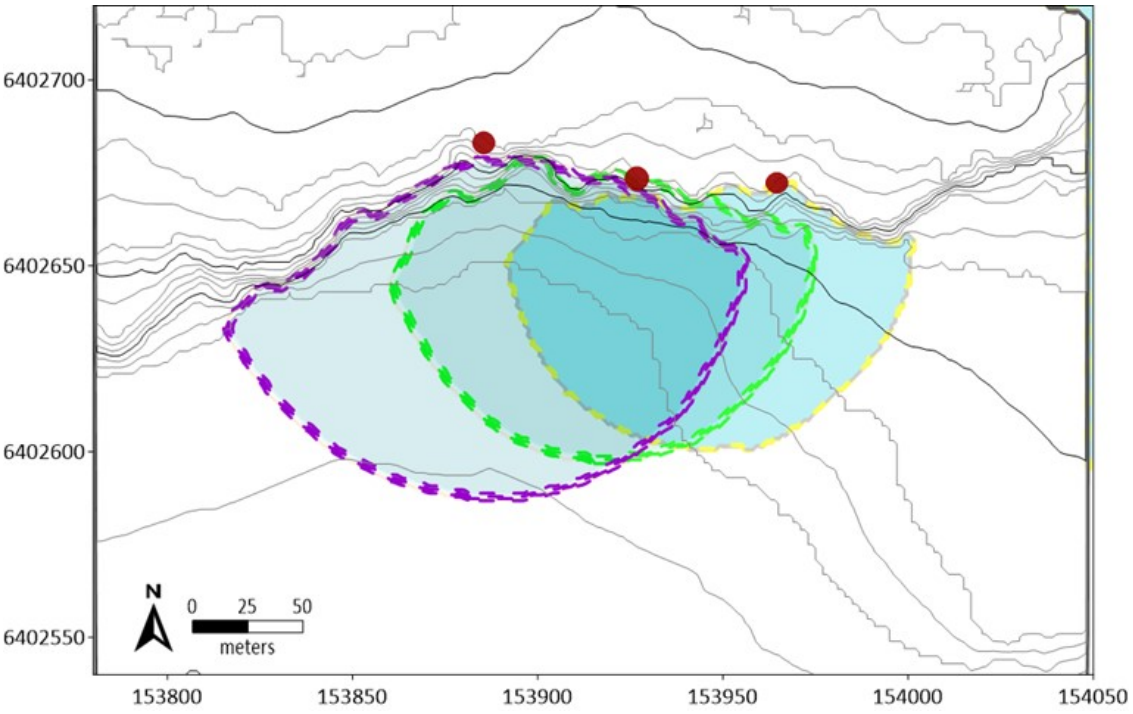

Fig. 48. Simulated runout zones using a cone slope angle of 33° for individual blocks in Fjällbo climbing area. The red dots show the location of the sources. Runout sources are delineated in purple, green and yellow for the West, Center and East sources, respectively.

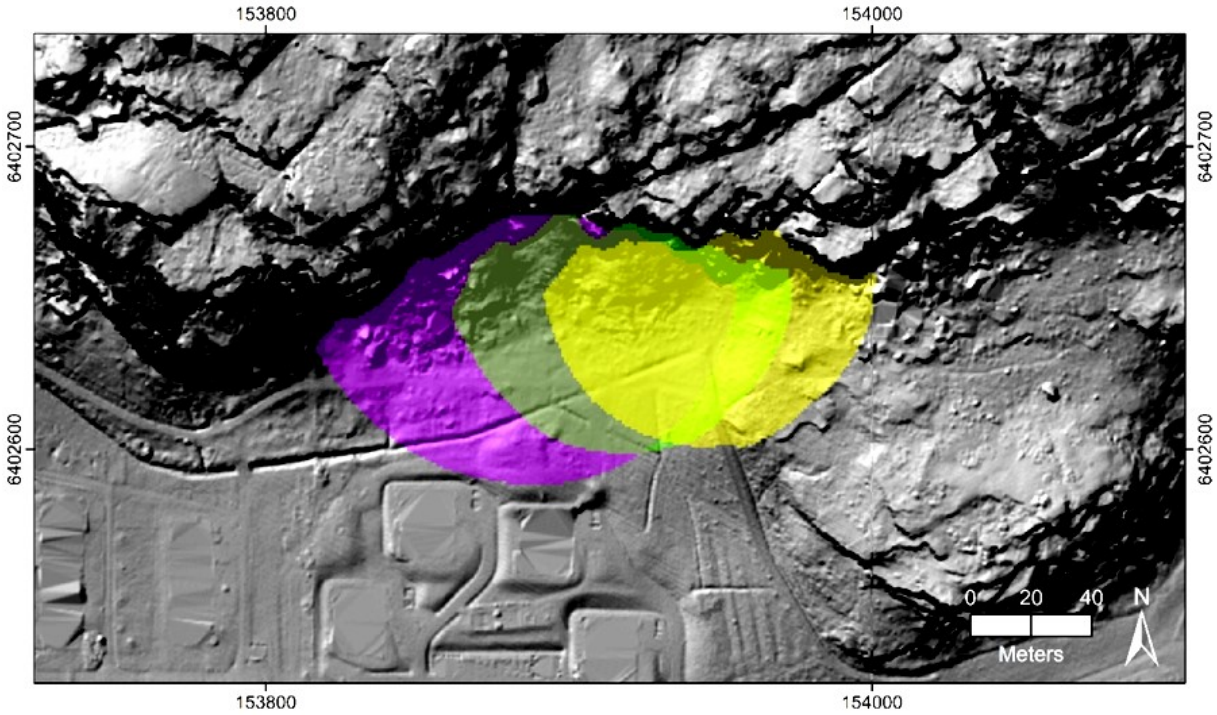

Fig. 49. Simulated runout zones superimposed on the hillshade map of Fjällbo. Runout zones are highlighted in purple, green and yellow for the West, Center and East sources, respectively.

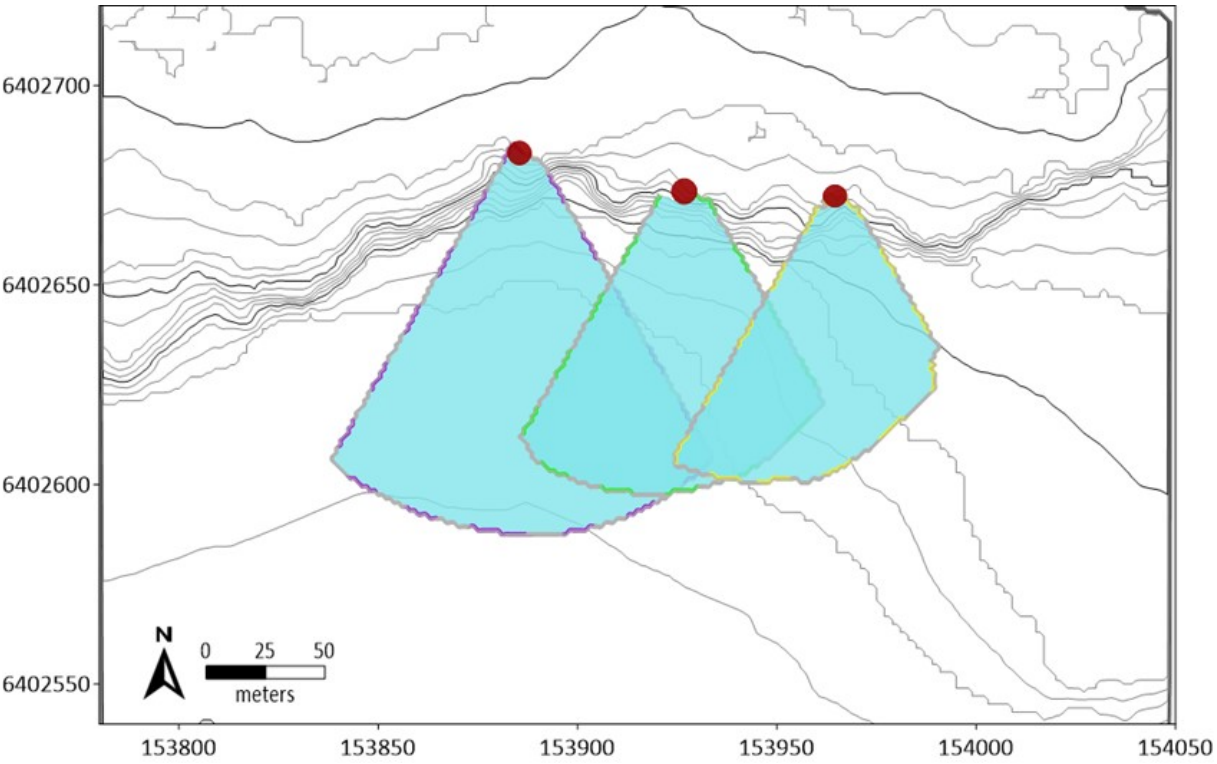

Fig. 50. Simulated runout zones using a cone slope angle of 33° and an aperture angle of 35° for individual blocks in Fjällbo climbing area. The red dots show the location of the sources. Runout sources are delineated in purple, green and yellow for the West, Center and East sources, respectively.

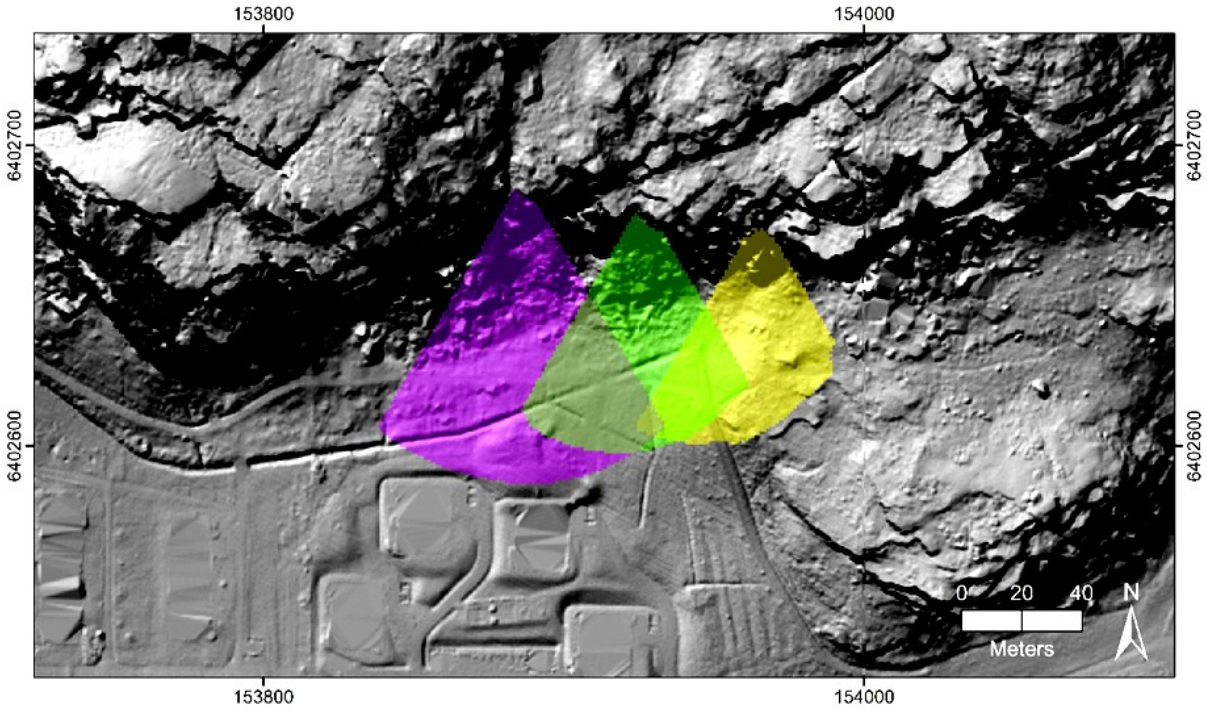

Fig. 51. Simulated runout zones (after setting the aperture angle constrain) superimposed on the hillshade map of Fjällbo. Runout zones are highlighted in purple, green and yellow for the West, Center and East sources, respectively.

5.3.3 Verification point: 2017 rockfall

As part of this local approach, and to verify the usefulness of the software, a source point was selected where the pillar that generated the 2017 rockfall in Fjällbo was located. The cone slope and aperture angle were set to the same values as in the previous simulations. For the previous simulations, however, the Fahrböschung energy line method was used, as the sources were located in the top part of the cliffs. In contrast, for the 2017 rockfall simulation, the shadow angle method was chosen (See section 2.3.2) as the source was located at an intermediate height in the rock wall. The resulting runout distance is 58 m and the lateral extent at longest runout is 62 m (Fig. 52), 14.5 m longer (from the longest real runout to the longest simulated runout) than the extent measured in the field; nevertheless, the limits of the lateral extent are well represented by the simulation (Fig. 53).

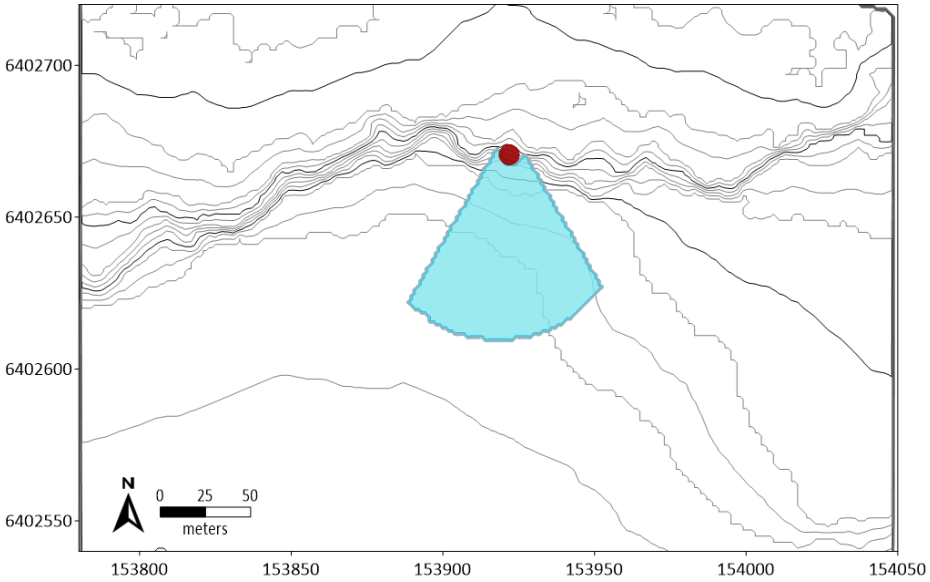

Fig. 52. Simulated runout zones using a cone slope angle of 33° and an aperture angle of 35° for the 2017 rockfall source in Fjällbo. The red dot shows the location of the source.

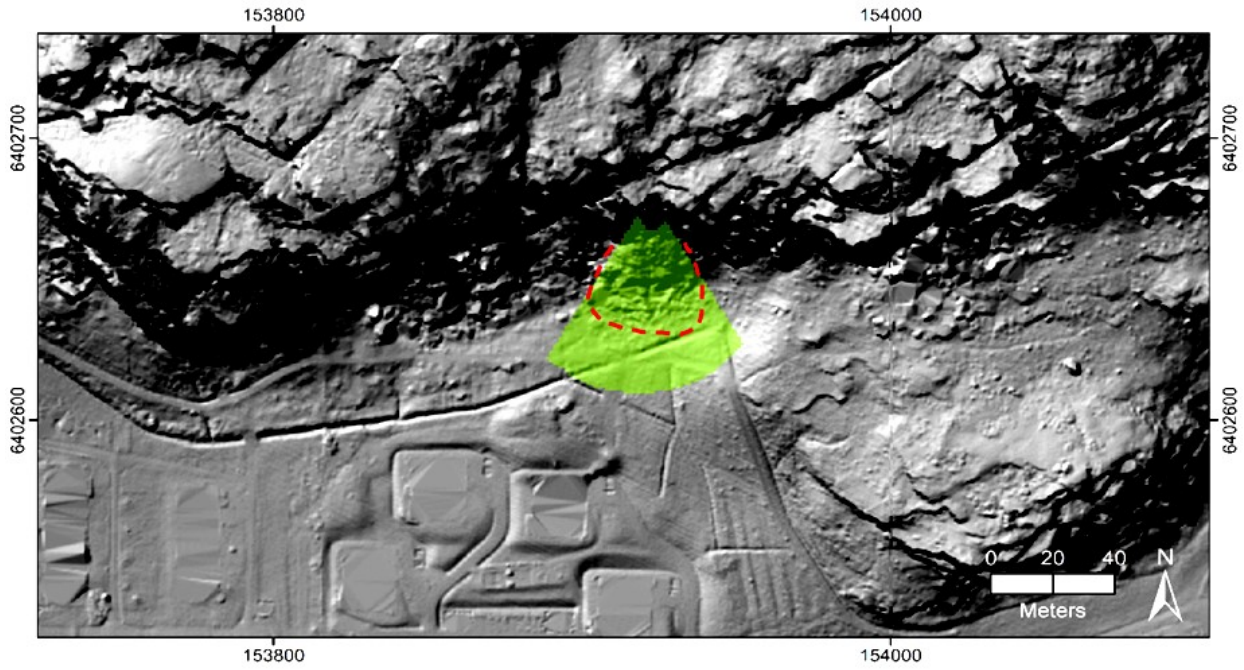

Fig. 53. Simulated runout zone of the 2017 rockfall superimposed on the hillshade map of Fjällbo. The dashed red line shows the measured extent of the 2017 rockfall.

5.4 RockyFor3D

The general configuration and principal elements in the Fjällbo climbing area are shown in Figure 54. Starting from this baseline, and, in order to test the sensitivity and effect of the parameters provided by RockyFor3D (Section 2.7.2), different settings for the simulations were tested. Runout distances are measured from north to south from the bottom of the cliff for the East source, considering that this source does not pose a talus slope, and from the top of the talus slopes for the Center and West sources, to the longest simulated point. The maximum lateral extent was measured from west to east in the longest position of the runout zones. Darker colors in all simulations outputs show the most likely path followed by the block; the trajectories that do not follow this direction are less likely but still possible.

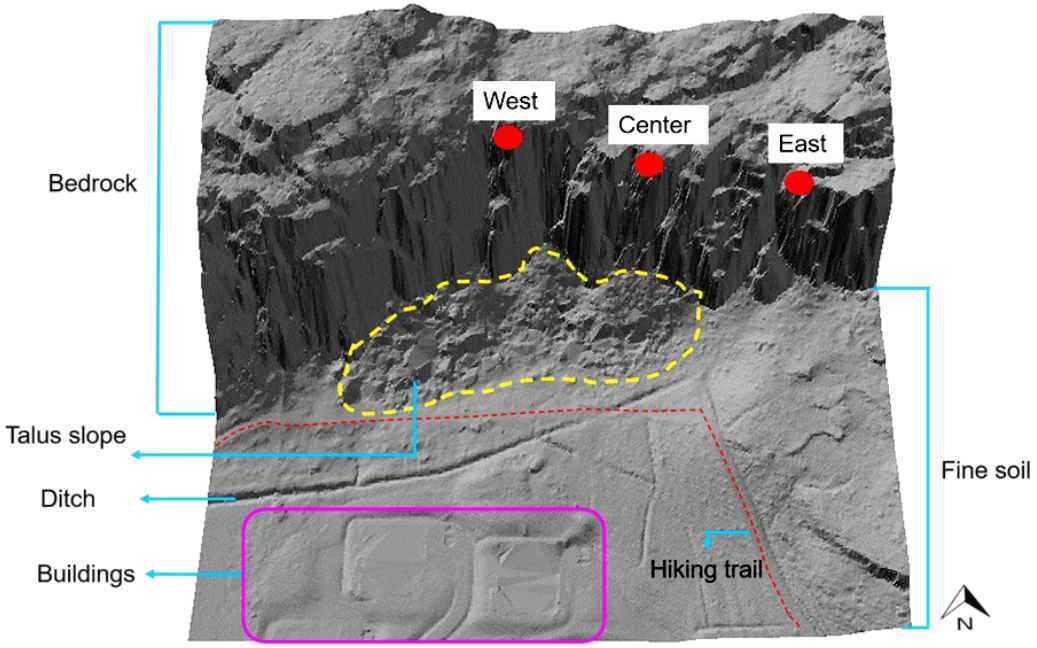

Fig. 54. General configuration of the Fjällbo climbing area.

5.4.1 Setting 1

Block shape chosen for the three sources was rectangular, block dimensions (height, width, length) for West = 3 x 4 x 6 m (V = 72 m^3 and M = 194.40 Ton), Center = 3 x 3 x 6 m (V = 54 m^3 and M = 145.80 Ton) and East = W = 3 x 4 x 4 m (V = 48 m^3 and M = 129.60 Ton). Methodology to calculate volume and mass is described in Section 4.5. As for the soil type, bedrock was chosen for sources and cliff wall, fine soil for the bottom of the cliff, and the ditch was considered as a water body (See section 2.7.2 for definition of soil type in the software). No trees in the area and zero roughness, were assumed. Figure 55 shows a runout distance of 53 m, 61 m and 76 m, and a lateral extent of 88 m, 102 m and 117 m, for East, Center and West, respectively.

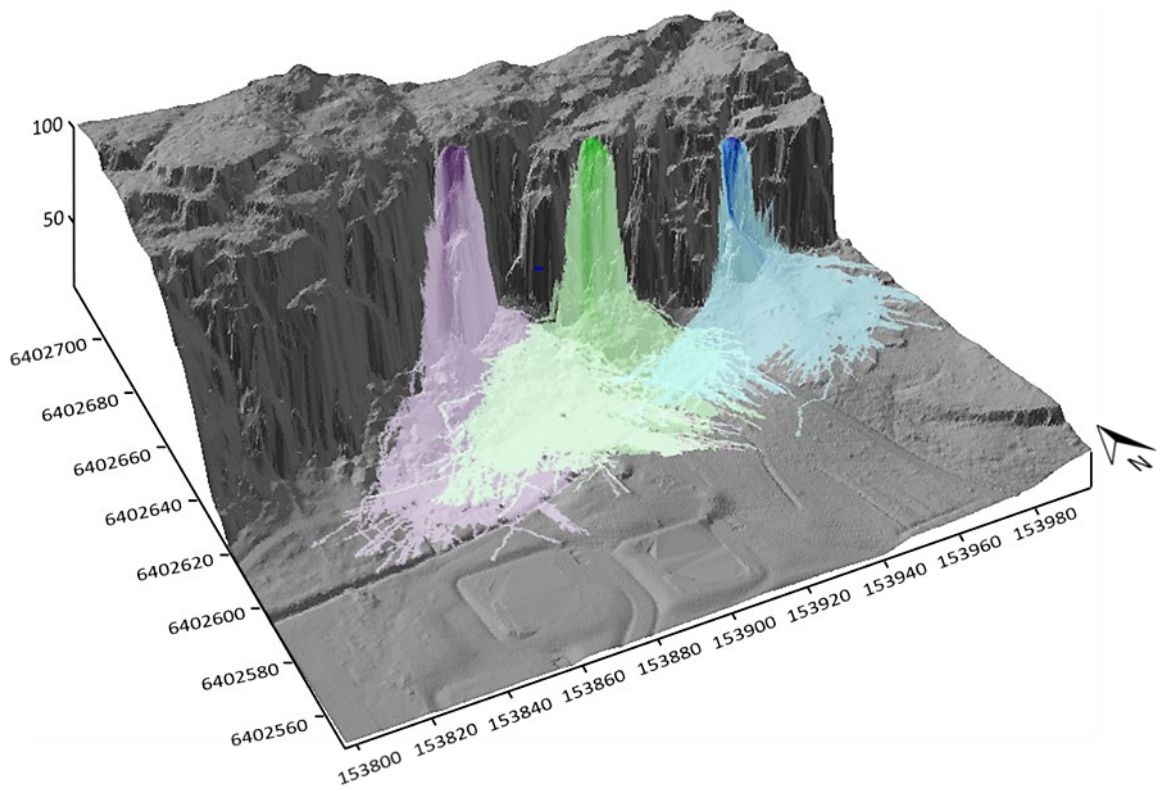

Fig. 55. Runout distances after simulation with parameters according to Setting 1. Runout zone for the West source = purple, runout zone for the Center source = green, runout zone for the East source = blue.

5.4.2 Setting 2

Block shape is spherical in this setting, dimensions were slightly changed in order to make them comparable to the ones in Setting 1, as volume calculations change. For West = 5 x 4.5 x 6 m (V = 71.864 m^3 and M = 194.03 Ton), Center = 3.5 x 5 x 6 m (V = 54.297 m3 and M = 146.60 Ton) and East = W = 4.5 x 4.5 x 5 m (V = 47.713 m^3 and M = 128.82 Ton). All other parameters were identical to Setting 1. Figure 56 shows a runout distance of 49 m, 67 m and 78 m, and a lateral extent of 80 m, 99 m and 130 m, for East, Center and West, respectively.

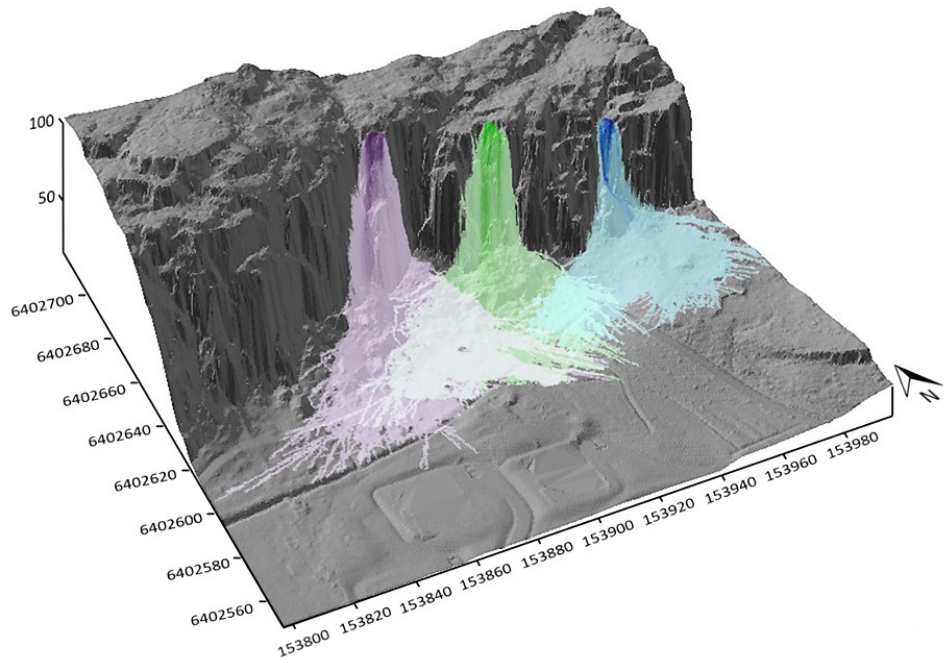

Fig. 56. Runout distances after simulation with parameters according to Setting 2. Runout zone for the West source = purple, runout zone for the Center source = green, runout zone for the East source = blue.

5.4.3 Setting 3

Block size in this setting was doubled. For West = 6 x 8 x 12 m (V = 576 m^3 and M = 1555.2 Ton), Center = 6 x 6 x 12 m (V = 432 m3 and M = 1166.4 Ton) and East = W = 6 x 8 x 8 m (V = 384 m^3 and M = 1036.8 Ton). All other parameters were identical to Setting 1. Figure 57 shows a runout distance of 47 m and 61 m, and a lateral extent of 81 m and 66 m, for East and Center, respectively. In this setting, an exception was made when measuring the lateral extent of West, since a particular trajectory exceeds the others in the west part at the bottom of the cliff (marked in Figure 57). Without this trajectory, the lateral extent is 92 m; with it, the extent is 130 m. The respective runout distance is 74 m.

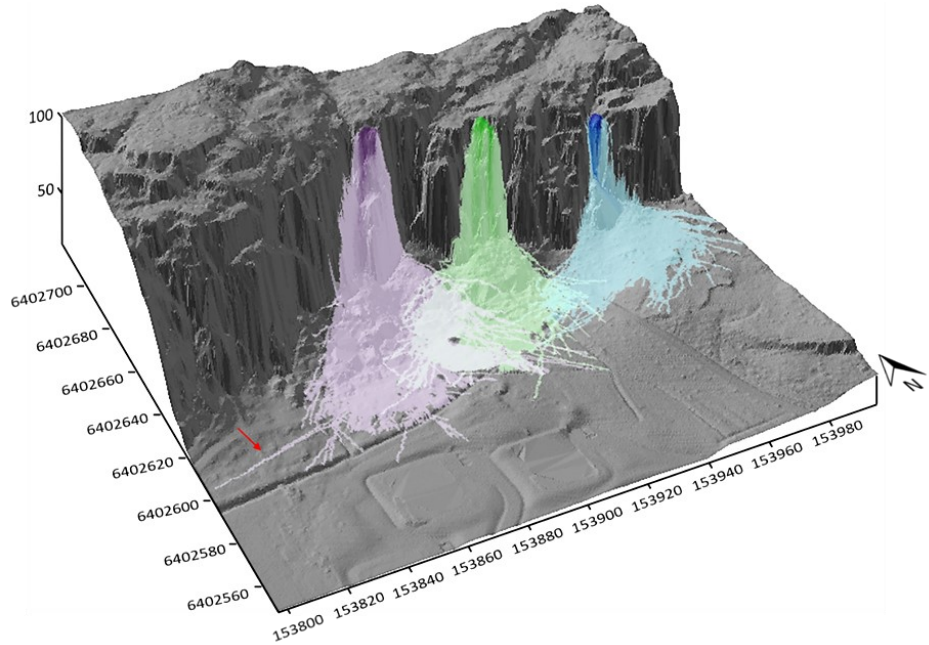

Fig. 57. Runout distances after simulation with parameters according to Setting 3. Runout zone for the West source = purple, runout zone for the Center source = green, runout zone for the East source = blue. The red arrow shows the exceptional trajectory (See text for explanation).

5.4.4 Setting 4

Block sizes and shapes are the same as originally (Setting 1). In order to see the effect of the coefficient of restitution on the runout zones, the soil type at the bottom of the cliff (including the talus slopes) were taken as 0, i.e. it was assumed as a material that blocks can penetrate completely (See section 2.7.2). Other conditions were the same as the original ones. Figure 58 shows a runout distance of 32 m, 54 m and 59 m, and a lateral extent of 60 m, 42 m and 46 m, for East, Center and West, respectively.

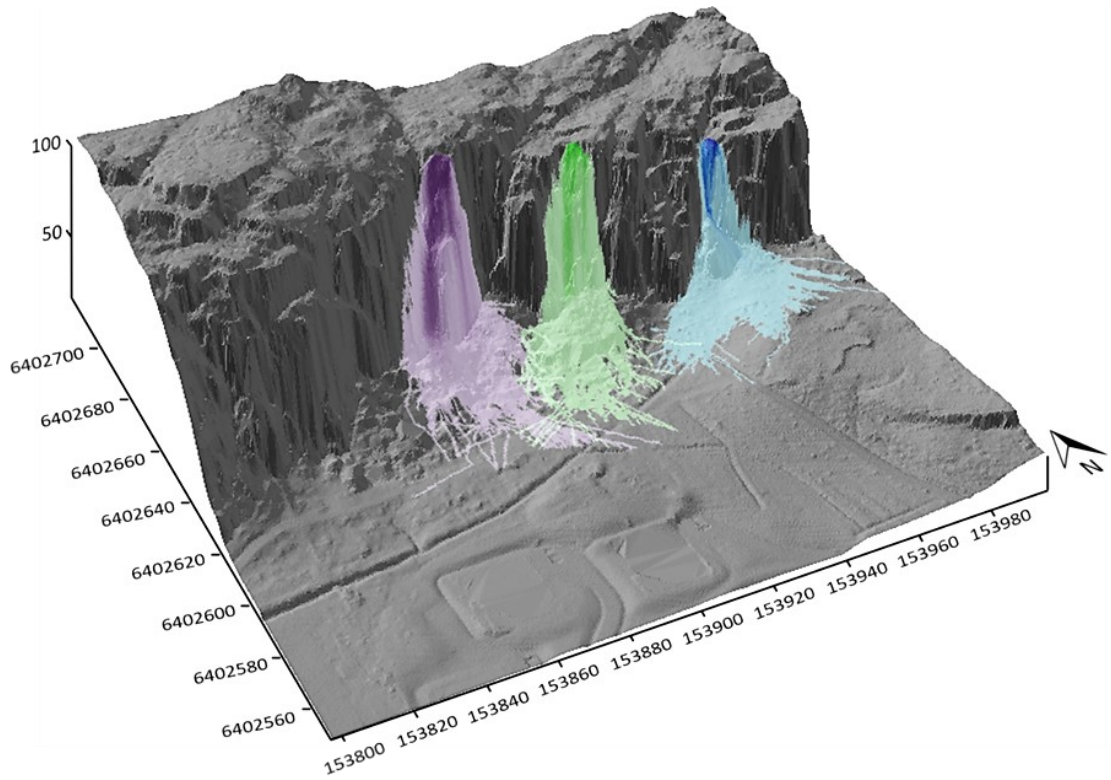

Fig. 58. Runout distances after simulation with parameters according to Setting 4. Runout zone for the West source = purple, runout zone for the Center source = green, runout zone for the East source = blue.

5.4.5. Setting 5

The complete opposite scenario, regarding the coefficient of restitution, was taken i.e. the soil type at the bottom of the cliff (including talus slopes and the ditch) was taken as 6, i.e. bedrock (See section 2.7.2); the ditch was assumed as a topographic low only. Other conditions were the same as the original ones. For better visualization purposes, in this case, the runout zones were separated. Figures 59 shows a runout distance of 85 m, and a lateral extent of 174 m for East. Figure 60 indicates a runout distance of 80 m, and a lateral extent of 150 m for Center. Lastly, Figure 61 indicates a runout distance of 84 m, and a lateral extent of 132 m for West.

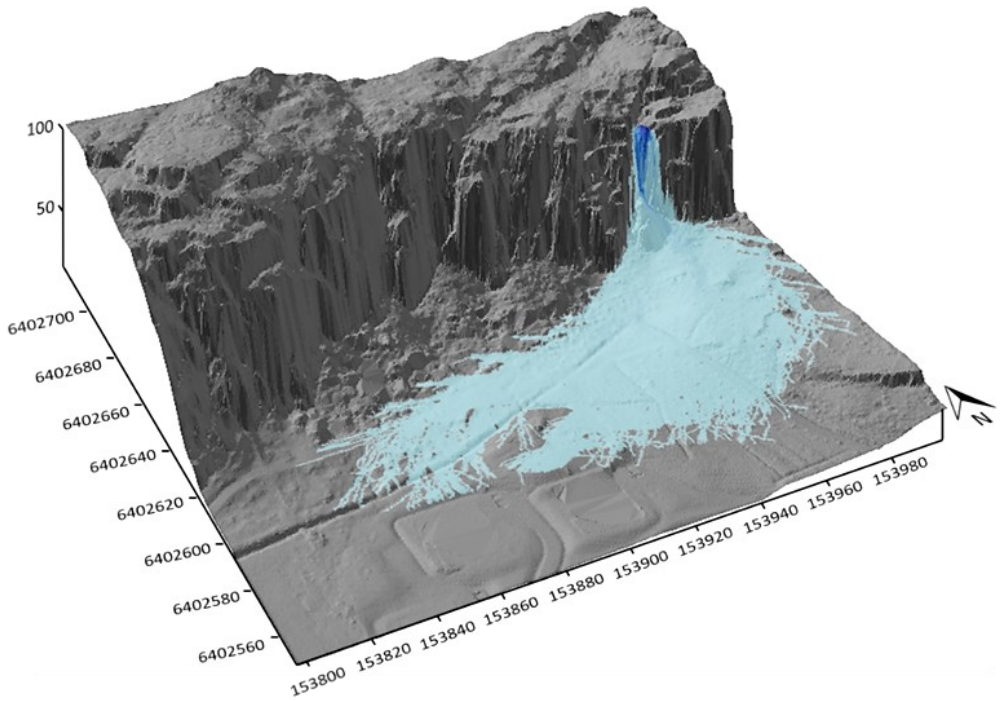

Fig. 59. Runout distances for the East source after simulation with parameters according to Setting 5.

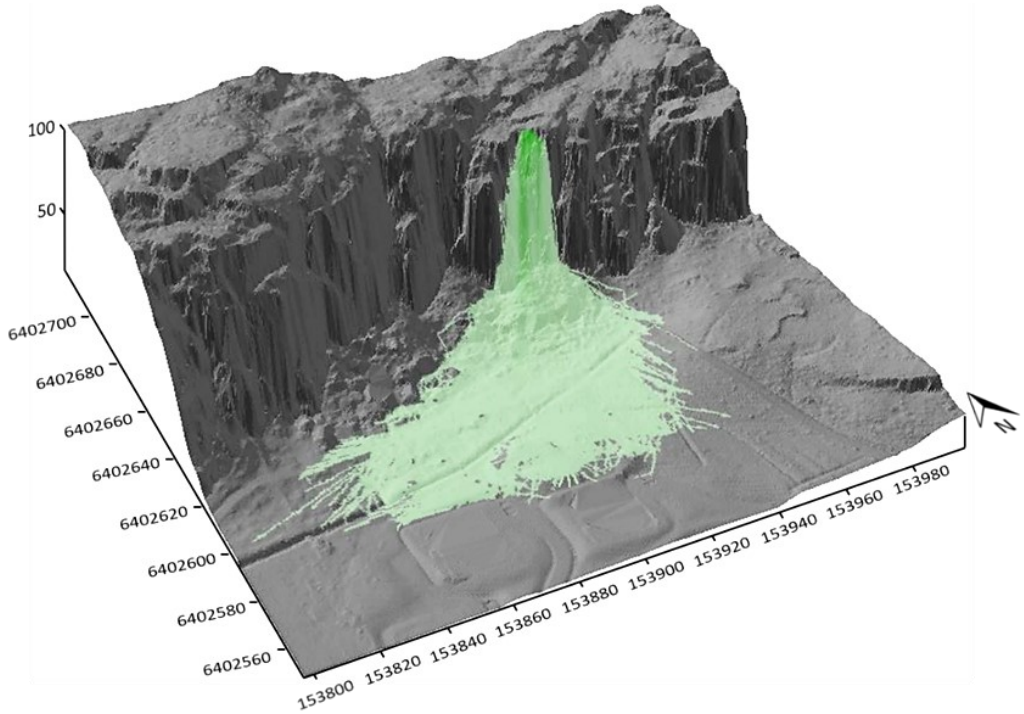

Fig. 60. Runout distances for the Center source after simulation with parameters according to Setting 5.

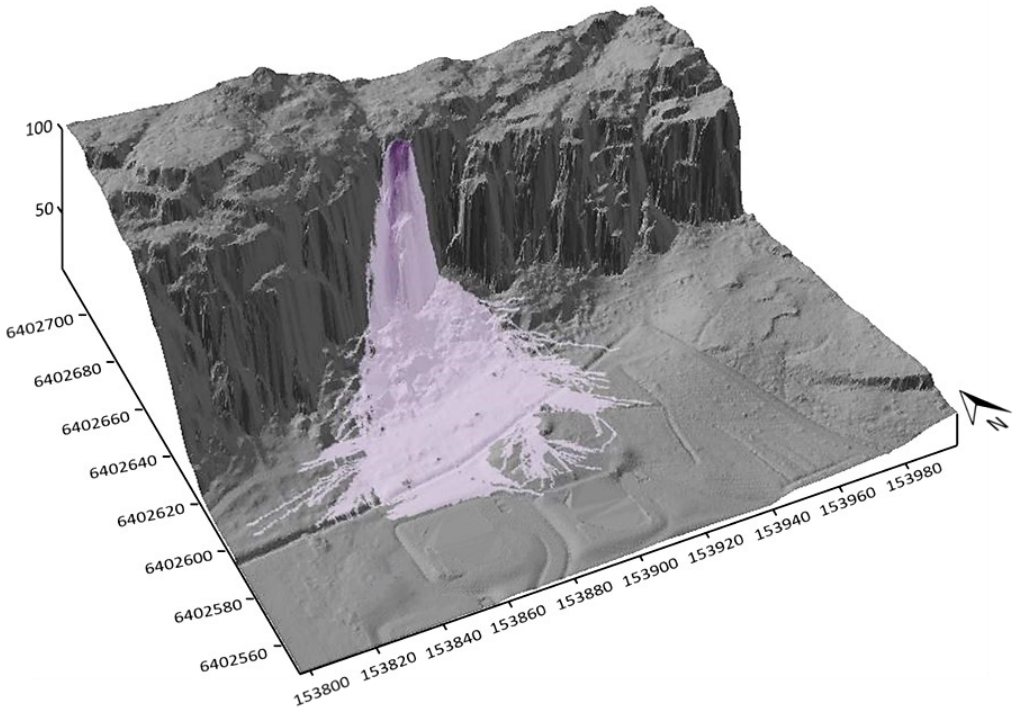

Fig. 61. Runout distances for the West source after simulation with parameters according to Setting 5.

5.4.6. Setting 6

This and the following two settings are focused on the protective effect that forest provides. The data taken in the field (Section 4.2) were plotted on the TIN and simulations were run with initial parameters unchanged (Setting 1) but adding data of the trees. Figure 62 displays the distribution of the trees as well as the runout zones in this simulation. It shows a runout distance of 41 m, 60 m and 63 m, and a lateral extent of 78 m, 76 m, and 118 m, for East, Center and West, respectively.

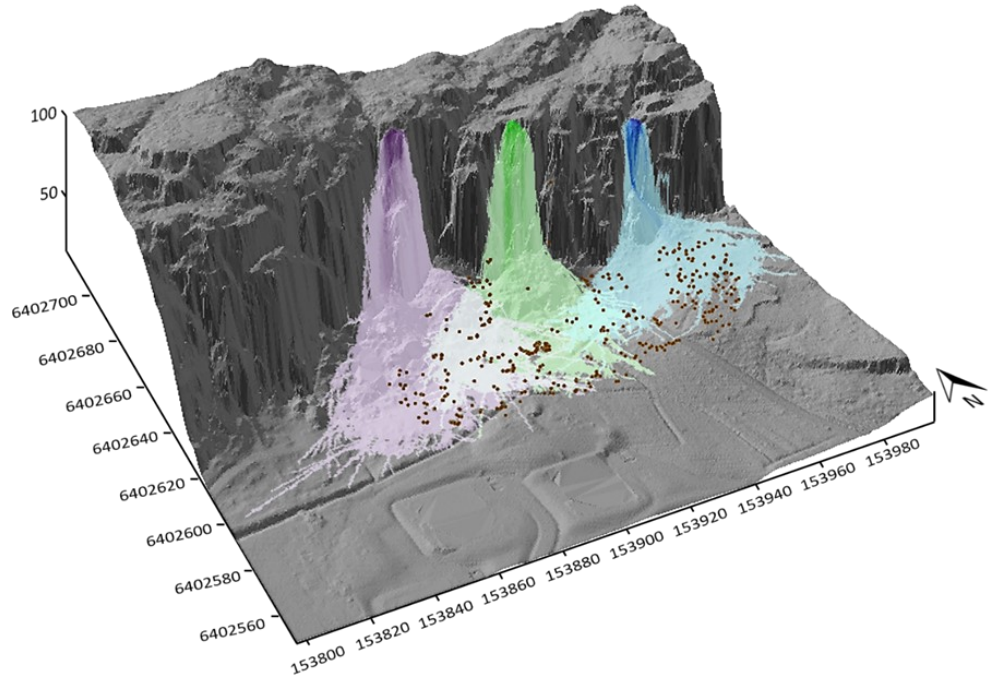

Fig. 62. Runout distances after simulation with parameters according to Setting 6. Runout zone for the West source = purple, runout zone for the Center source = green, runout zone for the East source = blue. The brown dots represent the measured trees.

5.4.7. Setting 7

For this setting, the DBH of all the three was manually increased by a factor of 3. All other parameters remained as original (Setting 1). Figure 63 displays the distribution of the trees as well as the runout zones. It shows a runout distance of 38 m, 63 m and 63 m, and a lateral extent of 77 m, 78 m, and 120 m, for East, Center and West, respectively.

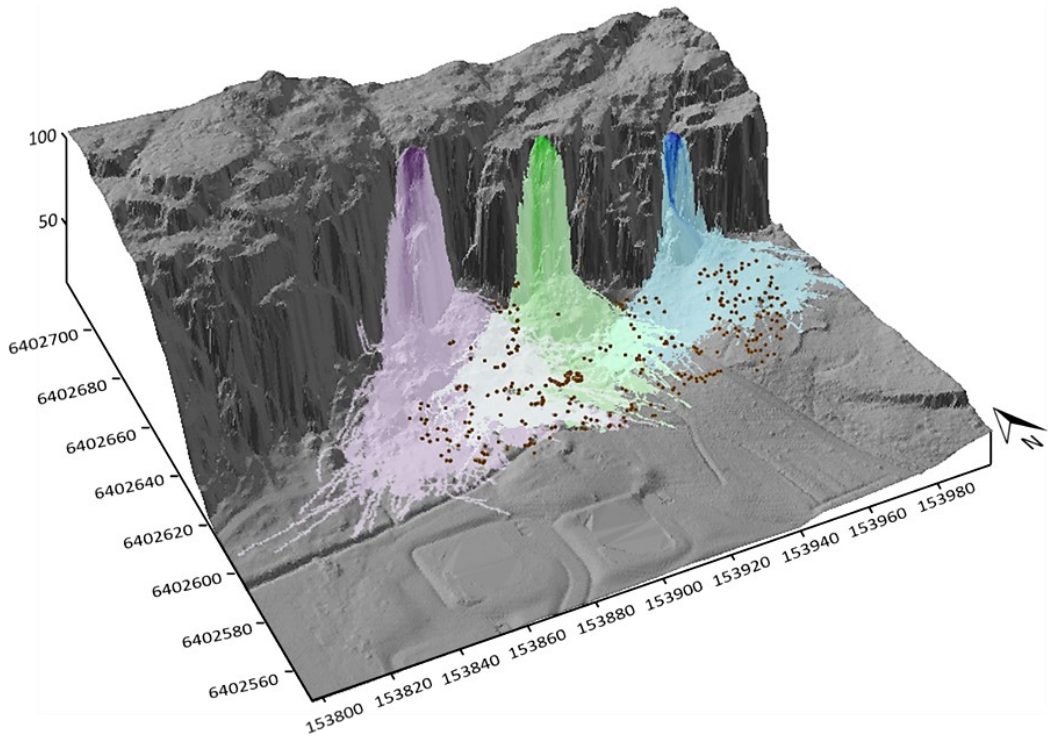

Fig. 63. Runout distances after simulation with parameters according to Setting 7. Runout zone for the West source = purple, runout zone for the Center source = green, runout zone for the East source = blue. The brown dots represent the measured trees.

5.4.8. Setting 8

For this setting, the density of the forest was increased. The new density consists of trees equally spaced every 2 m, DBH values correspond to random numbers between the lowest and highest values measured in the field. All other parameters were the same as in the original (Setting 1). Figure 64 displays the distribution of the trees as well as the runout zones. Figure 65 shows a runout distance of 28 m and 46 m, and a lateral extent of 62 m and 64 m, for East and Center, respectively. For West, an exception was made when measuring the runout distance, since a particular trajectory exceeds the others (marked in Figure 65). Without this trajectory the runout distance is 47 m, with it, the distance is 70 m, and the lateral extent is 78 m.

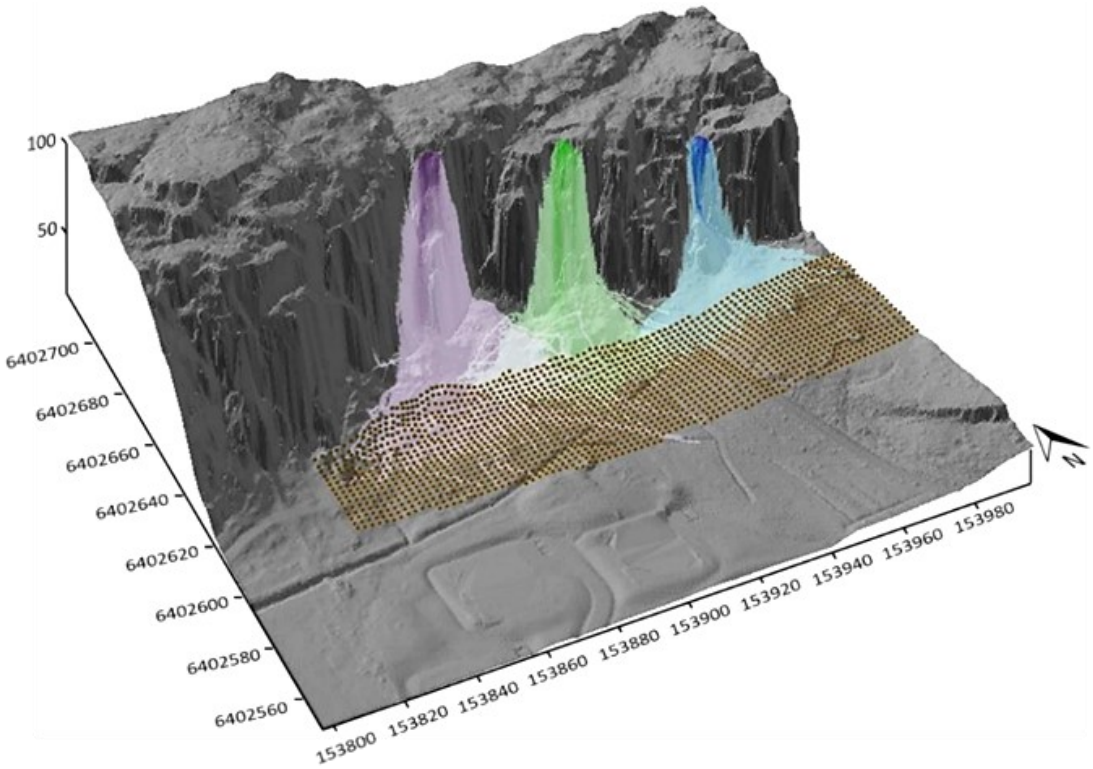

Fig. 64. Runout distances after simulation with parameters according to Setting 8. Runout zone for the West source = purple, runout zone for the Center source = green, runout zone for the East source = blue. The brown dots represent the tree cover ascribed for the simulation.

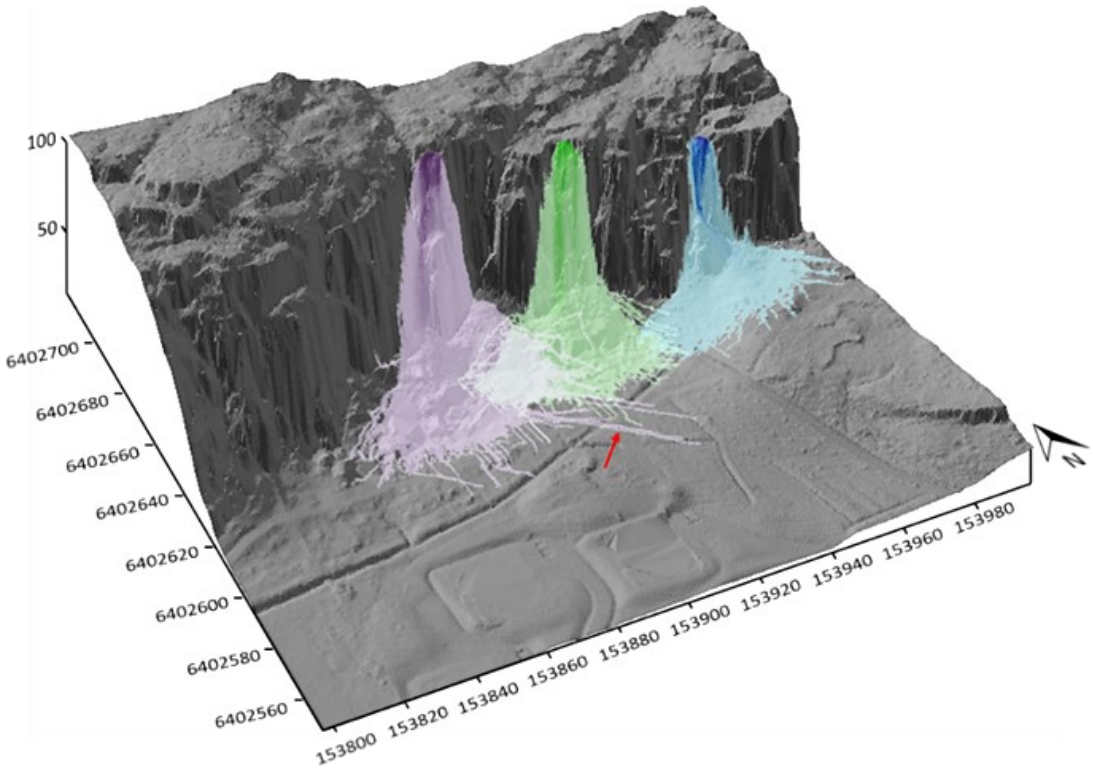

Fig. 65. Runout distances after simulation with parameters according to Setting 8. Runout zone for the West source = purple, runout zone for the Center source = green, runout zone for the East source = blue. The tree cover ascribed for the simulation is not shown. The red arrow shows the exceptional trajectory (See text for explanation)..

5.4.9. Setting 9

This setting is focused on surface roughness. Polygons with the MOH measurements taken in the field (Section 4.2; Annex 1) were added for each slope. All other parameters were the same as in the original (Setting 1). Figure 66 shows a runout distance of 31 m and 45 m, and a lateral extent of 61 m, 46 m, for East and Center, respectively. For West, an exception was made when measuring the runout distance, since a particular trajectory exceeds the others (marked in Figure 66). Without this trajectory the runout distance is 31 m, with it, the distance is 62 m, and the lateral extent is 53 m.

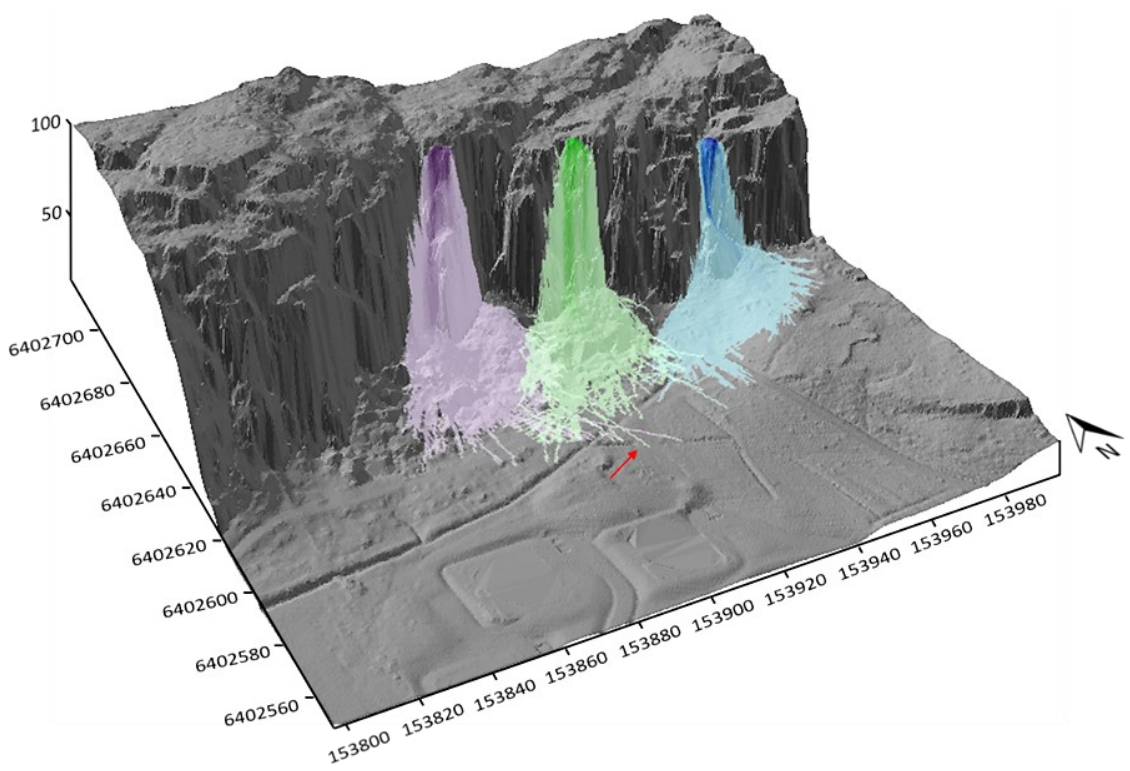

Fig. 66. Runout distances after simulation with parameters according to Setting 9. Runout zone for the West source = purple, runout zone for the Center source = green, runout zone for the East source = blue. The red arrow shows the exceptional trajectory (See text for explanation).

5.4.10. Setting 10

This setting represents a "combination" of Settings 6 and 9 and aims to be the most realistic scenario. Type of soil/rock, block size and block shape are the same as in Setting 1. Tree distribution and surface roughness (MOH) correspond to the measurements and observations made during the fieldwork. Figure 67 shows a runout distance of 29 m, 35 m and 43 m, and a lateral extent of 58 m, 42 m, and 52 m, for East, Center and West, respectively.

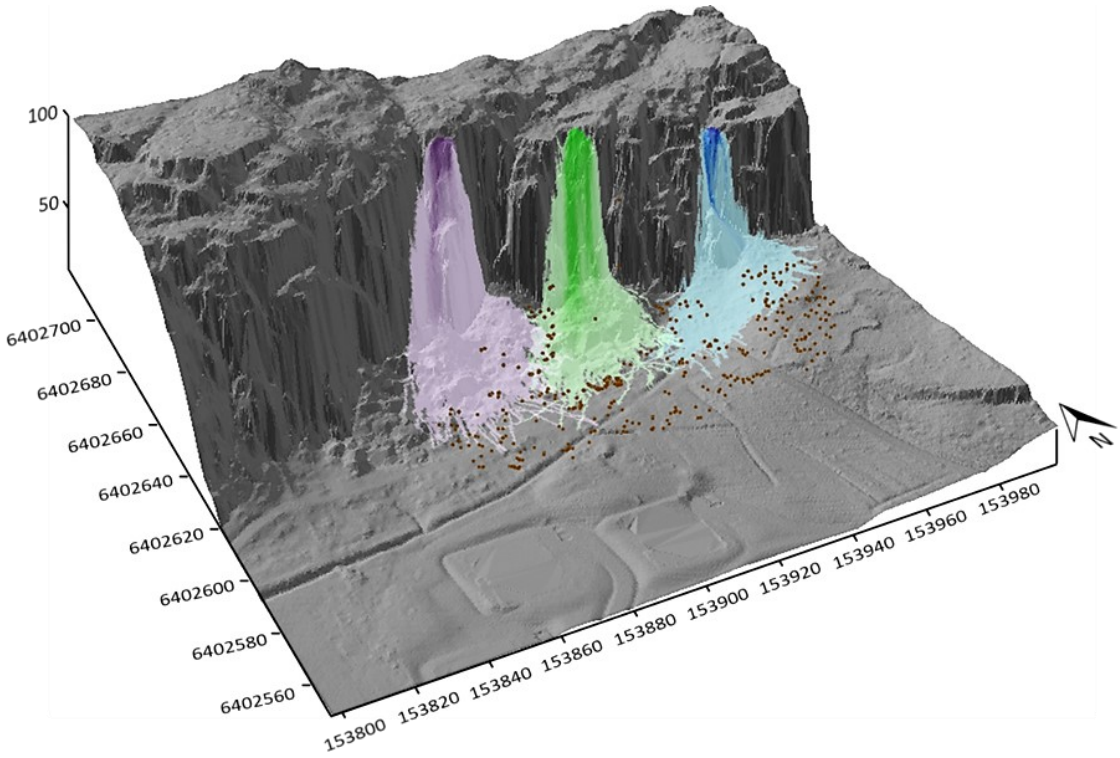

Fig. 67. Runout distances after simulation with parameters according to Setting 10. Runout zone for the West source = purple, runout zone for the Center source = green, runout zone for the East source = blue. The brown dots represent the measured trees.

5.4.11. Verification point: 2017 rockfall

With the help of aerial photos, and field verifications, the approximate extent of the 2017 rockfall was measured (Fig. 68). The runout distance is approximately 36 m (from the top of the talus slope, i.e., the vertical distance between the pillar and the top of the talus slope was not measured) and a lateral extent of 37 m. A simulation was performed applying similar conditions, i.e. a rectangular block that simulates the pillar of approximately 150 Ton, the tree distribution, type of soil and rock as described in the field. Considering there is evidence of older rockfalls, the surface roughness was estimated according to field observations, and only considering the blocks that seemed to be older than the ones brought down by the 2017 rockfall (See section 5.1); however, knowing what was exactly below these blocks and to measure their MOH is not possible. Figure 69 shows the simulated extent of the 2017 rockfall. The longest runout distance is 48 m and the lateral extent 68 m.

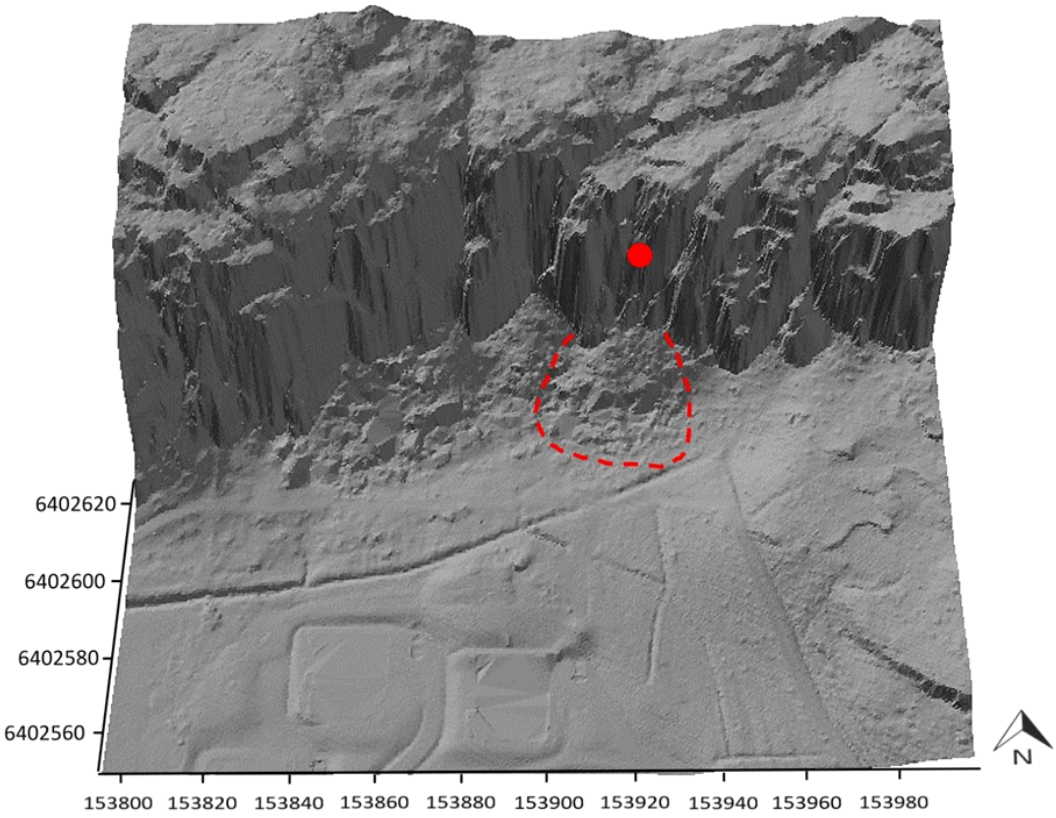

Fig. 68. Location of the 2017 rockfall source (red dot) and measured runout distance (red dashed line).

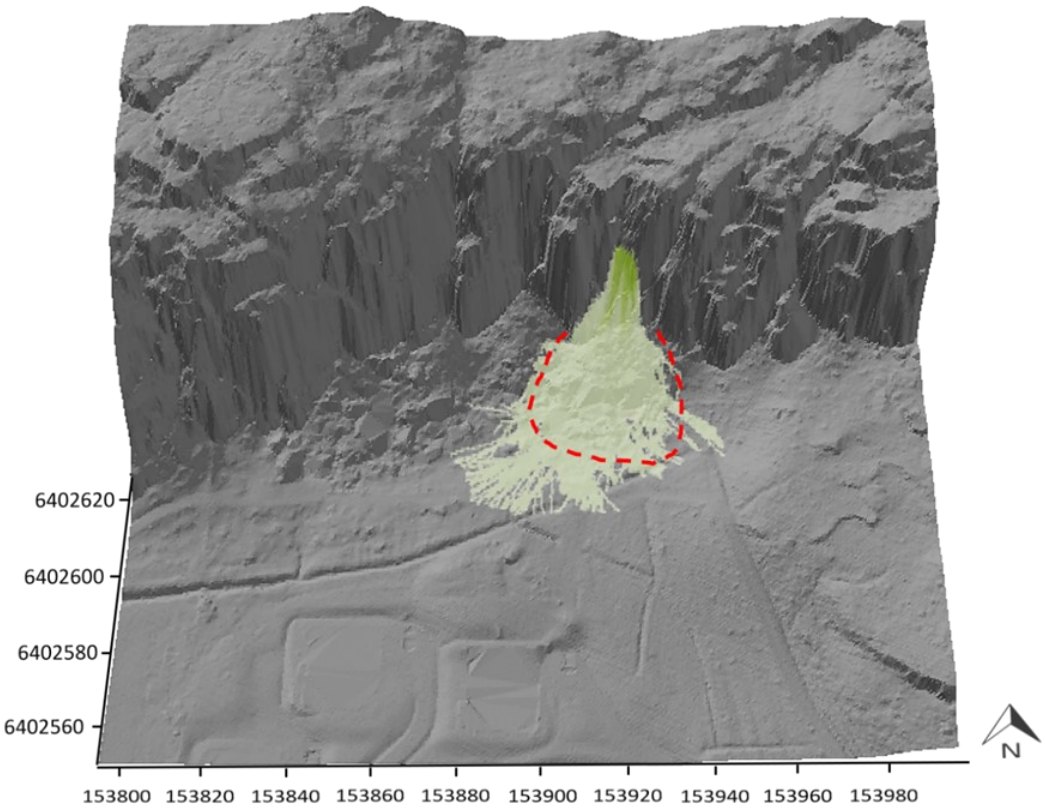

Fig. 69. In yellow: Simulated runout zone applying similar conditions to those for the 2017 rockfall. The red dashed line shows the measured extent of the rockfall.

Tables 8 and 9 summarize the vertical and lateral extent of simulated runouts for all settings.

VERTICAL EXTENT	Parameter evaluated	East	Center	West
Setting 1	Base configuration	53	61	76
Setting 2	Block shape (Spherical blocks)	49	67	78
Setting 3	Block size/mass (Heavier blocks)	47	67	74
Setting 4	Coefficient of restitution (CR = 0)	32	54	59
Setting 5	Coefficient of restitution (CR = 0.53)	85	80	84
Setting 6	Forest protection (Original distribution and size of the trees)	41	60	63
Setting 7	Forest protection (Increased size of the trees)	38	63	63
Setting 8	Forest protection (Increased density of the forest)	28	46	47/70
Setting 9	Surface roughness (Mean Obstacle Height)	31	45	31/62
Setting 10	Most realisitc model	29	35	43

Table 8. Vertical extent of the simulated runout for all settings. Values presented in m for each source. The values with "/" indicate the measurement with and without exceptions.

LATERAL EXTENT	Parameter evaluated	East	Center	West
Setting 1	Base configuration	88	102	117
Setting 2	Block shape (Spherical blocks)	80	99	130
Setting 3	Block size/mass (Heavier blocks)	81	66	92/130
Setting 4	Coefficient of restitution (CR = 0)	60	42	46
Setting 5	Coefficient of restitution (CR = 0.53)	174	150	132
Setting 6	Forest protection (Original distribution and size of the trees)	78	76	118
Setting 7	Forest protection (Increased size of the trees)	77	78	120
Setting 8	Forest protection (Increased density of the forest)	62	64	78
Setting 9	Surface roughness (Mean Obstacle Height)	61	46	53
Setting 10	Most realisitc model	58	42	52

Table 9. Lateral extent of the simulated runout for all settings. Values presented in m for each source. The values with "/" indicate the measurement with and without exceptions.

6 Discussion

6.1 SAD analysis

Although the SAD method is designed for regional studies (Loye et al. 2009; Michoud et al. 2012), with the aim of testing this method in a Swedish environment, and to see its validity at different scales, three different study areas around Fjällbo were chosen (Fig. 26).

The acquired LiDAR data for the area has a very high point density, and therefore, resolution; nevertheless, DEMs from XYZ data were generated with an intermediate resolution (5 m) for this analysis, since the geological data is required and the available maps are not very detailed, nor uniform in scale (1:25.000 – 1:100.000) as mapping was performed using different methodologies. As a result, the location of the contacts between units/deposits is not always accurate and the classification of soil cover is quite generalized.

For the first calculation of the SAFD, the decomposition in GDMUs according to their respective weight, mean and standard deviation, and their subsequent sum did not show to be a good fit for the SAFD curve (Fig. 30, 31, 32). The slope values corresponding to the plains and steep slopes MU range between low and high angle values (1° and 84°); hence, their mean and standard deviation values are very similar. Some of these high and low values were interpreted as outliers and discarded from the analysis for two reasons: i) high slope angle values in the plains MU are

mostly found close to the geological contacts with the bedrock units, and this can be interpreted as lack of accuracy considering the resolution of the mapping scale ii) low slope angle values in bedrock units that are below the mode of the till slopes are not steep enough and, hence, do not represent a potential rockfall source. See Figures 32, 33 and 34.

The SAFD curves show a general trend with higher frequencies for the low slope angle values; however, some individual values show large variations when compared with the general trend. This is probably explained by the resolution of the data. With a higher resolution, a smoother SAFD curve would be obtained but, in this case, it would not be comparable with the mapping scale of the geological data. Potential rockfall sources are associated with the bedrock topography, and most of them seem to be related to the regional-scale fold that runs through the area (See section 3). Area 3 shows the least outliers related to the lithological contacts (Fig. 35). This might be due to the compatibility between the regional scale of the geological mapping with the resolution of the DEM. This area is the one that shows the best fit ($R^2 = 0.93$; Fig. 40) and proves that this method is more suitable for regional studies.

The mode of the till slopes is the value above which slope angles start to be considered as potential rockfall sources (See section 2.3.1). In all cases, the mode of the till slopes is quite low (17° for Fjällbo, 19° for Area 2 and 22° for Area 3; Fig. 36, 38, 40). This may be due to the presence of till deposits mostly in plateau areas, as well as to its low abundance within the study area (See section 3.2). It has been proposed, however, that a minimum slope angle of 30 to 35 degrees is needed in order to initiate a rockfall (Toppe 1987; Jaboyedoff & Labiouse 2011).

On the other hand, the intersection angles between the till slopes MU and the steep slopes MU (40° for Fjällbo, and 42° for Areas 2 and 3; Fig. 36, 38, 40) are consistent with the previous estimations made by SGI (40°; SGI 2019). This value seems to cover well the minimum threshold of slope angle values that pose a risk for rockfalls and includes a wide range of areas, but, at the same time, it is not so low that it considers slopes with a very unlikely or even zero risk of rockfalls.

6.2 CONEFALL

As with the SAD analysis, this software was tested for application at different scales. Rockfall runout zones are simulated from two GRD files, containing the elevation data, and the location of potential rockfall source areas. No more input parameters or detailed information about the area is required.

Runout distances show a clear relationship with the height of the cliffs and the topography. This relationship is clearly illustrated by two examples (Fig. 46, 47). Firstly, in comparison to the Fjällbo cliffs and their corresponding runout distances, the cliffs located towards the west, by the Göta Älv river, show shorter distances, even though the topography at the bottom of the cliffs is very similar in both cases; however, Fjällbo source areas are located on higher cliffs. Secondly, in the southwest of the study area, cliffs with approximately the same height as the cliffs in Fjällbo show shorter runout distances, as the topography is more rugged in this region and does not allow the cones to spread farther.

Constraining the aperture angle allows the runout zone simulations to adjust well to the local topography and morphology (Fig. 50, 51, 52, 53). A verification of the accuracy of the method was conducted by comparing the simulated to the measured extent for the 2017 rockfall event (Fig. 53). The simulated and measured lateral extents are very similar to each other; the vertical runout is, however, 14.5 m longer than the measured, i.e. 25% longer than expected. The parameter affecting the runout distance is the cone slope angle. Suggested limits for this angle range between 27° and 37° (See section 2.7.1), which results in a rather conservative approach. Since the energy line method used by CONEFALL is based on empirical studies in very steep topographies (mostly alpine environments), the angle threshold that yields complete runout of the blocks is low (100% of the blocks being stopped; See section 2.3.2; Fig. 8). This may suggest that, when working in predominantly flat terrains (as in this study and many other areas in Sweden), a higher cone slope angle value must be chosen, i.e. an angle closer to 37 than 27, or even a higher value, although it would be outside the suggested limits by the creators of the software. The exact choice is best chosen after relevant field checks have been made. This also suggests that additional parameters of the slope and physical characteristics of the blocks should be included, which is not possible to do with this program.

Gridding resolution is important as this method focuses on the topography. Nearest neighbor method was used as gridding method; nevertheless, when creating maps from a GRD file the smoothness of the contours is partly lost (Fig. 48, 50, 52).

6.3 RockyFor3D

Due to all the required parameters to run simulations in RockyFor3D, this software is less suitable for regional studies. Simulations with this program were performed only for the Fjällbo climbing area, where fieldwork verifications and measurements were conducted. Starting from a base configuration (Fig. 54), the input parameters were tested using different combinations.

The conditions of each of the slopes under the selected rockfall sources have different characteristics that allow to visualize more clearly the effects of the

individual parameters (Fig. 54). Center and West were chosen because of their talus slopes; Center poses the talus slope partly created by the 2017 rockfall, but also by previous rockfalls, and West has a talus slope generated by older rockfalls. Moreover, these two sources are just in front of part of the growing residential area and the hiking trail. East was chosen because it has very little surface roughness and two important topographic changes at the bottom of the cliff. Towards the east, the slope angle is gentle, whereas a steeper slope is found towards the west. The eastern limit of the study area was not extended since it belongs to a different dataset and merging of data can lower the quality of the TIN; however, due to the flat character of the eastern part of the East source, it was assumed that runout zones are not much longer than the ones that can be visualized.

Due to the slope gradient (Fig. 27), and according to the assumptions of the program (See section 2.7.2), bouncing of the blocks was modelled when they were hitting the talus slopes, in this case only in sources West and Center. Outside the limits of the talus slope, rolling of the blocks was modelled. Rolling was also modelled for all the simulations in source East because of the low slope angle values at the bottom of the cliff.

Setting 1 (Fig. 55) represents the basal (original) setting as the input parameters were selected according to the general configuration of the area (Fig. 54). The outcomes from most of the other settings were compared to this first result to estimate how large the changes are when adjusting separate parameters.

The purpose of Settings 2 and 3 (Fig. 56 and 57) was to test the effect of block shape and block mass in the runout zones. In comparison to Setting 1, the runout distances are slightly longer for spherical blocks (between 2 and 6 m) for East and Center. West, however, shows a longer runout (by 4 m) for the rectangular block. The lateral extent is shorter for spherical blocks (between 3 and 8m) in East and Center. Large variations in the lateral extent for West are due to a few trajectories that, although unlikely to happen, are part of the modelled distances, and may be related to changes in the slope gradient towards the west of the study area. Nevertheless, the general trend coincides with the laboratory tests made by Hu et al. (2018) (See section 2.5), which suggest that due to the edges and corners of the rectangular blocks, they have more frictional resistance (yielding shorter runout distances), but more lateral spread since they can hit the surface in several ways.

Unlike the laboratory tests performed by Hu et al. (2018) (See section 2.5), Setting 3 shows shorter runout distances (between 2 and 6 m) and lateral extents (between 7 and 36 m) for heavier blocks when compared to Setting 1. This highlights the relevance and influence that the depth of penetration has on the energy loss and, hence, the deceleration of the blocks. In RockyFor3D, the depth of penetration is directly related to the dimension of the blocks, which, in turn, affect the volume and the mass (Dorren 2016). Towards the west of the area, in Setting 3 an exception shows a longer lateral extent, which might be due to the randomness algorithm the program uses that includes all possible, although unlikely scenarios.

Settings 4 and 5 (Fig. 58, 59, 60, and 61) show the sensitivity with respect to the tangential coefficient of restitution, which depends on the type of surface the block hits. As explained in Section 2.4, this coefficient expresses the amount of energy dissipated after collision with a surface. The closer the value of the coefficient gets to 1, the more perfectly elastic the collision is. The estimated values of the coefficient of restitution for easily penetrated materials (Setting 4) and bedrock (Setting 5) are 0 and 0.53, respectively. In comparison to Setting 1, the runout distances in Setting 4 are between 7 and 21 m shorter. The lateral extent is between 28 and 70 m shorter as well. Likewise, the variations in vertical (between 25 and 53 m) and lateral extent (between 86 and 114 m) when comparing Settings 4 and 5 are very high, showing the strong influence of the tangential coefficient of restitution on the runout zones.

Forest protection was tested in Settings 6, 7 and 8 (Fig. 62, 63, 65) using the distribution and size of the trees as measured in the field, increasing the DBH and increasing the density of the forest, respectively. In comparison to Setting 1, which is a scenario without trees, the runout distances in Setting 6 decreased between 1 and 13 m, and the lateral extent decreased between 10 and 26 m.

Modifications in the character of the forest were tested in Settings 7 and 8, which were compared with Setting 6. When increasing the DBH (Setting 7), the runout distances decreased between 3 and 18 m, and the lateral variations are not more than 1 or 2 m. Similarly, when increasing the density of the forest (Setting 8), the shortest runout zones were obtained, with runout distances decreasing between 13 and 35 m, and the lateral extent decreasing between 12 and 40 m, meaning that, even though all forested slopes provide protection to a certain extent, forest density has a stronger influence than DBH of the stems.

In Settings 6 and 7, longer trajectories can be seen towards the west because not so many trees were measured in this part of the study area, which represents a bias in the simulation. This can be confirmed in Setting 8, where the lateral extent in the west is shorter than in the previous simulations due to the presence of trees. The runout distance exception in Setting 8 is probably generated due to the randomness in the algorithm, that probably made individual simulations ran

through pixels that were not covered by trees and continued farther than the forest limit. However, this is a very unlikely scenario, as most of the blocks are halted by the first trees that they encounter.

Setting 9 (Fig. 66) considers the effect of the normal coefficient of restitution, defined by the MOH. In comparison with Setting 1, a scenario with no roughness, the vertical runout decreases between 16 and 45 m, while the lateral extent decreases between 27 and 64 m. The largest effect is found for the runout zone of the West source, as it has the highest values of MOH (larger and more blocks in the slope; See Annex 1).

Setting 1 represents the most conservative approach considering the conditions of the area (Fig. 54); in contrast, Setting 10 (Fig. 67) corresponds to the most realistic model. Both Settings consider realistic block sizes, block shapes and type of soil; nevertheless, Setting 10 includes the surface roughness parameter and the presence of forest, according to the measurements conducted in the field. For East, the vertical and lateral extent decreased by 24 and 30 m, respectively. Center showed a decrease in the vertical and lateral extent by 26 and 60 m, respectively. Lastly, for West the vertical and lateral spread was lower by 33 and 65 m, respectively. Between the conservative and realistic approaches, runout distances or vertical extent decreased between 43.4% and 45.2% and the lateral extent decreased between 34% and 58% for the three slopes. These percentages illustrate the effectiveness and influence that surface roughness and tree protection have on energy dissipation.

As RockyFor3D includes several input parameters, it was possible to perform a close replication of the conditions before the 2017 rockfall in Fjällbo. In comparison to the measured extent, the vertical and lateral simulated runouts have variations of 12 and 31 m, respectively, at the bottom of the cliff. The measured extent is, however, well covered and delimited by the simulated runout zone. The variations in the simulated runouts below the cliff are interpreted to have two reasons. Firstly, the existing talus slope has a greater slope gradient than the one that existed prior to the rockfall, therefore the model simulates more rebound, yielding a longer runout zone. Secondly, the surface roughness values were obtained from a combination of assumptions and measurements as it is not possible to know how the slope looked like before the rockfall, and the LiDAR data was acquired after the rockfall event. It was already seen in Setting 9 that model results are very sensitive to this parameter and, consequently, it should be carefully measured or estimated.

6.4 Applicability at different scales and recommendations

Considering that this thesis is a pilot study that evaluates methods to select potential rockfall sources and estimate runout zones that have not been previously tested in a Swedish environment, a general overview of the usefulness and applicability of these methods at different scales in Sweden is presented below:

The SAD procedure is more suitable for studies at a regional scale, especially considering the mapping scale of the Quaternary deposits and bedrock units currently available at SGU (See section 4.1). When using a high resolution in the DEM (e.g. 1 or 0.5 m as pixel size), ArcMap extracts a more accurate calculation of the slope angle values per pixel; however, to obtain reliable results, information about the geology of the area at a detailed scale is required. This information, of course, can be obtained more easily when conducting local studies, since field verifications can be carried out or improved where needed. Moreover, the MU classification used in this study applies to flat-dominated terrains, nevertheless, a higher pixel count for high slope angle values (values above 70°) may be obtained for areas with more rugged topography (e.g. northern Sweden). Thereby, the difference between the steep slopes and cliffs MU would become clearer, and the original MU classification (See section 2.3.1) may be used if it adapts well to the terrain.

Although the SAD procedure states that the intersection between the steep slopes and cliffs MU, or between the till slopes and the steep slopes MU (as in this study) is the angle above which all slope angles should be considered as potential rockfall sources, in some cases, there are rock slopes below the intersection that may present a risk as well. Individual cases should be assessed using the record of previous rockfalls, if available, and other determinant factors (See section 2.2). At the same time, this limit should be carefully chosen so that too low slope values are not considered as potential rockfall sources yielding an overestimation of the risk.

CONEFALL is a software that generates rather conservative results, and it can be used for both regional and local studies. It provides good approximations considering the few input data it requires, which is especially useful for remote areas, and when a fast or preliminary approach is needed. As seen in Section 6.2, it is highly dependent on the topography of the area and height of the cliffs at any scale it is used. In particular, the influence of the height at which potential rockfall sources are located is a fact that must be considered and weighted in the risk analysis since it is possible to have areas with high slope angle values that are located at low heights, and hence, represent a low risk. The lateral extent of the runout zones is not limited by the program, i.e. the default value is 360°;

therefore, it should be constrained, as it might lead to unrealistic estimations (Fig. 48, 49). For regional studies this can be challenging as the slope characteristics are not widely regular. However, for individual blocks, i.e. for local studies, it is easier to detect how the trajectories might be controlled by the local topography and morphology of the slopes and establish a limit for the aperture angle of the cone.

RockyFor3D should be used preferentially for local scale studies as it requires a thorough field study that involves characterization of the sources and the slope characteristics, i.e. dimensions, shape, mass and density of the blocks. Also, a description of the type of rock and soil in the area, and measurements of the MOH for each slope and the DBH of the trees are required. Estimations or extrapolations for larger areas where no measurements or detailed descriptions are performed can yield erroneous estimations of the runout zones as the parameters are highly sensitive. It is important to make clear that no validation of the algorithms used in the software was done in this thesis, and hence the calibrations and simplifications of the program (e.g. the tangential coefficient of restitution, which is based on theoretical values; See Table 1), were assumed as reliable. When it comes to forested slopes, it is imperative to measure as many trees as possible as density of the forest is the most important factor when this variable (presence of trees) is added to the simulation. For every slope, not necessarily with accumulations of previous rockfalls (talus slopes), surface roughness must be carefully measured as this parameter has a high influence on the vertical extent of the runout zones. And last, but not least, the pixel size of the DEM is also essential as it determines the resolution at which the program calculates the slope angle values and therefore determines the slope gradient, which is one of the most influencing variables when modelling rockfalls. Simulations obtained with RockyFor3D seem to present the best and most realistic estimate of the outcome of future rockfalls at the study area and other places in Sweden.

For all simulations, rockfall sources were assumed to be actual sources, without considering the probability of rockfall occurrence; therefore, further research including rock failure susceptibility and triggering mechanisms should be considered on an individual basis for specific areas of interest.

7 Conclusions

- The Slope Angle Distribution (SAD) procedure provides a systematic methodology to detect potential rockfall sources using criteria other than the slope angle. This method is, however, very sensitive to the resolution of the data, as all data have to be consistent in order to avoid outliers that yield erroneous interpretations or meaningless results.
- The classification of the morphological units (MU) into plains, till slopes and steep slopes showed to be suitable for areas with predominantly flat terrains. For the Fjällbo area and its surroundings, potential rockfall sources are controlled by the bedrock topography, and, according to the SAD method, the threshold slope angle above which all angles are considered potential rockfall sources is 40°- 42° in the study area.
- The SAD method can be used to perform preliminary rockfall hazard assessments, that can later be verified with fieldwork, and it can also be used for remote or less accessible areas. This methodology has proved to be more suitable for studies at a regional scale.
- CONEFALL is a cost-free and user-friendly program, that can be used for regional and local studies as a preliminary assessment of areas potentially affected by rockfalls. This software generates rather conservative results. In order to get a more realistic approach, for predominantly flat terrains, as in many places in Sweden, a high cone slope angle value could be selected, which is possible to implement in the software, although outside the suggested limits by its creators.
- The results in CONEFALL are highly dependent on the topography and morphology of the terrain and constraining the aperture angle is highly recommended in order to adjust the lateral extent of the runout zones to the local slope conditions.
- Due to all the required parameters to run simulations in RockyFor3D, this software is most suitable for local-scale studies. Although the slope gradient is the parameter that has the main influence on rockfall trajectories, runout zones and modes of motion is, the sensitivity and influence of other individual parameters were tested for the Fjällbo area.
- Block shape particularly influences the lateral extent of runout zones, as rectangular blocks can hit the ground in several different ways, which makes them radically change direction. Block mass controls the depth of penetration and, therefore, the energy dissipation and deceleration of the blocks.
- The coefficient of restitution has two components, the normal, which is associated with the Mean Obstacle Height (MOH), and the tangen-

tial, related to soil type in the slope. This parameter governs the bouncing properties of the blocks and thus most of the extent of the runout zones.

- The efficacy of forested slopes as protective agents is mostly controlled by the density of the forest, rather than the Diameter at Breast Height (DBH).

- The inclusion of a verification point when using a modelling software, i.e. the 2017 rockfall in Fjällbo in this study, offers a good opportunity to evaluate the applicability and accuracy of the models by replicating the environmental conditions of the previous rockfall.

- All methods and models used in this study comprise only rockfall parameters and mechanics, but not triggering mechanisms, nor probabilities of rockfall occurrence. These aspects are suggested to be subject of further research in Sweden.

- The SAD methodology for potential rockfall source detection, as well as the runout zone estimations obtained with CONEFALL and RockyFor3D models may serve as a foundation for further and more detailed risk assessment. These methods, however, are very sensitive to topography, morphology and geology of the area, and, therefore, it is paramount to perform verifications of the ground conditions in the study area with fieldwork and/or high-resolution remote sensing imagery.

8 Acknowledgments

I want to give special thanks to the Swedish Institute, for giving me the opportunity to come to Sweden to study the master's degree in Bedrock Geology at Lund University under the fully-funded Swedish Institute Study Scholarship Programme (SISSP). Thanks to my supervisor at SGI, Johan Berglund, for sharing his original idea about this project and his feedback along the way. Thanks to my supervisor at Lund University, Mats Rundgren, for his support, help and company during the field campaign and his valuable comments on my document. Thanks to Lund University for providing funding for the fieldwork. Thanks to my family, for their endless love, for believing in me and always encouraging me to pursue my dreams. And last, but not least, thanks to Hannes Pilser, for being a constant source of motivation, and for making this journey a lot more fun and full of amazing experiences.

9 References

Andersson, J., Möller, C. & Johansson, L., 2002: Zircon geochronology of migmatite gneisses along the Mylonite Zone (S Sweden): a major Sveconorwegian terrane boundary in the Baltic Shield. Precambrian Research 114, 121-147.

Anjar, J., Larsen, N. K., Håkansson, L., Möller, P., Linge, H., Fabel, D. & Xu, S., 2014: A 10 B e -based reconstruction of the last deglaciation in southern S weden. *Boreas 43*, 132-148.

Azzoni, A., La Barbera, G. & Zaninetti, A., 1995: Analysis and prediction of rockfalls using a mathematical model. *International journal of rock mechanics and mining sciences & geomechanics abstracts.* Elsevier. 709-724 pp.

Åhäll, K.-I. & Connelly, J. N., 2008: Long-term convergence along SW Fennoscandia: 330 my of Proterozoic crustal growth. *Precambrian Research 161*, 452-474.

Barnett, M. J., 2016: *Precipitation Triggered Landslide Risk Assessment and Relative Risk Modeling Using Cached and Real-Time Data*. University of Southern California.

Bergström, U., Stephens, M. B. & Wahlgren, C.-H., 2020: Polyphase (1.6–1.5 and 1.1–1.0 Ga) deformation and metamorphism of Proterozoic (1.7–1.1 Ga) continental crust, Idefjorden terrane, Sveconorwegian orogen. *Geological Society, London, Memoirs 50*, 397-434.

Bingen B., Andersson, J., Söderlund, U. & Möller, C., 2008: The Mesoproterozoic in the Nordic countries. Episodes 31.

CGS, 2020: Rockfalls. Retrieved 2020, from https://coloradogeologicalsurvey.org/hazards/rockfall/.

Dai, F., Lee, C. & Ngai, Y. Y., 2002: Landslide risk assessment and management: an overview. *Engineering geology 64*, 65-87.

Dorren, L., 2016: Rockyfor3D (v5. 2) revealed–Transparent description of the complete 3D rockfall model. ecorisQ paper (www. ecorisq. org): 33 p. Accessed.

Dorren, L., Berger, F. & Putters, U., 2006: Real-size experiments and 3-D simulation of rockfall on forested and non-forested slopes.

Dorren, L. K., 2003: A review of rockfall mechanics and modelling approaches. *Progress in Physical Geography 27*, 69-87.

Dorren, L. K. & Berger, F., 2006: Stem breakage of trees and energy dissipation during rockfall impacts. *Tree physiology 26*, 63-71.

Dorren, L. K., Domaas, U., Kronholm, K. & Labiouse, V., 2011. Methods for predicting rockfall trajectories and runout zones. John Wiley & Sons, ISTE ltd Report 1848212569.

Dorren, L. K. & Seijmonsbergen, A. C., 2003: Comparison of three GIS-based models for predicting rockfall runout zones at a regional scale. *Geomorphology 56*, 49-64.

Evans, S. & Hungr, O., 1993: The assessment of rockfall hazard at the base of talus slopes. *Canadian geotechnical journal 30*, 620-636.

Fanos, A. M. & Pradhan, B., 2018: Laser scanning systems and techniques in rockfall source identification and risk assessment: a critical review. *Earth Systems and Environment 2*, 163-182.

Gerber, W., 1994: Beurteilung des Prozesses Steinschlag. *Ganzheitliche Gefahrenbeurteilung. Kursunterlagen FAN-Kurs*.

Heim, A., 1932: *Bergsturz und menschenleben*. Fretz & Wasmuth.

Heidenreich, B., 2004. Small-and half-scale experimental studies of rockfall impacts on sandy slopes. EPFL Report.

Hellman, A., 2018: *Geohazard assesments of rock climbing sites.*, Göteborgs Universitet.

Highland, L., 2004. Landslide types and processes. Report 2327-6932.

Hu, J., Li, S., Shi, S., Li, L., Zhang, Q., Liu, H. & He, P., 2018: Experimental study on parameters affecting the Runout range of rockfall. *Advances in Civil Engineering 2018*.

Jaboyedoff, M., 2003: Conefall 1.0 User's Guide: Quanterra. *International Independent Center of Climate Change Impact on Natural Risk Analysis in Mountainous Area, Open Report–Soft-01*.

Jaboyedoff, M. & Labiouse, V., 2003: Preliminary assessment of rockfall hazard based on GIS data. *10th ISRM Congress.* International Society for Rock Mechanics and Rock Engineering.

Jaboyedoff, M. & Labiouse, V., 2011: Preliminary estimation of rockfall runout zones. *Natural Hazards and Earth System Sciences 11*, 819.

Jiménez-Perálvarez, J., Irigaray, C., El Hamdouni, R. & Chacón, J., 2009: Building models for automatic landslide-susceptibility analysis, mapping and validation in ArcGIS. *Natural hazards 50*, 571-590.

Johansson, M., Olvmo, M. & Lidmar-Bergström, K., 2001: Inherited landforms and glacial impact of different palaeosurfaces in southwest Sweden. *Geografiska Annaler: Series A, Physical Geography 83*, 67-89.

Lied, K., 1977: Rockfall problems in Norway. *ISMES Publication 90*, 51-53.

Loye, A., Jaboyedoff, M. & Pedrazzini, A., 2009: Identification of potential rockfall source areas at a regional scale using a DEM-based geomorphometric analysis. *Natural Hazards and Earth System Sciences 9*, 1643.

Lundqvist, J. & Wohlfarth, B., 2000: Timing and east–west correlation of south Swedish ice marginal lines during the Late Weichselian. *Quaternary Science Reviews 20*, 1127-1148.

Magnusson, E., 1978: *Beskrivning till jordartskartan Göteborg SO: Description to the quaternary map Göteborg SO*. Sveriges Geologiska Undersökning.

Michoud, C., Derron, M., Horton, P., Jaboyedoff, M., Baillifard, F., Loye, A., Nicolet, P., Pedrazzini, A. & Queyrel, A., 2012: Rockfall hazard and risk assessments along roads at a regional scale: example in Swiss Alps. *Natural Hazards & Earth System Sciences 12*.

Monnet, J., Clouet, N., Bourrier, F. & Berger, F., 2010: Using geomatics and airborne laser scanning for rockfall risk zoning: a case study in the French Alps.

Montgomery, D. R. & Brandon, M. T., 2002: Topographic controls on erosion rates in tectonically active mountain ranges. *Earth and Planetary Science Letters 201*, 481-489.

Nilsen, M. W., 2008: *Modelling of rockfall runout range: Employing empirical and dynamical methods*.

Olvmo, M. & Johansson, M., 2002: The significance of rock structure, lithology and pre-glacial deep weathering for the shape of intermediate -scale glacial erosional landforms. *Earth Surface Processes and Landforms 27*, 251-268.

Onofri, R. & Candian, C., 1979: Indagine sui limiti di massima invasione dei blocchi rocciosi franati durante il sisma del Friuli del 1976. *Reg. Aut. Friuli-Venezia-Giulia, CLUET 42*.

Park, R. G., Åhäll, K.-I. & Boland, M. P., 1991: The Sveconorwegian shear-zone network of SW Sweden in relation to mid-Proterozoic plate movements. Precambrian Research 49, 245-260.

Peng, B., 2000: Rockfall trajectory analysis: Parameter determination and application.

Pfeiffer, T. J. & Higgins, J. D., 1990: Rockfall hazard analysis using the Colorado rockfall simulation program. *Transportation Research Record*.

Pichler, B., Hellmich, C. & Mang, H. A., 2005: Impact of rocks onto gravel design and evaluation of experiments. *International Journal of Impact Engineering 31*, 559-578.

Påsse, T., 1987: Shore displacement during the Late Weichselian and Holocene in the Sandsjöbacka area, SW Sweden. *Geologiska Föreningen i Stockholm Förhandlingar 109*, 197-210.

Richards, L., 1988: Rockfall protection: a review of current analytical and design methods. *Secondo ciclo di conferenze di meccanica ed ingegneria delle rocce, MIR, Politecnico di Torino 11*, 1-13.

Ritchie, A. M., 1963: Evaluation of rockfall and its control. *Highway research record*.

Rouiller, J.-D., 1998: *Pentes instables dans le Pennique valaisan: Matterock: une méthodologie d'auscultation des falaises et de détection des éboulements majeurs potentiels*. vdf Hochschulverlag AG.

Samuelsson, L., 1978: *Beskrivning till berggrundskartan Göteborg SO: Description to the map of solid rocks Göteborg SO*. Sveriges Geologiska Undersökning.

Sartell, A., 2019: Metamorphic paragenesis and PT conditions in garnet amphibolite from the Median Segment of the Idefjorden Terrane, Lilla Edet. *Dissertations in Geology at Lund University*.

Scherstén, A., Larson, S. Å., Cornell, D. & Stigh, J., 2004: Ion probe dating of a migmatite in SW Sweden: the fate of zircon in crustal processes. *Precambrian Research 130*, 251-266.

Schön, J. H. 2015: Density. *In Developments in Petroleum Science*, 109-118. Elsevier.

SGI, 2018. Säkra bergslänter. Kunskapsläget och fallstudier. Statens geotekniska institut Report.

SGI, 2019: GIS- Inventering av bergslänter med Göteborgs stads höjddatabas. Statens geotekniska institut.

SGI, 2020: Ras, skred och slamströmmar. Retrieved 2020, from https://www.swedgeo.se/sv/vagledning-i-arbetet/ras--skred-och-slamstrommar/.

SGU, 2014. Produktbeskrivning - Jordarter 1:25 000-1:100 0000. Sveriges geologiska undersökning Report.

SGU, 2020: SGUs kartvisare - Jordarter 1:25 000 - 1:100 000. Retrieved 2020, from https://apps.sgu.se/kartvisare/kartvisare-jordarter-25-100.html?zoom=305060.0659366815,6394733.604272217,343308.14243283455,6413129.64106429

Starmer, I., 1996: Oblique terrane assembly in the late paleoproterozoic during the Labradorian-Gothian Orogeny in southern Scandinavia. *The Journal of Geology 104*, 341-350.

Stephens, M. B., Bergström, U. & Wahlgren, C.-H., 2020: Regional context and lithotectonic framework of the 1.1–0.9 Ga Sveconorwegian orogen, southwestern Sweden. *Geological Society, London, Memoirs 50*, 337-349.

Stevens, R. L. & Hellgren, L.-G., 1990: A generalized lithofacies model for glaciomarine and marine sequences in the Göteborg area, Sweden. *Geologiska Föreningen i Stockholm Förhandlingar 112*, 89-105.

Strahler, A. N., 1950: Equilibrium theory of erosional slopes approached by frequency distribution analysis. Part I. *American Journal of Science 248*, 673-696.

Stroeven, A. P., Hättestrand, C., Kleman, J., Heyman, J., Fabel, D., Fredin, O., Goodfellow, B. W., Harbor, J. M., Jansen, J. D. & Olsen, L., 2016: Deglaciation of fennoscandia. *Quaternary Science Reviews 147*, 91-121.

Söderlund, U., Hellström, F. A. & Kamo, S. L., 2008: Geochronology of high-pressure mafic granulite dykes in SW Sweden: tracking the P–T–t path of metamorphism using Hf isotopes in zircon and baddeleyite. Journal of Metamorphic Geology 26, 539-560.

Thorbjörnson Lind, T., 2016: Rockfalls from rock cuts beside Swedish railroads: A full scale fieldtest, to investigate rockfalls and how rock bounces.

Toppe, R., 1987: Terrain models: a tool for natural hazard mapping. *IAHS, Publication 162*.

Varnes, D. J., 1978: Slope movement types and processes. *Special report 176*, 11-33.

Vo, T. D., 2015: RAMMS::Rockfall versus Rockyfor3D in rockfall trajectory simulations at the Community of Vik, Norway.

Volkwein, A., Schellenberg, K., Labiouse, V., Agliardi, F., Berger, F., Bourrier, F., Dorren, L. K., Gerber, W. & Jaboyedoff, M., 2011: Rockfall characterisation and structural protection-a review.

Wang, B. & Cavers, D. S., 2008: A simplified approach for rockfall ground penetration and impact stress calculations. *Landslides 5*, 305.

Wang, Y., Jiang, W., Cheng, S., Song, P. & Mao, C., 2018: Effects of the impact angle on the coefficient of restitution in rockfall analysis based on a medium-scale laboratory test. *Natural Hazards and Earth System Sciences 18*, 3045-3061.

ANNEX 1

Measurements of block heights in the slopes in cm. Values in red are the calculated average in this case (MOH).

WEST		
70%	20%	10%
90	0	230
41	0	160
82		498
79		225
40		153
30		350
55		650
37		245
28		215
50		230
27		295.6
35		
37		
37		
55		
40		
39		
68		
31		
35		
38		
47		
38		
54		
36		
57		
49		
48		
55		
43		
31		
33		
36		
37		
51		
16		
31		
32		
40		
69		
57		
17		
26		
41		
34		
29		
72		
49		
28		
25		
47		
37		
33		
41		
27		
38		
48		
34		
51		
52		
37		
25		
28		
38		
44		
42		
54		
26		
22		
71		
42.14		

CENTER		
70%	20%	10%
50	24	154
53	18	245
40	25	104
78	13	385
62	21	120
38	29	186
72	14	108
61	12	210
59	26	320
60	8	155
54	25	198.7
50	23	
92	26	
34	23	
44	19	
88	24	
66	30	
71	10	
44	18	
47	12	
73	20	
42		
71		
57		
72		
65		
63		
58		
53		
46		
59		
55		
88		
89		
44		
53		
71		
91		
65		
82		
75		
54		
81		
73		
75		
98		
53		
56		
74		
53		
67		
48		
53		
65		
35		
42		
71		
58		
37		
38		
46		
56		
40		
48		
82		
56		
49		
51		
62		
25		
59.73		

EAST		
70%	20%	10%
0	175	35
0	105	30
	153	38
	117	28
	78	30
	165	51
	75	44
	196	47
	177	35
	183	24
	98	53
	95	56
	134.75	37
		54
		29
		30
		25
		38

ANNEX 2

Location of the trees in Fjällbo, measured circumference and calculation of the DBH.

Y COORD	X COORD	CIRCUMFERENCE	DBH
153890.6	6402655	26	8.28
153886.7	6402659	143	45.52
153885.5	6402659	47	14.96
153889	6402652	17	5.41
153892.7	6402650	25	7.96
153894.3	6402646	28	8.91
153894.9	6402646	40	12.73
153897.1	6402646	47	14.96
153896.8	6402646	82	26.10
153896.8	6402646	130	41.38
153901.2	6402649	202	64.30
153900.4	6402649	125	39.79
153903.2	6402650	26	8.28
153905.7	6402656	20	6.37
153905.7	6402656	25	7.96
153905.4	6402656	14	4.46
153903.7	6402653	26	8.28
153905.6	6402654	19	6.05
153905.6	6402655	17	5.41
153908.2	6402658	32	10.19
153907.9	6402658	41	13.05
153906.9	6402656	44	14.01
153901.2	6402652	46	14.64
153903.2	6402650	41	13.05
153904.1	6402651	36	11.46
153919.3	6402653	240	76.39
153919.3	6402637	34	10.82
153935.1	6402667	198	63.03
153889.6	6402619	32	10.19
153889.3	6402621	17	5.41
153887.8	6402613	28	8.91
153885.7	6402607	34	10.82
153892.5	6402610	30	9.55
153887.7	6402611	29	9.23
153887.6	6402611	38	12.10
153887.6	6402611	24	7.64
153887.2	6402612	13	4.14
153887.2	6402612	31	9.87

153887.2	6402612	27	8.59
153886.4	6402611	17	5.41
153885.4	6402612	167	53.16
153880.1	6402612	15	4.77
153880.2	6402612	35	11.14
153880.5	6402613	45	14.32
153880.4	6402613	33	10.50
153880.6	6402613	58	18.46
153879.4	6402616	176	56.02
153885.5	6402626	23	7.32
153880.4	6402636	31	9.87
153880.3	6402634	34	10.82
153878.6	6402631	33	10.50
153876.3	6402628	31	9.87
153875.3	6402629	86	27.37
153874.3	6402624	28	8.91
153875.3	6402624	30	9.55
153874.2	6402624	20	6.37
153872.9	6402622	17	5.41
153872.8	6402623	201	63.98
153875.3	6402620	19	6.05
153875.3	6402616	29	9.23
153875.2	6402616	13	4.14
153873.3	6402614	20	6.37
153874.2	6402613	28	8.91
153873.5	6402613	33	10.50
153873.5	6402613	26	8.28
153872.3	6402611	28	8.91
153871.8	6402611	18	5.73
153871.7	6402611	30	9.55
153871.6	6402610	218	69.39
153871.7	6402610	199	63.34
153871.2	6402612	20	6.37
153871.1	6402611	26	8.28
153871.2	6402611	82	26.10
153871.2	6402611	22	7.00
153870.6	6402612	43	13.69
153870.9	6402612	15	4.77
153870.6	6402612	14	4.46
153870.3	6402613	18	5.73
153864.2	6402615	23	7.32

153863.1	6402616	31	9.87
153864	6402615	153	48.70
153881.5	6402641	32	10.19
153882.2	6402642	15	4.77
153882.1	6402642	22	7.00
153882.1	6402642	38	12.10
153869.1	6402628	26	8.28
153868.7	6402629	140	44.56
153872.9	6402636	27	8.59
153879.7	6402642	31	9.87
153879.6	6402642	148	47.11
153880.9	6402643	242	77.03
153943.8	6402626	25	7.96
153943.8	6402626	38	12.10
153945.8	6402625	46	14.64
153962	6402636	96	30.56
153962	6402636	15	4.77
153963.9	6402644	153	48.70
153965.7	6402646	22	7.00
153965.8	6402646	16	5.09
153967.6	6402647	9	2.86
153971.4	6402644	152	48.38
153971.3	6402643	158	50.29
153972.7	6402645	142	45.20
153968.9	6402643	193	61.43
153969.6	6402644	20	6.37
153967	6402644	41	13.05
153968.3	6402639	174	55.39
153966.1	6402635	32	10.19
153964.7	6402633	42	13.37
153963.8	6402633	48	15.28
153963.8	6402632	31	9.87
153963.1	6402631	19	6.05
153963.3	6402630	160	50.93
153965.1	6402631	141	44.88
153963.5	6402626	43	13.69
153964.6	6402625	42	13.37
153964.6	6402625	16	5.09
153971.7	6402621	24	7.64
153972.2	6402620	100	31.83
153969	6402621	13	4.14

153969.4	6402620	24	7.64
153965.2	6402622	116	36.92
153963.9	6402622	19	6.05
153961	6402623	39	12.41
153960.5	6402619	19	6.05
153960.8	6402618	28	8.91
153959	6402616	124	39.47
153960.9	6402618	17	5.41
153960.9	6402618	26	8.28
153964	6402616	35	11.14
153964.9	6402613	120	38.20
153964.9	6402613	17	5.41
153963.1	6402612	12	3.82
153963.2	6402612	15	4.77
153963.2	6402612	127	40.43
153962.7	6402612	18	5.73
153962.7	6402612	25	7.96
153962.6	6402612	19	6.05
153961.8	6402612	20	6.37
153960.5	6402613	14	4.46
153959	6402612	16	5.09
153959	6402612	13	4.14
153958.4	6402610	123	39.15
153958.5	6402608	18	5.73
153959.9	6402608	128	40.74
153958	6402609	16	5.09
153958.6	6402608	48	15.28
153961.2	6402608	9	2.86
153963.7	6402609	21	6.68
153963.7	6402604	152	48.38
153961.8	6402605	49	15.60
153959.2	6402604	190	60.48
153956.6	6402603	152	48.38
153951.5	6402615	148	47.11
153948.4	6402619	73	23.24
153947.2	6402618	54	17.19
153947.3	6402619	126	40.11
153947.3	6402620	81	25.78
153948.2	6402621	26	8.28
153948	6402622	64	20.37
153948.1	6402623	194	61.75

153945.7	6402631	81	25.78
153945.7	6402631	26	8.28
153945.9	6402631	31	9.87
153945.9	6402631	27	8.59
153945.9	6402645	43	13.69
153943.1	6402652	29	9.23
153943	6402652	18	5.73
153942.7	6402652	290	92.31
153946.1	6402650	42	13.37
153948	6402650	40	12.73
153947.5	6402648	168	53.48
153940.5	6402651	26	8.28
153940	6402652	27	8.59
153939.3	6402652	51	16.23
153940.1	6402650	81	25.78
153940.6	6402647	15	4.77
153941.7	6402645	187	59.52
153938.8	6402643	24	7.64
153938.8	6402641	194	61.75
153943	6402632	42	13.37
153943.1	6402630	44	14.01
153942.2	6402629	33	10.50
153942.8	6402629	63	20.05
153938.5	6402625	50	15.92
153937.9	6402615	29	9.23
153938.1	6402615	49	15.60
153939.3	6402614	42	13.37
153940	6402612	18	5.73
153940.9	6402610	90	28.65
153940.4	6402609	117	37.24
153942.1	6402609	25	7.96
153942	6402610	30	9.55
153943.6	6402609	14	4.46
153944.7	6402609	25	7.96
153945.9	6402608	91	28.97
153945.4	6402608	85	27.06
153946.9	6402608	110	35.01
153947.7	6402608	113	35.97
153942.1	6402608	109	34.70
153939.1	6402611	114	36.29
153938.2	6402614	48	15.28

153937	6402611	70	22.28
153933.7	6402608	91	28.97
153934.1	6402611	58	18.46
153933.3	6402611	78	24.83
153933.3	6402611	111	35.33
153931.4	6402613	41	13.05
153931.2	6402615	112	35.65
153929.7	6402623	12	3.82
153930.9	6402623	26	8.28
153930.7	6402624	247	78.62
153933.6	6402627	28	8.91
153932.9	6402628	20	6.37
153932.7	6402629	13	4.14
153932.9	6402629	19	6.05
153932.7	6402629	24	7.64
153932.4	6402629	34	10.82
153933.9	6402630	37	11.78
153938.2	6402637	32	10.19
153933	6402663	197	62.71
153928.7	6402638	200	63.66
153930.4	6402632	19	6.05
153926.5	6402637	31	9.87
153925.5	6402638	63	20.05
153936.9	6402629	37	11.78
153914.3	6402633	240	76.39
153914.3	6402633	32	10.19
153914.3	6402633	16	5.09
153914.2	6402632	21	6.68
153914	6402632	42	13.37
153914.8	6402633	18	5.73
153914.7	6402633	152	48.38
153914.2	6402632	250	79.58
153914.2	6402632	18	5.73
153914.6	6402631	48	15.28
153913.5	6402630	15	4.77
153913.4	6402630	30	9.55
153913.6	6402630	17	5.41
153913.9	6402629	152	48.38
153913	6402630	14	4.46
153911	6402633	32	10.19
153911.3	6402633	25	7.96

153911.1	6402633	26	8.28
153911.4	6402633	38	12.10
153911.4	6402633	19	6.05
153911.4	6402633	25	7.96
153912.2	6402634	177	56.34
153912.3	6402634	16	5.09
153912.9	6402634	26	8.28
153912.9	6402634	19	6.05
153913	6402634	12	3.82
153913	6402634	21	6.68
153913.4	6402629	26	8.28
153913.5	6402630	52	16.55
153913.4	6402630	61	19.42
153912.8	6402630	19	6.05
153912.7	6402630	179	56.98
153913.1	6402630	46	14.64
153912.6	6402630	15	4.77
153912.6	6402630	179	56.98
153912.6	6402630	25	7.96
153912.4	6402630	19	6.05
153912.3	6402630	33	10.50
153912.3	6402631	15	4.77
153912.4	6402631	25	7.96
153912.7	6402631	213	67.80
153912.3	6402632	31	9.87
153912.2	6402635	121	38.52
153911.2	6402634	43	13.69
153911.1	6402634	28	8.91
153910.4	6402631	174	55.39
153910.5	6402631	24	7.64
153909.6	6402631	20	6.37
153909.6	6402631	29	9.23
153909.6	6402631	26	8.28
153908.4	6402630	52	16.55
153907.9	6402631	53	16.87
153907.3	6402631	25	7.96
153907.3	6402631	119	37.88
153907.5	6402632	33	10.50
153907.5	6402632	23	7.32
153907.5	6402631	46	14.64
153907	6402631	42	13.37

153907	6402632	32	10.19
153907	6402633	20	6.37
153906.7	6402633	210	66.85
153905.9	6402634	26	8.28
153906.2	6402633	28	8.91
153905.9	6402634	24	7.64
153905.9	6402634	28	8.91
153903.6	6402633	41	13.05
153903.6	6402633	25	7.96
153903.6	6402632	56	17.83
153900.2	6402630	28	8.91
153900.3	6402631	24	7.64
153899.9	6402628	27	8.59
153899.3	6402627	210	66.85
153899.3	6402627	14	4.46
153899.5	6402626	16	5.09
153898.9	6402626	17	5.41
153898.7	6402626	15	4.77
153898.9	6402626	18	5.73
153898.2	6402625	16	5.09
153898.3	6402625	24	7.64
153897.3	6402626	26	8.28
153897.4	6402626	38	12.10
153896.8	6402626	19	6.05
153896.6	6402626	165	52.52
153895.6	6402627	20	6.37
153920.4	6402636	262	83.40
153978	6402633	96	30.56
153978	6402633	15	4.77
153979.9	6402641	153	48.70
153971.1	6402638	22	7.00
153972.4	6402637	16	5.09
153982.9	6402641	9	2.86
153977.2	6402641	152	48.38
153977.1	6402641	158	50.29
153978.5	6402643	142	45.20
153974.8	6402641	193	61.43
153971.9	6402640	20	6.37
153972.8	6402641	41	13.05
153984.3	6402637	174	55.39
153982.1	6402632	32	10.19

153980.7	6402630	42	13.37
153973.5	6402632	48	15.28
153979.8	6402630	31	9.87
153971.3	6402628	19	6.05
153971.4	6402636	160	50.93
153981.1	6402628	141	44.88
153971.5	6402617	43	13.69
153972.5	6402616	42	13.37
153972.5	6402616	16	5.09
153976.3	6402627	24	7.64
153976.8	6402625	100	31.83
153973.6	6402626	13	4.14
153974	6402625	24	7.64
153973.1	6402612	116	36.92
153971.8	6402612	19	6.05
153969	6402614	39	12.41
153968.5	6402610	19	6.05
153968.8	6402609	28	8.91
153968.9	6402609	17	5.41
153968.9	6402609	26	8.28
153977.6	6402625	43	13.69
153978.6	6402624	42	13.37
153978.6	6402624	16	5.09
153979.2	6402621	116	36.92
153978	6402621	19	6.05
153975.1	6402622	39	12.41
153974.6	6402619	19	6.05
153974.9	6402617	28	8.91
153975	6402617	17	5.41
153975	6402617	26	8.28
153966	6402628	153	48.70
153967.7	6402630	22	7.00
153967.9	6402630	16	5.09
153969.7	6402631	9	2.86
153969.1	6402628	41	13.05
153959.1	6402629	42	13.37
153958.2	6402628	31	9.87
153959.6	6402627	141	44.88
153956	6402624	43	13.69
153957	6402623	42	13.37
153957	6402623	16	5.09

153957.6	6402620	116	36.92
153956.4	6402619	19	6.05
153950.7	6402648	24	7.64
153950.6	6402646	194	61.75
153950.1	6402642	32	10.19
153922.1	6402618	32	10.19
153921.7	6402620	17	5.41
153920.2	6402612	28	8.91
153915.2	6402608	34	10.82
153924.9	6402609	30	9.55
153920.2	6402610	29	9.23
153920	6402610	38	12.10
153920.1	6402610	24	7.64
153919.6	6402611	13	4.14
153919.6	6402611	31	9.87
153919.6	6402611	27	8.59
153918.9	6402610	17	5.41
153917.8	6402611	167	53.16
153912.5	6402611	15	4.77
153912.6	6402611	35	11.14
153912.9	6402612	45	14.32
153912.8	6402612	33	10.50
153913	6402612	58	18.46
153903.1	6402619	176	56.02
153906.8	6402623	28	8.91
153907.7	6402623	30	9.55
153906.6	6402623	20	6.37
153905.3	6402621	17	5.41
153905.2	6402622	201	63.98
153907.7	6402619	19	6.05
153899	6402619	29	9.23
153898.9	6402619	13	4.14
153905.8	6402613	20	6.37
153906.6	6402612	28	8.91
153904	6402612	33	10.50
153904	6402612	26	8.28
153910.3	6402607	28	8.91
153908	6402611	18	5.73
153909.7	6402607	30	9.55
153909.6	6402607	218	69.39
153909.7	6402607	199	63.34

153912.6	6402606	20	6.37
153927.2	6402606	26	8.28
153914.8	6402607	82	26.10
153923.6	6402605	22	7.00
153903.3	6402609	43	13.69
153922.9	6402605	15	4.77
153901	6402611	14	4.46
153902.9	6402610	18	5.73
153896.6	6402614	23	7.32
153895.6	6402615	31	9.87
153896.5	6402614	153	48.70
153862.1	6402637	174	55.39
153865.5	6402619	24	7.64
153862.9	6402618	13	4.14
153864.9	6402636	22	7.00
153866.2	6402635	16	5.09
153868.6	6402639	193	61.43
153865.7	6402638	20	6.37
153866.6	6402639	41	13.05
153867.3	6402630	48	15.28
153865.1	6402626	19	6.05
153865.3	6402634	160	50.93
153867.4	6402624	13	4.14
153867.8	6402623	24	7.64
153868.9	6402620	39	12.41
153861.6	6402628	22	7.00
153861.7	6402628	16	5.09
153863.5	6402629	9	2.86
153862.9	6402626	41	13.05
153886.8	6402637	153	48.70
153897.9	6402634	22	7.00
153898.1	6402634	16	5.09
153899.9	6402635	9	2.86
153894.3	6402636	152	48.38
153894.2	6402636	158	50.29
153895.6	6402638	142	45.20
153891.8	6402636	193	61.43
153892.5	6402636	20	6.37
153889.9	6402637	41	13.05
153891.2	6402632	174	55.39
153894.7	6402633	20	6.37

153895.7	6402634	41	13.05
153904.1	6402665	13	4.14
153904.6	6402664	24	7.64
153911	6402665	28	8.91
153912	6402665	30	9.55
153910.9	6402665	20	6.37
153909.6	6402663	17	5.41
153909.8	6402661	201	63.98
153907.1	6402661	202	64.30
153904.4	6402662	125	39.79
153907.1	6402664	46	14.64

Tidigare skrifter i serien ”Examensarbeten i Geologi vid Lunds universitet”:

540. Christiansen, Emma, 2018: Mikroplast på och i havsbotten - Utbredningen av mikroplaster i marina bottensediment och dess påverkan på marina miljöer. (15 hp)
541. Staahlnacke, Simon, 2018: En sammanställning av norra Skånes prekambriska berggrund. (15 hp)
542. Martell, Josefin, 2018: Shock metamorphic features in zircon grains from the Mien impact structure - clues to conditions during impact. (45 hp)
543. Chitindingu, Tawonga, 2018: Petrological characterization of the Cambrian sandstone reservoirs in the Baltic Basin, Sweden. (45 hp)
544. Chonewicz, Julia, 2018: Dimensionerande vattenförbrukning och alternativa vattenkvaliteter. (15 hp)
545. Adeen, Lina, 2018: Hur lämpliga är de geofysiska metoderna resistivitet och IP för kartläggning av PFOS? (15 hp)
546. Nilsson Brunlid, Anette, 2018: Impact of southern Baltic sea-level changes on landscape development in the Verkeån River valley at Haväng, southern Sweden, during the early and mid Holocene. (45 hp)
547. Perälä, Jesper, 2018: Dynamic Recrystallization in the Sveconorwegian Frontal Wedge, Småland, southern Sweden. (45 hp)
548. Artursson, Christopher, 2018: Stratigraphy, sedimentology and geophysical assessment of the early Silurian Halla and Klinteberg formations, Altajme core, Gotland, Sweden. (45 hp)
549. Kempengren, Henrik, 2018: Att välja den mest hållbara efterbehandlingsmetoden vid sanering: Applicering av beslutsstödsverktyget SAMLA. (45 hp)
550. Andreasson, Dagnija, 2018: Assessment of using liquidity index for the approximation of undrained shear strength of clay tills in Scania. (45 hp)
551. Ahrenstedt, Viktor, 2018: The Neoproterozoic Visingsö Group of southern Sweden: Lithology, sequence stratigraphy and provenance of the Middle Formation. (45 hp)
552. Berglund, Marie, 2018: Basaltkuppen - ett spel om mineralogi och petrologi. (15 hp)
553. Hernnäs, Tove, 2018: Garnet amphibolite in the internal Eastern Segment, Sveconorwegian Province: monitors of metamorphic recrystallization at high temperature and pressure during Sveconorwegian orogeny. (45 hp)
554. Halling, Jenny, 2019: Characterization of black rust in reinforced concrete structures: analyses of field samples from southern Sweden. (45 hp)
555. Stevic, Marijana, 2019: Stratigraphy and dating of a lake sediment record from Lyngsjön, eastern Scania - human impact and aeolian sand deposition during the last millennium. (45 hp)
556. Rabanser, Monika, 2019: Processes of Lateral Moraine Formation at a Debris-covered Glacier, Suldenferner (Vedretta di Solda), Italy. (45 hp)
557. Nilsson, Hanna, 2019: Records of environmental change and sedimentation processes over the last century in a Baltic coastal inlet. (45 hp)
558. Ingered, Mimmi, 2019: Zircon U-Pb constraints on the timing of Sveconorwegian migmatite formation in the Western and Median Segments of the Idefjorden terrane, SW Sweden. (45 hp)
559. Hjorth, Ingeborg, 2019: Paleomagnetisk undersökning av vulkanen Rangitoto, Nya Zeeland, för att bestämma dess utbrottshistoria. (15 hp)
560. Westberg, Märta, 2019: Enigmatic worm-like fossils from the Silurian Waukesha Lagerstätte, Wisconsin, USA. (15 hp)
561. Björn, Julia, 2019: Undersökning av påverkan på hydraulisk konduktivitet i förorenat område efter in situ-saneringsförsök. (15 hp)
562. Faraj, Haider, 2019: Tolkning av georadarprofiler över grundvattenmagasinet Verveln - Gullringen i Kalmar län. (15 hp)
563. Bjermo, Tim, 2019: Eoliska avlagringar och vindriktningar under holocen i och kring Store Mosse, södra Sverige. (15 hp)
564. Langkjaer, Henrik, 2019: Analys av Östergötlands kommande grundvattenresurser ur ett klimtperspektiv - med fokus på förstärkt grundvattenbildning. (15 hp)
565. Johansson, Marcus, 2019: Hur öppet var landskapet i södra Sverige under Atlantisk tid? (15 hp)
566. Molin, Emmy, 2019: Litologi, sedimentologi och kolisotopstratigrafi över krita–paleogen-gränsintervallet i borrningen Limhamn-2018. (15 hp)
567. Schroeder, Mimmi, 2019: The history of European hemp cultivation. (15 hp)
568. Damber, Maja, 2019: Granens invandring i sydvästa Sverige, belyst genom pollenanalys från Skottenesjön. (15 hp)
569. Lundgren Sassner, Lykke, 2019: Strandmorfologi, stranderosion och stranddeposition, med en fallstudie på Tylösand sandstrand, Halland. (15 hp)
570. Greiff, Johannes, 2019: Mesozoiska konglomerat och Skånes tektoniska utveckling. (15 hp)

571. Persson, Eric, 2019: An Enigmatic Cerapodian Dentary from the Cretaceous of southern Sweden. (15 hp)
572. Aldenius, Erik, 2019: Subsurface characterization of the Lund Sandstone – 3D model of the sandstone reservoir and evaluation of the geoenergy storage potential, SW Skåne, South Sweden. (45 hp)
573. Juliusson, Oscar, 2019: Impacts of subglacial processes on underlying bedrock. (15 hp)
574. Sartell, Anna, 2019: Metamorphic paragenesis and P-T conditions in garnet amphibolite from the Median Segment of the Idefjorden Terrane, Lilla Edet. (15 hp)
575. Végvári, Fanni, 2019: Vulkanisk inverkan på klimatet och atmorsfärcirkulationen: En litterarurstudie som jämför vulkanism på låg respektive hög latitud. (15 hp)
576. Gustafsson, Jon, 2019: Petrology of platinum-group element mineralization in the Koillismaa intrusion, Finland. (45 hp)
577. Wahlquist, Per, 2019: Undersökning av mindre förkastningar för vattenuttag i sedimentärt berg kring Kingelstad och Tjutebro. (15 hp)
578. Gaitan Valencia, Camilo Esteban, 2019: Unravelling the timing and distribution of Paleoproterozoic dyke swarms in the eastern Kaapvaal Craton, South Africa. (45 hp)
579. Eggert, David, 2019: Using Very-Low-Frequency Electromagnetics (VLF-EM) for geophysical exploration at the Albertine Graben, Uganda - A new CAD approach for 3D data blending. (45 hp)
580. Plan, Anders, 2020: Resolving temporal links between the Högberget granite and the Wigström tungsten skarn deposit in Bergslagen (Sweden) using trace elements and U-Pb LA-ICPMS on complex zircons. (45 hp)
581. Pilser, Hannes, 2020: A geophysical survey in the Chocaya Basin in the central Valley of Cochabamba, Bolivia, using ERT and TEM. (45 hp)
582. Leopardi, Dino, 2020: Temporal and genetical constraints of the Cu-Co Vena-Dampetorp deposit, Bergslagen, Sweden. (45 hp)
583. Lagerstam Lorien, Clarence, 2020: Neck mobility versus mode of locomotion – in what way did neck length affect swimming performance among Mesozoic plesiosaurs (Reptilia, Sauropterygia)? (45 hp)
584. Davies, James, 2020: Geochronology of gneisses adjacent to the Mylonite Zone in southwestern Sweden: evidence of a tectonic window? (45 hp)
585. Foyn, Alex, 2020: Foreland evolution of Blåisen, Norway, over the course of an ablation season. (45 hp)
586. van Wees, Roos, 2020: Combining luminescence dating and sedimentary analysis to derive the landscape dynamics of the Velická Valley in the High Tatra Mountains, Slovakia. (45 hp)
587. Rettig, Lukas, 2020: Implications of a rapidly thinning ice-margin for annual moraine formation at Gornergletscher, Switzerland. (45 hp)
588. Bejarano Arias, Ingrid, 2020: Determination of depositional environment and luminescence dating of Pleistocene deposits in the Biely Váh valley, southern foothills of the Tatra Mountains, Slovakia. (45 hp)
589. Olla, Daniel, 2020: Petrografisk beskrivning av Prekambriska ortognejser i den undre delen av Särvskollan, mellersta delen av Skollenheten, Kaledonska orogenen. (15 hp)
590. Friberg, Nils, 2020: Är den sydatlantiska magnetiska anomalin ett återkommande fenomen? (15 hp)
591. Brakebusch, Linus, 2020: Klimat och väder i Nordatlanten-regionen under det senaste årtusendet. (15 hp)
592. Boestam, Max, 2020: Stränder med erosion och ackumulation längs kuststräckan Trelleborg - Abbekås under perioden 2007-2018. (15 hp)
593. Agudelo Motta, Laura Catalina, 2020: Methods for rockfall risk assessment and estima-tion of runout zones: A case study in Gothenburg, SW Sweden. (45 hp)

LUNDS UNIVERSITET

Geologiska institutionen
Lunds universitet
Sölvegatan 12, 223 62 Lund